이학박사 학위논문

Studies on the physiological roles of UCHL1

UCHL1의 생체기능 연구

2022년 8월

서울대학교 대학원

생명과학부

이 대 원

UCHL1의 생체기능 연구

지도교수 정 종 경

이 논문을 이학박사 학위논문으로 제출함

2022년 6월

서울대학교 대학원

생명과학부

이 대 원

이대원의 이학박사 학위논문을 인준함

2022년 6월

위 원 장 _____ (인)

부위원장 _____ (인)

위 원 _____ (인)

위 원 _____ (인)

위 원 _____ (인)

Studies on the physiological roles of UCHL1

Professor Jongkyeong Chung

Submitting a Ph.D. Dissertation of
Biological Sciences

June, 2022

School of Biological Sciences
Seoul National University
Biological Sciences Major

Daewon Lee

Confirming the Ph.D. Dissertation written by
Daewon Lee
June, 2022

Chair	_____	(Seal)
Vice Chair	_____	(Seal)
Examiner	_____	(Seal)
Examiner	_____	(Seal)
Examiner	_____	(Seal)

Abstract

Studies on the physiological roles of UCHL1

Daewon Lee

School of Biological Sciences

The Graduate School

Seoul National University

Ubiquitin carboxy-terminal hydrolase L1 (UCHL1) hydrolyzes a glycine peptide bond at the C-terminus of ubiquitin and replenishes the cellular pool of free ubiquitin monomers. Although UCHL1 is abundantly expressed in the human brain, accounting for 1 to 2 percent of total brain proteomes, the physiological functions of UCHL1 and its implications for human disease are poorly identified. Therefore, I observed the biological roles

of UCHL1 and related phenotypes using mammalian cell lines and *Drosophila* models.

In PART 1, I studied an energy-dependent mitophagy pathway and anti-Parkinsonian effects induced by UCHL1 inhibition. Through a small-scale genetic screen using fruit flies, I found that the loss of UCHL1 ameliorated Parkinson's disease (PD)-related phenotypes, including impaired locomotor activities and the death of dopaminergic neurons, developed by PTEN-induced kinase 1 (PINK1) or Parkin mutants. Furthermore, I generated UCHL1 knockout cell lines and found that pyruvate production and ATP levels were decreased in these cell lines. These findings led to the identification of a direct substrate of UCHL1, pyruvate kinase (PKM). As a result, the loss of UCHL1 elevated the ubiquitination of PKM and destabilized PKM. Therefore, cellular glycolysis was reduced, which elevated the activity of AMP-activated protein kinase (AMPK). AMPK activated Unc-51-like kinase 1 (ULK1) and triggered a mitophagy mediated by Fun14 domain-containing 1 (FUNDC1). Further genetic analyses demonstrated that this PINK1/Parkin-independent mitophagy pathway underlies the anti-Parkinsonian effects of UCHL1 deficiency. In addition, I identified that tripartite motif-containing 63 (TRIM63) ubiquitinated PKM and exhibited an antagonistic role against UCHL1.

In PART 2, I studied insulin signaling and observed type 2 diabetes (T2D) phenotypes in *Drosophila* UCHL1 mutants. T2D symptoms, including

hyperglycemia and insulin resistance, were shown in the UCHL1 knockout flies. Also, these mutants exhibited the impairments of sensory neurons in the fly legs, which induced numbness to the physically or chemically noxious stimulations. Conversely, UCHL1 overexpression completely rescued these diabetic phenotypes from high sugar diet (HSD)-induced T2D model flies. In addition, downregulated insulin signaling was observed in UCHL1 KO cell lines. Through measuring protein levels of the components of insulin signaling, I revealed that UCHL1 controls insulin signaling and T2D-like phenotypes by deubiquitinating insulin receptor substrate 1 (IRS1). I also identified the E3 ligase cullin-1 (CUL1) as an antagonistic enzyme of UCHL1. Intriguingly, the expression of CUL1 was elevated by HSD in *Drosophila*. In addition, HSD-mediated CUL1 transcription was regulated by glycogen synthase kinase 3 (GSK3)/Snail pathway. As CUL1 is fully activated by its neddylation, I observed that the diabetic symptoms were mitigated by genetic suppression of CUL1 neddylation.

Since UCHL1 targets PKM and IRS1, two of which are the most indispensable molecules for glucose metabolism, I suggest UCHL1 as an important regulator of cellular metabolism. Also, I propose that chemical and genetic regulation of UCHL1 activity might be effective strategies for rehabilitating metabolic diseases.

Keywords: UCHL1, PKM, Parkinson's disease, mitophagy, IRS1, type 2 diabetes, insulin signaling

***Student number*:** 2015-22638

TABLE OF CONTENTS

List of Figures

List of Tables

Introduction

Ubiquitination

Ubiquitination is one of the most prevalent posttranslational modifications (PTMs) of proteins in which a ubiquitin is attached to a target protein (Rape, 2018). This process occurs when the last amino acid of ubiquitin, glycine 76, binds to a lysine residue of the target protein. Three main enzymes, ubiquitin-activating enzyme (E1), ubiquitin-conjugating enzymes (E2), and ubiquitin ligases (E3), are required for this binding (Swatek and Komander, 2016). These enzymes induce different types of substrate ubiquitination, monoubiquitination, and polyubiquitination. Monoubiquitination is the addition of a ubiquitin monomer to a substrate protein and regulates the cellular roles of the protein (Hicke, 2001). For example, the monoubiquitination of voltage-dependent anion channel 1 (VDAC1) by the E3 ligase Parkin is associated with apoptosis by elevating mitochondrial calcium uptake (Ham et al., 2021). Also, Ste2p, a pheromone G protein-coupled receptor in *Saccharomyces cerevisiae*, located at cell surface is transported into the cytoplasm by monoubiquitination (Shih et al., 2000). Polyubiquitination is the addition of a ubiquitin chain on a lysine residue of the substrate protein. These polyubiquitin chains are generated by binding the glycine residue of a ubiquitin molecule to a lysine of ubiquitin bound to a substrate protein. As ubiquitin has seven lysine residues, including 6, 11, 27, 29, 33, 48, and 63, and first methionine as ubiquitination sites, many patterns of polyubiquitin chains are observed in cells (Komander and Rape, 2012). For example, K48-linked ubiquitination of lysine demethylase 4A

(KDM4A) is induced by ring finger protein 168 (RNF168) and the ubiquitinated KDM4A is degraded by proteasomal degradation (Mallette et al., 2012). Also, K63-linked ubiquitination at 376 lysine residues of receptor-interacting protein kinase 1 (RIPK) decreases its kinase activity and induces apoptosis (Tang et al., 2019). Therefore, both monoubiquitination and polyubiquitination of proteins are critical for the appropriate regulation of protein functions and cellular processes.

Deububiquitination and deubiquitinases (DUBs)

Ubiquitination is reversed by deubiquitinases (DUBs), so-called deubiquitination. Two types of DUBs, including cysteine proteases and metalloproteases, can cleave the amide bond between ubiquitin and protein substrate. Through this reaction, a ubiquitinated protein is deubiquitinated. In addition, free monomeric ubiquitin is formed and cells recycle this ubiquitin for other ubiquitination processes (Amerik and Hochstrasser, 2004). Therefore, deubiquitination also regulates various cellular processes like ubiquitination. For example, Jab1/Mov34/Mpr1 Pad1 N-terminal+ (MPN+) (JAMM) domain proteases, the only metalloprotease family among DUB families, regulate physiological processes. Proteasome 26S subunit, non-ATPase 14 (PSMD14), belonging to the JAMM family, deubiquitinates S-Cdk inhibitor (Sic1) and blocks the entry of ubiquitinated proteins into the proteasome complexes in yeast (Verma et al., 2002). Also, USP15 and USP30 under ubiquitin-specific proteases (USPs) subfamily are the regulators of mitochondrial clearance, mitophagy. They deubiquitinate mitochondrial substrates of Parkin, an E3 ubiquitin ligase, and suppress Parkin-mediated mitophagy (Bingol et al., 2014; Cornelissen et al., 2014; Cunningham et al., 2015). In addition, BRCA1-associated protein 1 (BAP1), belonging to the ubiquitin C-terminal hydrolases (UCHs) family, deubiquitinates and stabilizes type 3 inositol-1,4,5-trisphosphate receptor (IP3R) and regulates calcium homeostasis. BAP1 heterozygous mutant mice exhibit malignant mesothelioma (Bononi et al., 2017).

Ubiquitin C-terminal hydrolase L1 (UCHL1)

UCHL1 belongs to the UCH family. Similar to other cysteine proteases, UCHL1 hydrolyzes small C-terminal adducts of ubiquitin and generates free monomeric ubiquitins. Although other deubiquitinases in the UCH family except UCHL1 are dominantly expressed in muscles, heart, and lymphoid tissues (Ouyang et al., 2020; Sun, 2008; Szczepanski and Wang, 2021), UCHL1 is mainly expressed in various neurons and constitutes 1 percent of total central nervous system (CNS) proteins (Doran et al., 1983). Therefore, UCHL1 mutations are closely linked with neuronal physiology. UCHL1 knockout mice exhibit sensory disorders at an early age, followed by locomotor dysfunctions at a later stage (Saigoh et al., 1999). These phenotypes have resulted from the degeneration of the gracile nucleus in the medulla oblongata, so-called gracile axonal dystrophy (GAD) (Yamazaki et al., 1988). Furthermore, the expression of UCHL1 is increased in high-grade pediatric glioma cell lines, including UW479, SF188, and SJ-GBM2 (Sanchez-Diaz et al., 2017). Similarly, the metastasis of U251 and T98-G glioma cell lines is decreased by UCHL1 knockdown (Sui and Piao, 2020). Although GAD and glioma phenotypes of UCHL1 mutations reflect the importance of UCHL1 in neuronal disorders, the exact target of UCHL1 has not been identified yet.

Parkinson's disease (PD)

Parkinson's disease (PD) is one of the most common neurodegenerative disorders worldwide. One of the main symptoms of PD is impaired movement, caused by the death of dopaminergic (DA) neurons in the substantia nigra, a region of the midbrain (Poewe et al., 2017; Rabey and Hefti, 1990). Since DA neurons regulate movement by regulating the functions of motor neurons or basal ganglia, one of the motor centers, most of the PD symptoms are related to locomotion. Also, it has been reported that about twenty genes are closely associated with the development of PD or loss of DA neurons. For example, SNCA (α-synuclein; PARK1) overexpression in the brain of mouse or *Drosophila* induces loss of dopaminergic neurons and the defects related to movements. However, the reasons why DA neurons are vulnerable in the pathogenesis of PD are still unclear. According to previous researches, DA neurons are classified as one of the cell types that require massive energy supplies to sustain energetic and functional demands. Therefore, glucose metabolism is elevated in DA neurons, which creates excessive reactive oxygen species (ROS) as by-products (Bolam and Pissadaki, 2012; Surmeier et al., 2017). Consequently, DA neurons are vulnerable to oxidative stress, and mitochondrial damage caused by ROS may be a contributing factor to the death of DA neurons in PD patients. Consistently, DA neuronal death was developed by administrating 1-methyl-4-phenyl-1,2,3,6-tetrahydropyridine (MPTP) and 1,1'-dimethyl-4,4'-bipyridinium (paraquat) with animal models for blocking electron transport

chain (ETC) in mitochondria (Callio et al., 2005; Fukushima et al., 1997; Richardson et al., 2005; Vila and Przedborski, 2003). Thus, the molecular link between glucose metabolism and mitochondrial homeostasis has been crucial for identifying the susceptibility of DA neurons in PD pathogenesis.

Mitophagy and PD genes

Mitochondrial damages were mainly caused by oxidative stress. If these impairments are accumulated, the mitochondria are not able to produce energy at a normal level. Therefore, cells have to clear the damaged mitochondria via mitochondria-specific autophagy, mitophagy. Especially, two of the PD genes discovered from genetic analyses, PTEN-induced kinase 1 (PINK1; also known as PARK6) and E3 ligase Parkin (also known as PARK2), form a major signaling axis, and play a crucial role in modulating mitophagy (Palikaras et al., 2018; Park et al., 2006; Pickrell and Youle, 2015). In response to mitochondrial injury, PINK1 phosphorylates Parkin, which translocates Parkin from cytosol to the mitochondria (Springer and Kahle, 2011). Mitochondrial proteins are ubiquitinated by mitochondrial Parkin, then recognized by mitophagy adaptors and mitophagosomes **(Fig. 1)** (Vives-Bauza et al., 2010; Youle and Narendra, 2011). Other PD-causative genes, including DJ-1 (Dodson and Guo, 2007; Repici and Giorgini, 2019), leucine-rich repeat kinase 2 (LRRK2) (Bonello et al., 2019), high-temperature requirement protein A2 (htrA2) (Plun-Favreau et al., 2007), and F-box only protein 7 (FBXO7) (Burchell et al., 2013), also interact with PINK1/Parkin pathway.

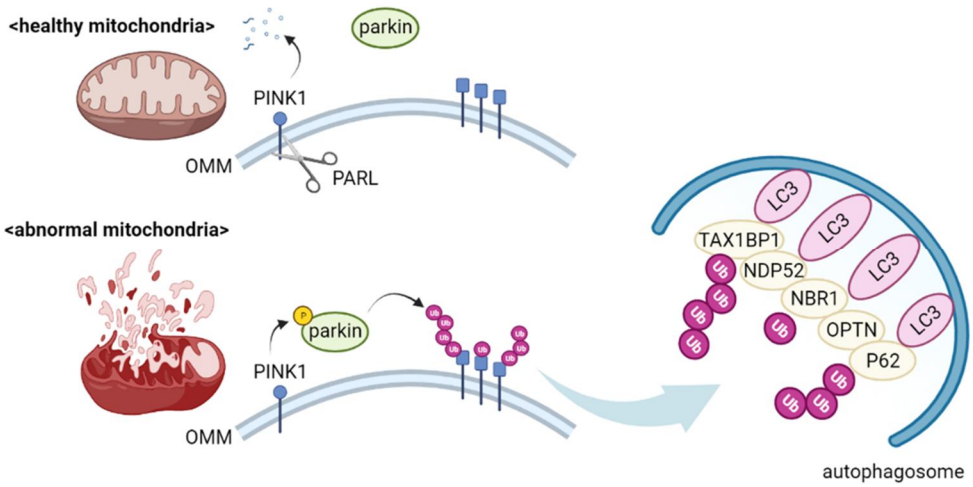

Figure 1. PINK1/Parkin pathway and mitophagy.

In healthy mitochondria, PINK1, located onto the mitochondrial outer membrane (OMM), is degraded by a protease, presenilin associated rhomboid-like (PARL). However, in unhealthy mitochondria, PARL cannot cleave PINK1. Therefore, PINK1 phosphorylates an E3 ligase, Parkin, which translocates cytosolic Parkin to mitochondria. Mitochondrial Parkin ubiquitinates various proteins in OMM. These ubiquitination processes are recognized by autophagosomes comprised of microtubule-associated protein 1 light chain 3 (LC3), Tax1 binding protein 1 (TAX1BP1), calcium-binding and coiled-coil domain 2 (NDP52), next to BRCA1 gene 1 protein (NBR1), optineurin (OPTN), and sequestosome 1 (p62). Finally, the unhealthy mitochondria are removed by these autophagosomes. Image was generated from Biorender.

UCHL1 as a PD gene

Since ubiquitination of mitochondrial proteins is a key modification for mitophagy, UCHL1, which has deubiquitinase (DUB) activity, has been considered as an important PD gene (Chakraborty and Ziviani, 2020). However, the precise roles of UCHL1 and its molecular targets have yet to be identified. As a member of the UCH family of deubiquitinating enzymes (DUBs), UCHL1 cuts glycine peptide bonds at the C-terminal of ubiquitins and occupies about 2 percent of total brain proteins (Larsen et al., 1998; Wilkinson et al., 1989). Unexpectedly, one family with familial PD in Germany was found to have the I93M mutation in the UCHL1 gene, providing the first evidence to classify UCHL1 as a PD-susceptible gene (Leroy et al., 1998). Also, impairments in motor neurons similar to PD were shown when the seventh amino acid of UCHL1, glutamate, is changed into alanine (Bilguvar et al., 2013). Oppositely, several statistical analyses suggested that PD pathogenesis is decreased by a polymorphism S18Y in UCHL1 (Carmine Belin et al., 2007; Kyratzi et al., 2008; Lincoln et al., 1999; Maraganore et al., 2004b; Xilouri et al., 2012). Despite these epidemiological findings, the questions of whether the mutations of UCHL1 are directly linked to PD are still barely answered.

Type 2 diabetes and insulin signaling

Diabetes mellitus is a disorder causing blood glucose levels to be abnormally high. The reasons for elevated glucose are categorized into two mechanisms. When the pancreas fails to produce insulin at appropriate levels, cells cannot intake glucose from the blood, and the glycemia increases, so-called type 1 diabetes (T1D) (Katsarou et al., 2017). However, the blood glucose can be elevated despite the normal secretion of insulin. When insulin is secreted into the blood from the pancreas, insulin is attached to the insulin receptor (IR) which is located on the cellular membrane facing the extracellular matrix (ECM) (Haeusler et al., 2018). The insulin-IR complex passes the signals by phosphorylating insulin receptor substrate 1 (IRS1) (Gual et al., 2005). As a signaling adaptor, IRS1 plays a key role in transmitting signals from insulin to intracellular pathways composed of phosphoinositide 3-kinase (PI3K), protein kinase B (PKB/AKT), target of rapamycin (TOR), glycogen synthase kinase 3 (GSK3), and AKT substrate of 160 kDa (AS160) (Boucher et al., 2014; Cohen and Frame, 2001; Hoxhaj and Manning, 2020; Um et al., 2006). Especially, AS160 is phosphorylated by AKT after insulin stimulation, which results in the translocation of glucose transporter 4 (GLUT4) from vesicle to plasma membrane (Eguez et al., 2005; Mîinea et al., 2005) **(Fig. 2)**. Therefore, the glucose from blood is transported to the cytosol by insulin signaling. However, when cells cannot convey the insulin signals into the cytosolic molecules, they are not able to utilize the

glucose from the blood and the glycemia elevates, classified as type 2 diabetes (T2D) (Davies et al., 2018; DeFronzo et al., 2015; Olokoba et al., 2012).

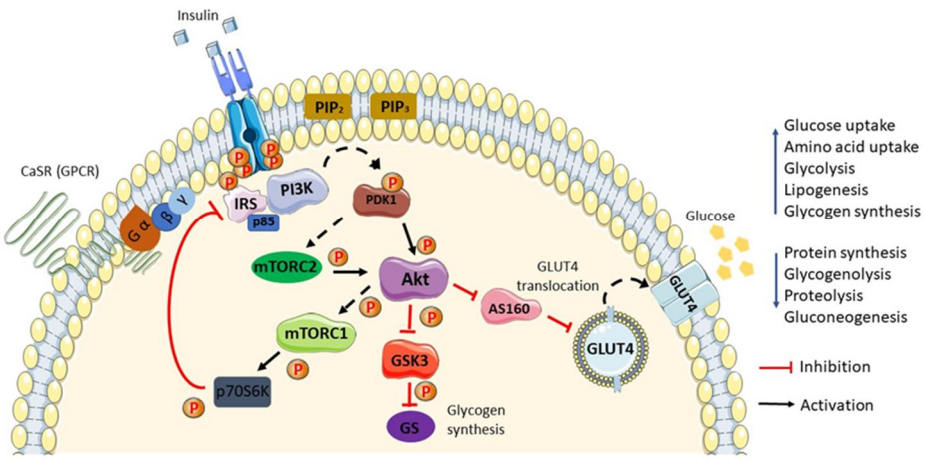

Figure 2. A schematic for insulin signaling.

When extracellular insulin binds to insulin receptor (IR), the binding triggers autophosphorylation of IR. Autophosphorylated IR phosphorylates IRS1 and enhances insulin signaling. Then, the signals are transmitted to PI3K and AKT which activates TOR and inactivates GSK3 and AS160. Activated TOR phosphorylates ribosomal protein S6 kinase (S6K) and phosphorylated S6K phosphorylates IRS1, which inactivates IRS1 and insulin signaling for negative feedback. Inactivated GSK3 activates glycogen synthase (GS), generating glycogen for the storage of glucose. AS160 is inactivated by AKT phosphorylation, which causes translocation of GLUT4 vesicles into the plasma membranes. Image from (Zakaria et al., 2021).

Insulin resistance and IRS1

Insulin resistance, defined as the impairment of intracellular glucose transport in spite of the normal concentration of insulin, is the main symptom of T2D (Yaribeygi et al., 2019). Although it has been reported that enormous genetic and environmental factors can contribute to insulin resistance in various model organisms (Islam and Loots du, 2009; Stott and Marino, 2020), human studies proposed that downregulated insulin signaling by IRS1 dysfunction is a common and comprehensive reason for T2D pathogenesis (DeFronzo and Tripathy, 2009; Karlsson and Zierath, 2007). As IRS1 is a 180 kDa protein and has various lysine residues for ubiquitination, IRS1 regulation by ubiquitination is critical for understanding insulin resistance (Boura-Halfon and Zick, 2009; Copps and White, 2012). For example, the E3 ligase mitsugumin 53 (MG53) ubiquitinates IRS1, and insulin resistance induced by high fat diet (HFD) is improved by MG53 knockout in mice models (Park et al., 2018; Yi et al., 2013). Also, cullin 7 (CUL7) ubiquitinates IRS1 while interacting with S-phase kinase-associated protein 1 (Skp1). CUL7 KO mice show increased insulin signaling and IRS1 accumulation (Xu et al., 2008). Thus, identifying the regulatory mechanisms for IRS1 ubiquitination should be focused on to comprehend insulin resistance. Although several E3 ligases are known to ubiquitinate IRS1, the exact lysine sites for the ubiquitination by these ligases and the deubiquitinases of IRS1 are not studied well.

Relations between PD and diabetes

It has been reported that the remedies for PD can be connected to developing hyperglycemia, one of the main symptoms of T2D. For example, levodopa, one of the PD medications, treatment induces hyperglycemia. In mouse models, intravenous injection of levodopa elevates the level of blood glucose (Håkanson et al., 1967). Also, patients with parkinsonism after 0.5 to 1.0 g of levodopa therapy have increased levels of plasma glucose (Sirtori et al., 1972). Similar to these results, other drug treatments or genetic manipulations for mitigating PD induce hyperglycemia. Feeding rapamycin, an inhibitor of TOR, rescues the death of dopaminergic neurons in fruit flies (Tain et al., 2009) and the mice injected with rapamycin show hyperglycemia (Blagosklonny, 2019; Schindler et al., 2014). Also, over-expressing F-box only protein 7 (FBXO7) in *Drosophila* ameliorates PD-related phenotypes (Burchell et al., 2013) and a bioinformatic analysis revealed that FBXO7 expression is increased in T2D patients (Zhu et al., 2020). Therefore, identifying the correlation between PD and T2D is pivotal for understanding both diseases.

Specific Aims

Aim 1 – To identify the roles of UCHL1 in mitophagy and Parkinson's disease

- Explore the interactions between UCHL1 and PINK1/Parkin using *Drosophila* genetics
- Reveal how UCHL1 controls an energy-dependent mitophagy pathway using human cell biology
- Investigate a specific target of UCHL1 which can regulate mitophagy and Parkinson's disease-related phenotypes

Aim 2 – To understand the roles of UCHL1 in insulin signaling and type 2 diabetes

- Observe *Drosophila* phenotypes related to type 2 diabetes and insulin signaling in human cell lines
- Discover a substrate of UCHL1 which can control insulin signaling
- Decipher an E3 ligase playing an antagonistic role of UCHL1 and its upstream signaling

Materials and Methods

Plasmid constructs and chemical reagents

Wild-type UCHL1 (NM_004181) was cloned into pcDNA3.1 zeo (+) C-terminal Myc-tagged vector or pCMV 14 C-terminal Flag-tagged vector. DNA constructs of UCHL1 carrying point mutations (E7A, S18Y, C90S, I93M, and R178Q) were generated by the site-directed point mutagenesis method. N-terminus HA-tagged human ubiquitin was inserted into pRK5 vector. The C-terminus Myc-tagged human PKM (PKM1; NM_002654.5 and PKM2; AB528306.1) was inserted into pcDNA3.1 zeo (+) vector. The N-terminus Flag-tagged human TRIM63 (NM_032588.3) was cloned into pCMV10 vector. The N-terminal Flag-tagged human IRS1 (NM_005544.3) was cloned into pcDNA3.1 zeo (+) vector. Cells were treated with carbonyl cyanide m-chlorophenyl hydrazone (CCCP, Calbiochem), rotenone (Sigma), oligomycin (Sigma), 2-DG (Sigma), antimycin A (Sigma), Compound C (Sigma), carbobenzoxy-Leu-Leu-leucinal (MG132, Calbiochem) or insulin (Roche, 11376497001).

Cell culture and transfection

HEK293 cells and HEK293E cells were used and cultured in DMEM (Welgene, Korea) supplemented with 10% fetal bovine serum (Invitrogen) at 37°C in a humidified atmosphere composed of 5% CO_2. These cells were transfected using lipofectamine 3000 (Invitrogen) as instructed by the manufacturer. For siRNA transfection, I used RNAi max (Invitrogen).

Generation of UCHL1 KO HEK293

The CRISPR genome editing technique was used for the generation of UCHL1 KO cells. To generate UCHL1 KO HEK293 cells, the guide RNA sequence (GTGGCGCTTCGTGGACGTGC) was cloned into the PX459 vector (Addgene, #62988). I generated UCHL1 KO cells using the previously reported method (Ran et al., 2013). The plasmid was transfected into HEK293 cells. 48 h after transfection, transfected cells were selected with 5 μg/ml puromycin for 3 days, and then single colonies were transferred onto 96-well plates with one colony in each well. The UCHL1 KO clones were screened by immunoblot analysis with rabbit anti-UCHL1 antibody (Cell Signaling).

Antibodies

For immunoblot analysis, the following antibodies were used; mouse anti-MFN1 (Abcam), rabbit anti-TOM20 (Cell Signaling), mouse anti-TIM23 (BD Science), rabbit anti-COXIV (Cell Signaling), rabbit anti-UCHL1 (Cell Signaling), mouse anti-tubulin (DSHB), rabbit anti-phospho-AMPK alpha (T172, Cell Signaling), rabbit anti-phoshpo-ULK1 (S555, Cell Signaling), mouse anti-AMPK (Abcam), rabbit anti-ULK1 (Cell Signaling), rabbit anti-FUNDC1 (Novus Biologicals), mouse anti-VDAC1 (Abcam), mouse anti-NDUFS3 (Abcam), rabbit anti-Flag (Cell Signaling), rabbit anti-HA (Cell Signaling), mouse anti-Myc (MBL, Japan), mouse anti-TRIM63 (Santacruz), rabbit anti-PKM antibody (Cell Signaling), mouse anti-phospho-AKT (S473, Cell Signaling), rabbit anti-phospho-S6K (T389, Abcam), and rabbit anti-

IRS1 (Cell signaling). Peroxidase-conjugated secondary antibodies were purchased from Jackson Laboratory.

Immunoprecipitation and immunoblotting

For immunoprecipitation, cells were lysed using a lysis buffer A (20 mM Tris pH 7.5, 100 mM NaCl, 1 mM EDTA, 2 mM EGTA, 50 mM β-glycerophosphate, 50 mM NaF, 1 mM sodium vanadate, 2 mM DTT, 1 mM PMSF, 10 μg/ml leupeptin, 1 μg/ml pepstatin A, and 1% Triton X-100) and were subjected to immunoprecipitation and immunoblotting according to standard procedures. Cell lysates were centrifuged at 13,000 rpm, 4°C for 20 min and were incubated overnight after the addition of primary antibodies. Lysates were then incubated with protein A/G agarose beads for 2 h at 4°C, washed 4 times in detergent-free lysis buffer A, and eluted with 2× Laemmli buffer at 95°C. For the Immunoblot analysis of mitochondrial proteins, I used RIPA buffer (50 mM Tris pH 8.0, 150 mM NaCl, 0.5% sodium deoxycholate, 1% NP-40, 0.1% SDS, 2 mM DTT, 1 mM PMSF, 10 μg/ml leupeptin, and 1 μg/ml pepstatin A). Total proteins were quantified using the BCA protein assay kit (Pierce). Lysates were subjected to SDS-PAGE analysis followed by immunoblotting according to standard procedures. The blots were developed and viewed under LAS-4000 (Fujifilm).

Fly stocks and diet preparation

The *Drosophila* lines used in the experiments were *mef2*-GAL4 (27390; Bloomington *Drosophila* Stock Center), *hs*-GAL4 (2077; Bloomington *Drosophila* Stock Center), *th*-GAL4 (8848; Bloomington *Drosophila* Stock Center), *elav*-GAL4 (8765; Bloomington *Drosophila* Stock Center), *cg*-GAL4 (7011; Bloomington *Drosophila* Stock Center), *OK371*-GAL4 (26160; Bloomington *Drosophila* Stock Center) $PINK1^{B9}$ (34749; Bloomington *Drosophila* Stock Center), $park^{1}$ (34747; Bloomington *Drosophila* Stock Center), *tub*-$GAL80^{TS}$ (7017; Bloomington *Drosophila* Stock Center), *DILP2*-GAL4 (37516; Bloomington *Drosophila* Stock Center), UAS-DILP2 (80936; Bloomington *Drosophila* Stock Center), UAS-nlsGFP (4776; Bloomington *Drosophila* Stock Center), UAS-InR^{CA} (8263; Bloomington *Drosophila* Stock Center), UAS-$PI3K^{CAAX}$ (8294; Bloomington *Drosophila* Stock Center), UAS-myrAKT (80935; Bloomington *Drosophila* Stock Center), UAS-UBA3 RNAi (83571; Bloomington *Drosophila* Stock Center), UAS-RBX1 RNAi (32362; Bloomington *Drosophila* Stock Center), UAS-CUL1 RNAi (36601; Bloomington *Drosophila* Stock Center), UAS-Cbl RNAi (27500; Bloomington *Drosophila* Stock Center), UAS-CUL3 RNAi (28899; Bloomington *Drosophila* Stock Center), UAS-TRAF4 RNAi (81497; Bloomington *Drosophila* Stock Center), UAS-Sgg^{CA} (5255; Bloomington *Drosophila* Stock Center), UAS-Sgg^{DN} (5359; Bloomington *Drosophila* Stock Center), UAS-Zda RNAi (5482R-2; Japanese National Institute of Genetics), UAS-Bnip3 RNAi (5059R-1; Japanese National Institute of Genetics), UAS-p62 RNAi (10360R-1; Japanese National

Institute of Genetics), UAS-FUNDC1 RNAi (5676R-1; Japanese National Institute of Genetics), UAS-AMPK RNAi (3051R-1; Japanese National Institute of Genetics), UAS- ULK1 RNAi (10967R-1; Japanese National Institute of Genetics), UAS-UBE2M RNAi (7375R-2; Japanese National Institute of Genetics), UAS-Snail RNAi (3956R-2; Japanese National Institute of Genetics), UAS-AMPK^{CA} (previously described) (Lee et al., 2007), UAS-IRS1 (previously described) (Naganos et al., 2012), UAS-FUNDC1 (F004027; FlyORF), UAS-CUL1 (F001068; FlyORF), UAS-Snail (F000066; FlyORF), UAS-PKM RNAi (7070R-2; Japanese National Institute of Genetics), UAS-TRIM9 RNAi (31721R-2; Japanese National Institute of Genetics), UAS-TRIM9 (received from Dr. Bing Ye) (Yang et al., 2014), UAS-GLUT1 RNAi (28645; Bloomington *Drosophila* Stock Center), UAS-NDUFS3 RNAi (12079R-1; Japanese National Institute of Genetics), UAS-ATPsynβ (8189R-1; Japanese National Institute of Genetics). *Drosophila* PKM cDNA (UFO11109) and UCH cDNA (GH02396) were obtained from *Drosophila* Genomics Resource Center (Indiana University) and UAS-PKM-HA and UAS-UCH-HA were generated by microinjecting pUAST-PKM-HA into w1118 embryos. *Drosophila* UCH cDNA (GH02396) was obtained from *Drosophila* Genomics Resource Center (Indiana University) and UAS-UCH-HA was generated by microinjecting pUAST-UCH-HA into w1118 embryos. The UAS-PD gene RNAi lines were described in **Table 1**. All flies were grown in the standard cornmeal-yeast-agar medium at 25°C. For high sugar diet, the food was made by mixing 15 grams of agar, 250 grams of sucrose,

100 grams of yeast, and 3 mL of propionic acid to make 1 L of high sugar food. For high fat diet, the food was made by mixing 15 grams of agar, 50 grams of sucrose, 100 grams of yeast, and 3 mL of propionic acid, 200 grams of coconut oil to make 1 L of high sugar food.

Generation of UCH KO and KI flies

For the generation of UCH KO flies, I used *CAS-0001* fly from Japanese National Institute of Genetics. After selecting a Cas9 target site as far forward as possible in the UCH 1st exon, I made sgRNA using in vitro transcription as previously described (Bassett and Liu, 2014). As both UCH gene and *nos-Cas9* are on the 2nd chromosome, I crossed *CAS-0001* with *w1118* and collected embryos. After injecting sgRNA into the embryos, the adult male flies were crossed with *bc*/*cyo*. To exclude the case that a DNA break had occurred on the *nos-Cas9* chromosome, I sorted out the flies that did not carry *nos-Cas9* by PCR. Then, I amplified the target loci by PCR and analyzed the sequence.

For the generation of UCH KI flies, I injected three different kinds of plasmids into fly embryos; Cas9 expression vector (pHsp70-Cas9; Addgene, #45945), sgRNA expression vectors, and donor plasmids for homologous recombination (38). To construct sgRNA expression vectors, 24-bp oligonucleotides with 20-bp sgRNA sequence and 4-bp Bbs1 restriction enzyme site were synthesized and inserted into pU6-Bbs1-chiRNA vector (Addgene, #45946). For preparing donor plasmids, I extracted fly genomic

DNA and amplified the homology arms which have a length of about 2-kb and a PAM sequence at the center by PCR. After cloning the homology arms into pBS vector, I made each point mutation by site-directed mutagenesis. Also, as the homology arms need the sequences which sgRNA could recognize, sgRNA sequences in the homology arms were modified by a site-directed mutagenesis to avoid changing the UCH protein sequence. Finally, all the three completed vectors were injected into fly embryos to generate various UCH KI flies. The KI flies were identified by PCR and subsequent DNA sequencing.

Measurement of ATP levels

I used ATP Bioluminescence Assay Kit HS II (Roche) and analyzed ATP levels according to the manufacturer's instructions. To measure ATP levels in cells, HEK293 WT or KO cells were cultured in 96 wells for 24 h, and I treated rotenone (Sigma), oligomycin (Sigma), and 2-DG (Sigma) for 12 h before measuring ATP levels. Samples were incubated with cell lysis reagents for 5 min at room temperature and were added with luciferase reagents. The luminescence was measured by Tecan Plate Reader Infinite 200. Three independent experiments were performed for data quantification. To measure ATP levels in flies, five 3rd instar larvae were collected and ground in lysis reagents. After lysis, luciferase reagents were added to the supernatants and the luminescence was measured by Tecan Plate Reader Infinite 200. Feeding flies with 2-DG (Brown et al., 2020), rotenone (Doktór

et al., 2019), and oligomycin (Bahadorani et al., 2010) was performed as previously described.

Detecting mitophagy in cells

Mitophagy was measured by using a mitophagy detection kit (Dojindo Molecular Technologies, Korea) according to the manufacturer's instructions. HEK293 UCHL1 WT or KO cells were seeded on 10 mm coverslips in 12-well plates and cultured at 37°C overnight. HEK293 cells were treated with 20 μM CCCP for 12 h and measured mitophagy as suggested by the manufacturer's instruction (Iwashita et al., 2017). The cells were observed by LSM 710 confocal microscope. Three independent experiments were performed for quantification and the red fluorescence dots per cell were counted using Image J.

Glucose isotope tracing for metabolomics

For metabolites extraction from cells, 200 μl of an ice-cold mixture of methanol, acetonitrile, and distilled water (5:3:2) were mixed with cell pellet (cell number = 5 × 106), and 400 μL of an ice-cold mixture of methanol and acetonitrile (5:3:2) was added to the 100 μl culture media. This mixture was vortexed for 20 sec and frozen in liquid nitrogen for 2.5 min. It was then thawed at 25°C for 1.5 min. This freeze-and-thaw cycle was repeated twice and the cell homogenate was centrifuged at 15,000×g for 20 min at 4°C. The supernatant was concentrated by vacuum evaporation in VS-802 Speed-Vac

(Vision Scientific, Korea). The dried samples were reconstituted in 25 µl of a chilled mixture of acetonitrile/water (1:1) for mass spectrometry analysis. 13C-labeled metabolites derived from the U-13C glucose tracer were measured by Q Exactive (QE) focus mass spectrometer (Thermo Fisher Scientific, Germany). The LC separation was performed with a ZIC-pHILIC column (150 × 2.1 mm, 5 µm, Merck kGaA, Germany) on Acquity UPLCTM system (Waters). The column temperature was set at 35°C with a flow rate of 0.2 ml/min, and the analytes were eluted with a linear gradient (mobile phase A: acetonitrile, mobile phase B: 10 mM ammonium carbonate in water, pH 9.0) as follows: 80% A in 0-4.5 min, 80%-5% in 4.5-13.5 min, 5% in 13.5-19.5 min, 5%-80% 19.5-22.5 min, 80% 22.5-26.5 min. Prior to injection, samples were kept at 4°C in an auto-sampler and the injection volume was 5 µl. For the mass detection, Thermo Orbitrap was operated in full scan of negative ion mode with mass range from 64 to 830 m/z, and the instrument parameters were as follows: 4.2 kV of spray voltage, the capillary temperature at 270°C, and sheath gas, auxiliary gas, and sweep gas at flow rates of 46, 12, and 6 arbitrary units, respectively. Metabolites were identified by accurate mass measurement (accuracy of <6 ppm) and confirmed by comparing the m/z and retention time with those of the standard compounds **(Table 2)**. The peak area of metabolites and those isotopologues were measured using Xcalibur software (Thermo Fisher Scientific).

For sample preparation, HEK293 UCHL1 WT and KO cells were cultured in 60 mm plate with DMEM media (Gibco) for 48 h. Cells were

washed twice with DPBS (Gibco) and media were changed with 25 mM U-13C-glucose (Cambridge Isotope Laboratories) in DMEM without glucose (Gibco) supplemented with 10% dialyzed FBS (Gibco). Cells were harvested after 12 h incubation in U-13C-glucose media. Cells were trypsinized and centrifuged at 5,000 rpm at 4°C for 3 min. Cell pellets were washed twice with DPBS and were frozen in liquid nitrogen and stored at -80°C prior to metabolite extraction.

Quantification of wing and thorax abnormality in *Drosophila*

To quantify the abnormality of wing and thorax, the percentage of 3-day-old male flies showing crushed thorax and downturned or upturned wing out of ten flies was measured. Ten independent experiments were performed for quantification (Ham et al., 2021; Ham et al., 2020).

Mitochondria staining and TUNEL assay in *Drosophila*

3-day-old male flies were fixed with 4% paraformaldehyde. After fixation, the thoraces of flies were collected and stained. For mitochondria staining, streptavidin was used to observe mitochondria (1:200, Alexa Fluor 488 streptavidin, Invitrogen) and phalloidin was used to observe actin filament (1:200, phalloidin-tetramethylrhodamine B isothiocyanate, Merck). For the TUNEL assay, in situ cell death detection kit (Roche) was used to visualize apoptosis and Hoechst was used to stain nucleus (1:200, Hoechst 33258, Invitrogen).

To quantify the percentage of flies having mitochondrial abnormalities, a fly with a mitochondrion having a length of more than 5 μm and a width more than 3 μm was defined as the fly having abnormal mitochondria. To quantify the percentage of flies showing apoptosis, a fly having more than ten TUNEL dots in any of 6 dorsal longitudinal muscles of the indirect flight muscles was defined as the fly showing apoptosis (Ham et al., 2021; Ham et al., 2020). Ten 3-day-old male flies were counted to quantify these percentages. Ten independent experiments were performed for data quantification.

Climbing assay in *Drosophila*

3-day-old male flies were transferred in groups of ten to 18-cm-long vials and were incubated for 5 min at room temperature for recovery period. All the flies were moved to the bottom of the vial by gently tapping, and the percentage of flies arriving over 15 cm within 12 sec was measured. The assay was repeated ten times per group of the flies, and ten groups of each genotype were performed for data quantification.

DA neuron staining in *Drosophila*

30-day-old male flies were fixed with 4% paraformaldehyde and the brains were dissected. DA neurons were stained with anti-TH mouse antibody (1:200, Immunostar). For counting the number of DA neurons, the brains were observed by LSM710 confocal microscope (Carl Zeiss) via Z-stack

analysis. DA neurons from ten flies of each genotype were measured for data quantification.

Generation of recombinant UCHL1 proteins

E. coli BL21 (DE3) strain was used for transformation, cloning, and protein production. Human UCHL1, *Drosophila* UCH, and their mutants (E7A, S18Y, C90S, and I93M in human UCHL1/ E8A, H19Y, C93S, and V96M in *Drosophila* UCH) were cloned into pGEX 4T-1 vector. 20 ml of overnight pre-cultures were used to inoculate 500 ml of LB supplemented with ampicillin. Cultures were incubated at 37°C with 180 rpm shaking. When the OD600nm reached 0.6, protein expression was induced by adding 0.1 mM IPTG for about 1-2 h. Cells were harvested by centrifugation at 12,000 rpm for 30 min at 4°C. Cell pellets were re-suspended in a lysis buffer (25 mM Tris-HCl pH 7.5, 150 mM NaCl, 1 mM EDTA) supplemented with protease inhibitors (1 mM PMSF, 10 μg/ml leupeptin, and 1 μg/ml pepstatin A) and 0.5% Triton X-100. Cells were disrupted by sonication and the lysate was clarified by centrifugation at 10,000 rpm for 10 min at 4°C. GST-tagged proteins in the supernatant were purified by binding to GST beads (GE Healthcare) for 2 h at 4°C. GST beads were washed 3-4 times with a lysis buffer without Triton X-100. GST-tagged proteins were eluted with an elution buffer (10 mM reduced glutathione, 50 mM Tris-HCl, 5% glycerol, pH 8.0).

DUB activity assay

The DUB activity of each UCHL1 or UCH mutant protein was measured using a DUB activity assay kit (Biovision, K485). 1 mg/ml of UCHL1 or UCH recombinant protein was used and DUB substrate (Ub-AMC) was diluted into DUB assay buffer (1:44). To initiate the reaction, 5 μL of UCHL1 or UCH protein and 5 μL of DUB substrate were mixed. Using Tecan Plate Reader Infinite 200, the fluorescence emitted from the DUB reaction and the AMC standard were measured every 3 min for 30 min (Bilguvar et al., 2013).

Measurement of hemolymph glucose in *Drosophila*

40 female flies were collected and punctured through the thorax with a micro dissecting needle. These flies were then transferred into a small tube with a perforated bottom. This tube was placed onto 1.5 mL collection tube and centrifuged at 5,000 rpm for 5 min at 4 ℃. Afterward, the collected hemolymph was diluted 1/10 and the free glucose from the 10-fold diluted hemolymph was measured using glucose assay kit (Sigma, G3293) (Moraru et al., 2018).

Measurement of TAG and glycogen in *Drosophila*

8 female flies were homogenized in 0.5 mL of 0.05% PBST and the lysates were then incubated at 70 ℃ for 5 min. The cooled-down lysates were centrifuged at 14,000 rpm for 5 min. The levels of TAG content were measured using 150 μL free glycerol reagent (Sigma, F6428) by mixing

supernatant with 15 μL. For glycogen measurement, 30 μL of supernatant was mixed with 1 μL of amyloglucosidase (Sigma, 10115) at 50 ℃ for 1 hour. Afterward, 15 μL of this solution was mixed with 150 μL of glucose reagent (Sigma, G3293) for 37 ℃ for 30 min and the 340 nm absorbance was measured (Moraru et al., 2018).

Measurement of trehalose in *Drosophila*

8 female flies were homogenized in 0.5 mL of 70% ethanol. The lysates were centrifuged at 14,000 rpm for 10 min. Then, the lysates were vacuum-centrifuged for 1 hour until the samples were dried. The pellets were resuspended in 200 μL of 2 % NaOH and boiled at 100 ℃ for 10 min. 40 μL of these samples were mixed with 1 mL of 0.2% Anthrone reagent in 72% sulfuric acid and the mix solutions were incubated at 90 ℃ for 20 min. The trehalose contents were determined by measuring 620 nm absorbance of the cooled-down solutions (Moraru et al., 2018).

RNA preparation and measurement of gene expressions in *Drosophila*

For RNA preparation, 10 female flies were homogenized in 0.5 mL of TRIzol reagent (Invitrogen, 15596018) and centrifuged at 14,000 rpm for 15 min at 4 ℃. 0.4 mL of supernatant was mixed with 0.1 mL of chloroform. After 14,000 rpm centrifugation at 4 ℃, 0.2 mL of the transparent supernatant was mixed with 0.2 mL of isopropanol and the mixture was centrifuged at

14,000 rpm at 4 ℃. After washing with 70% ethanol, the pellet was resuspended in 15 μL of RNase-free water.

For cDNA synthesis, 10 μL of RNA solution was mixed with 1 μL of random primer. The mixture was incubated at 70 ℃ for 10 min. Afterward, 4 μL of dNTP, 4 μL of RT buffer, and 1 μL of RT (Promega, A3802) were mixed into the solution at 37 ℃ for 2 hours. After incubation, the cDNA solution was incubated at 95 ℃ for 10 min.

For measuring gene expressions, CFX96 Optical Reaction Module for Real-Time PCR Systems (Bio-rad, 1845096) was used.

Drosophila food intake assay

For measuring food intake by CAFE assay, two capillaries were filled with 5 μL of 5 % sucrose solution and were provided to 4 flies in a vial. After 24 hours, the decreased volume of the capillaries was measured.

For imaging of stomach containing food, 5 female flies were starved for 1 day in a vial only with a tissue soaked by water. After fasting, the starved flies were fed on the colored food (10 % sucrose + 1 % green dye solution) (Min et al., 2016).

Measurement of pain responses of _Drosophila_

Flies were placed onto the 43 ℃ plate or the petri dish filled with 10 % sulphuric acid. I measured the time when the flies jumped for the first time.

Drosophila leg staining and the quantification of sensory somas

Flies were fixed with 4% paraformaldehyde for 20 min. After fixation, the prothoracic legs of flies were collected and mounted on a slide glass. For quantifying sensory somas, the green signal was measured at the 3, 4, and 5 tarsus segments (Fernius et al., 2017).

Glucose tolerance test and insulin tolerance test of *Drosophila*

For the glucose tolerance test, 3-day-old female flies fasted for 24 hours. After that, the flies were fed on 10 % glucose food for 1 hour. After 1-hour feeding, the flies fasted again and the glycemia was measured every 30 min.

For the insulin tolerance test, I generated *tub-GAL80^{TS}, DILP2>DILP2* flies which can overexpress DILP2 at 30 ℃. These flies were grown at 18 ℃ at all stages. Before heat shock, the flies fasted for 6 hours. After 18 ℃ fasting, the flies were transferred to 30 ℃ incubator for 30 min while keeping fast. After heat shock, the flies were transferred at 18 ℃ while keeping fast again and the glycemia was measured every 15 min.

Drosophila movement tracking and analysis

Three male flies were incubated for 5 min in a petri dish of 5.5 cm radius which is molded with silicon at the bottom to make *Drosophila* not soar. After 5 min-incubation, the flies were recorded by a camera (Logitech HD Pro Webcam C910) for 5 min. The fly videos were converted into mat.

flies using Caltech Multiple Walking Fly Tracker software (Ctrax). The mat. files were analyzed using MATLAB R2020b. Using 'total distances walked' code, the walking distances of the three flies were measured (Branson et al., 2009).

Statistical analysis

A blind manner was used in all experiments and analysis. Image areas were selected randomly during observing samples. For computing *p* values, one-way ANOVA (Dunnett's multiple comparison test and Tukey's multiple comparison test), two-way ANOVA (Sidak's multiple comparison test and Tukey's multiple comparison test), and Student's t tests, log-rank (Mantel-Cox) were used. All the tests were examined via GraphPad Prism v.8 for the statistics.

Results and Discussion

PART 1

Loss of UCHL1 rescues the defects related to Parkinson's disease by suppressing glycolysis

Results

Mitophagic failure is one of the most common reasons for PD pathogenesis, and the PINK1/Parkin pathway plays a compelling role in the mitophagy triggered by mitochondrial impairments. Therefore, I used *Drosophila* models to undertake a small-scale genetic screen to find a novel regulatory mechanism of mitophagy associated with PD.

A genetic screen for identifying a new interactor of PINK1/Parkin pathway, UCHL1

In the first screen, I crossed PINK1 KO flies (*PINK1*^{B9}) expressing *mef2*-GAL4 drivers with upstream activation sequence (UAS)-RNA interference (RNAi) lines for 15 different fly genes orthologous to PD-causative human genes **(Table 1 and Fig. 3)**. Thus, I generated PINK1 mutant flies with knocking down PD genes in the fly muscles. I tried to identify whether the impaired morphology of mitochondria in the PINK1 KO flies was ameliorated by the RNAi lines **(Fig. 4)**. After 1st screening, I also observed the mitochondrial morphology of Parkin KO mutants (*park*^{1}) with the knockdown lines which exhibited positive outcomes at 1st screen. Finally, I found that two knockdown lines rescued the morphology of damaged mitochondria in *PINK1*^{B9} and *park*^{1} **(Fig. 5)**. These two lines were to be the RNAi lines for *Drosophila UCH* (*cg4265*), identical with human UCHL1 gene.

Locus	Human gene name	Fly ortholog	RNAi#1	RNAi#2
PARK1	SNCA	SNCA		
PARK2	Parkin	Parkin	BL31259	BL38333
PARK3	-	-		
PARK4	SNCA	SNCA		
PARK5	UCHL1	UCH	V103614	V26468
PARK6	PINK1	PINK1		
PARK7	DJ-1	DJ-1 alpha	BL31260	BL51177
		DJ-1 beta	BL31261	BL38378
PARK8	LRRK2	LRRK2	BL32457	BL39019
PARK9	ATP13A2	ATP13A2	V105477	V29174
PARK10	-	-		
PARK11	GIGYF2	GIGYF2	BL28896	V18158
PARK12	-	-		
PARK13	HTRA2	HTRA2	BL28544	BL55165
PARK14	PLA2G6	PLA2G6	BL36129	V108294
PARK15	FBOX7	x		
PARK16	-	-		
PARK17	VPS35	VPS35	BL38944	V22180
PARK18	EIF4G1	EIF4G1	BL33049	V17002
	GBA	Gba1a	BL38379	BL39064
		Gba1b	BL38970	BL38977
	BST1	x		
	MAPT(tau)	tau	V101386	V25023
	ATXN2	ATXN2	BL44012	BL36114
	ATXN3	x		

Table 1. List of PD-causative genes and their knockdown fly lines used for the genetic screen.

BL#stock was obtained from Bloomington *Drosophila* Stock Center (BDSC) and V#stock was obtained from Vienna *Drosophila* Stock Center (VDRC).

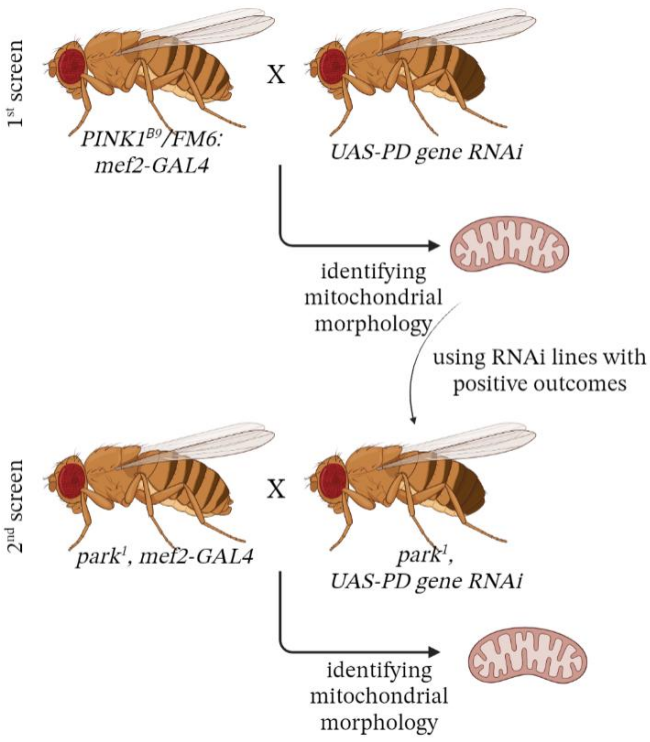

Figure 3. Schemes of the screens for identifying a new interactor of PINK1 and Parkin.

Image was generated from Biorender.

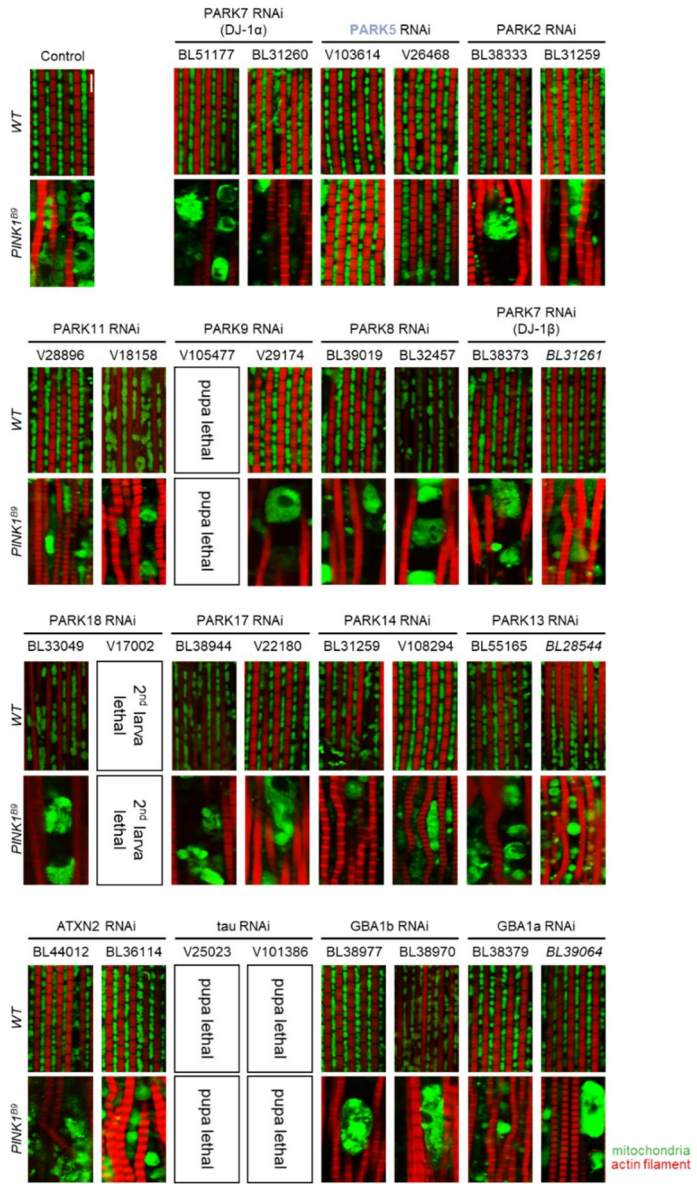

Figure 4. Mitochondrial morphologies of *PINK1^{B9}* with the muscle-specific knockdown of PD genes.

Fluorescence images of the adult muscles with indicated genotypes using confocal microscopy. Green indicates mitochondria and red indicates actin filament. Scale bar, 5 μm.

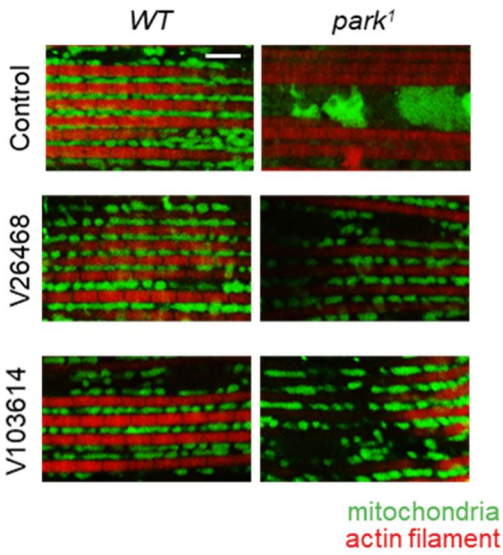

Figure 5. Mitochondrial morphologies of *park[1]* with RNAi lines that showed positive results in Figure 4.

Fluorescence images of the adult muscles with indicated genotypes using confocal microscopy. Green indicates mitochondria and red indicates actin filament. Scale bar, 5 μm.

Loss of UCHL1 rescued PD-related phenotypes in *Drosophila*

To repeat these knockdown results more precisely, I used CRISPR/Cas9 system and generated UCH deletion mutant flies by introducing an early-stop frame shift mutation **(Fig. 6)**. None of the PD-related phenotypes were shown in UCH^{KO} flies **(Fig. 7, 8, 9, 10, and 11)**. However, I observed that PD-related phenotypes, including crushed thoraces **(Fig. 7A and 7A')** and abnormal wing postures **(Fig. 7B and 7B')**, induced by PINK1 or Parkin KO were completely rescued by UCH deletion. In addition, swollen mitochondria **(Fig. 8)**, apoptosis in the indirect flight muscles **(Fig. 9)**, decreased climbing abilities **(Fig. 10)**, and the loss of DA neurons in the protocerebral posterior medial 1/2 (PPM1/2) **(Fig. 11A)** and posterior protocerebrum lateral 1 (PPL1) **(Fig. 11B)** of adult fly brains were mitigated by UCH^{KO}. Therefore, I proposed that PD-like pathologies in $PINK1^{B9}$ or $park^{1}$ mutants were ameliorated by UCH deletion.

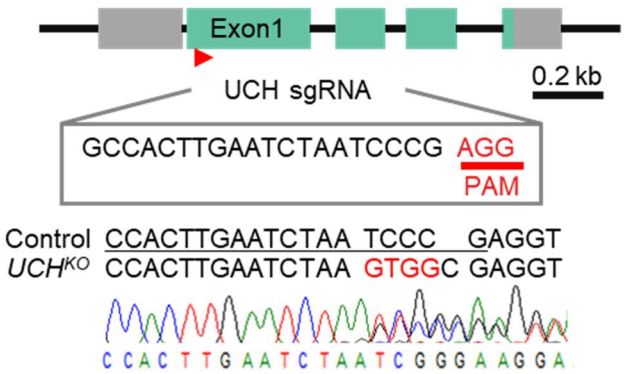

Figure 6. Generation of *UCH*^{KO} flies using CRISPR/Cas9 system.

The sgRNA sequence is GCCACTTGAATCTAATCCCG and PAM sequence is AGG. TCCC in WT flies is changed into GTGGC in *UCH*^{KO}.

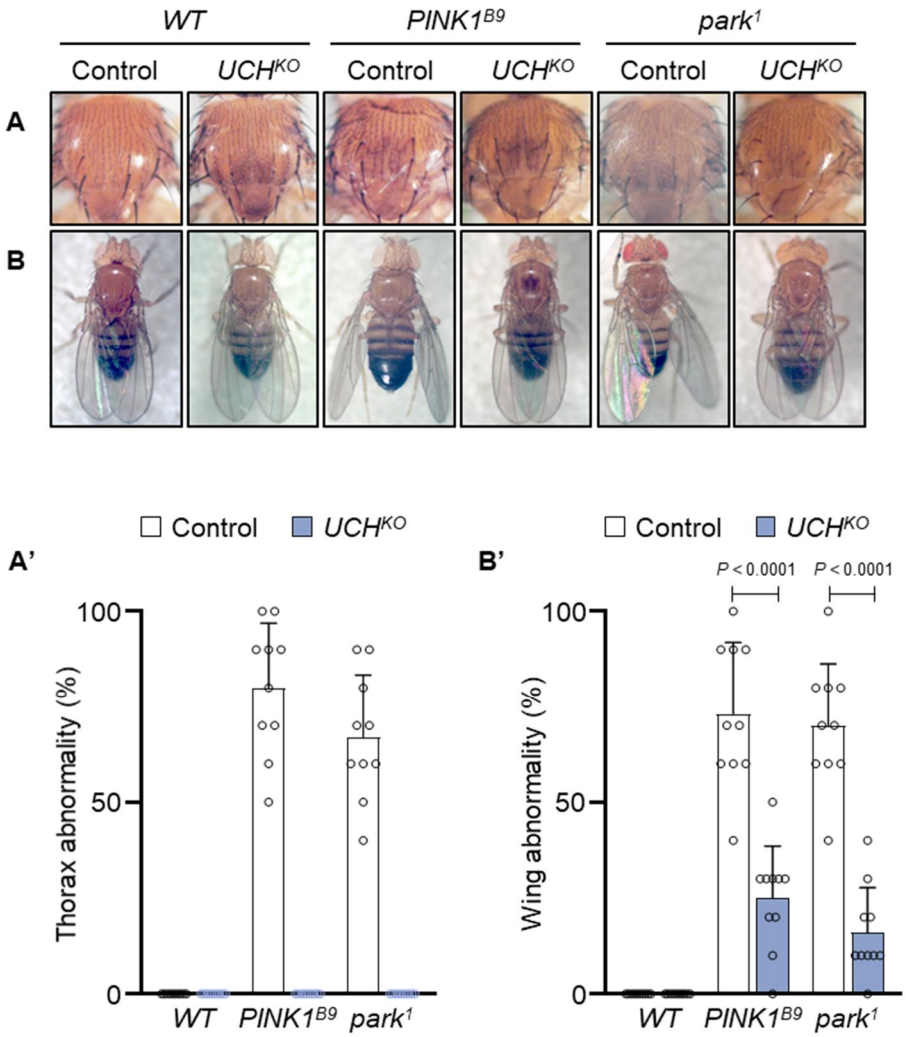

Figure 7. Loss of UCH rescued the crushed thoraces and abnormal wing postures induced by PINK1 or Parkin KO.

(A and A') Images of the fly thoraces **(A)** and percentages of the flies having crushed thoraces **(A')** of indicated genotypes. *n* = 10. **(B and B')** Images of the fly wings **(B)** and percentages of the flies having abnormal wing postures **(B')** of indicated genotypes. *n* = 10. Two-way analysis of variance (ANOVA) with Sidak's multiple comparison test was used **(B')**. All data were presented as mean + SD.

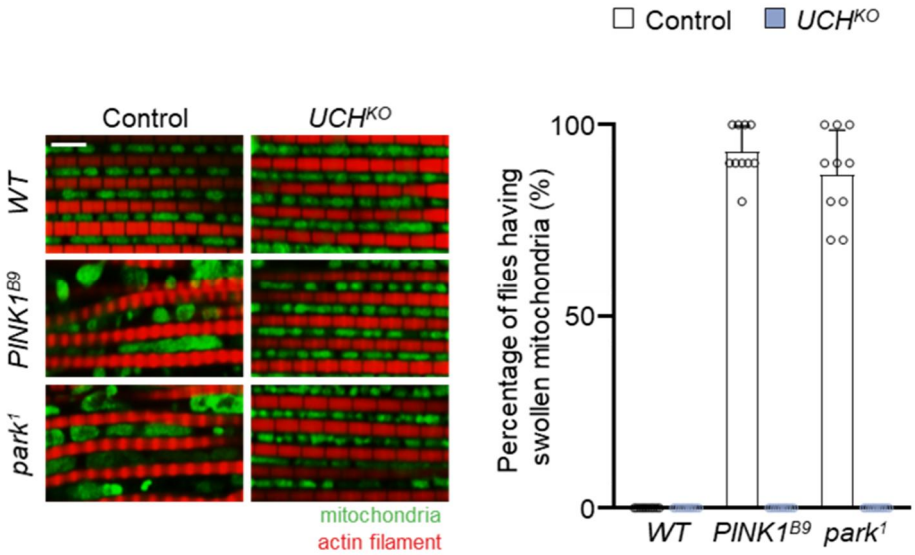

Figure 8. Loss of UCH rescued swollen mitochondria developed by PINK1 or Parkin deficiency.

Left, confocal fluorescence images of adult flight muscles in *Drosophila*. Green indicates mitochondria, and red indicates actin filament. Scale bar, 5 μm. Right, percentages of the flies having swollen mitochondria. $n = 10$. Data were presented as mean + SD.

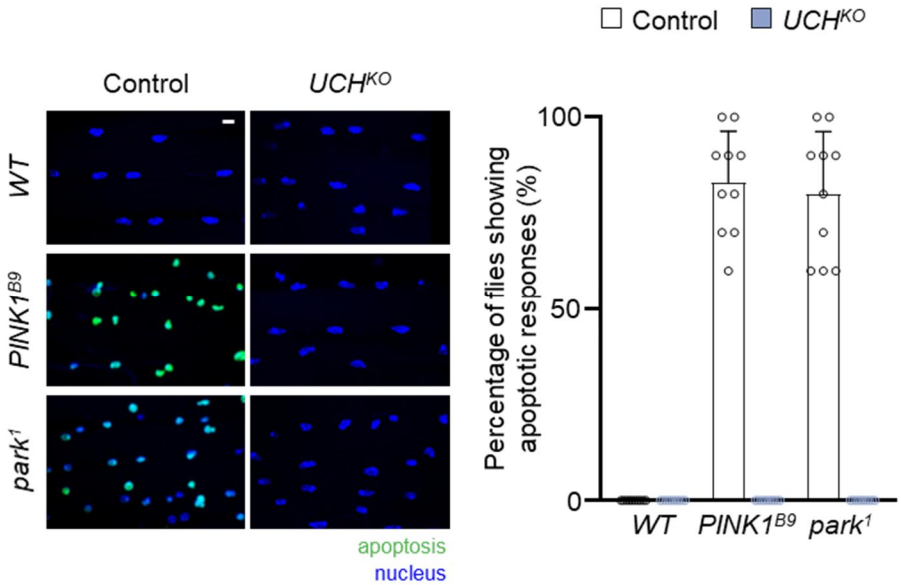

Figure 9. Increased apoptotic signals in *PINK1*^{B9} and *park*^{1} were decreased by UCH KO.

Left, confocal fluorescence images for terminal deoxynucleotidyl transferase-mediated deoxyuridine triphosphate nick end labelling (TUNEL) assays of the adult flight muscles in *Drosophila*. Green indicates apoptosis, and blue indicates nucleus. Scale bar, 20 μm. Right, percentages of the flies showing apoptotic responses. n = 10. Data were presented as mean + SD.

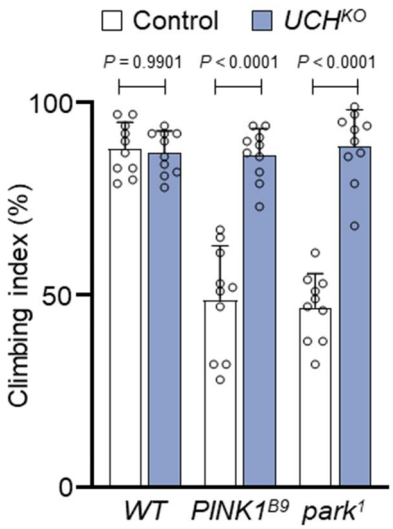

Figure 10. UCH KO rescued the impaired climbing abilities developed by PINK1 or Parkin deletion.

Climbing abilities in the adult flies of indicated genotypes. n = 10. Two-way ANOVA with Sidak's multiple comparison test was used. Data were presented as mean + SD.

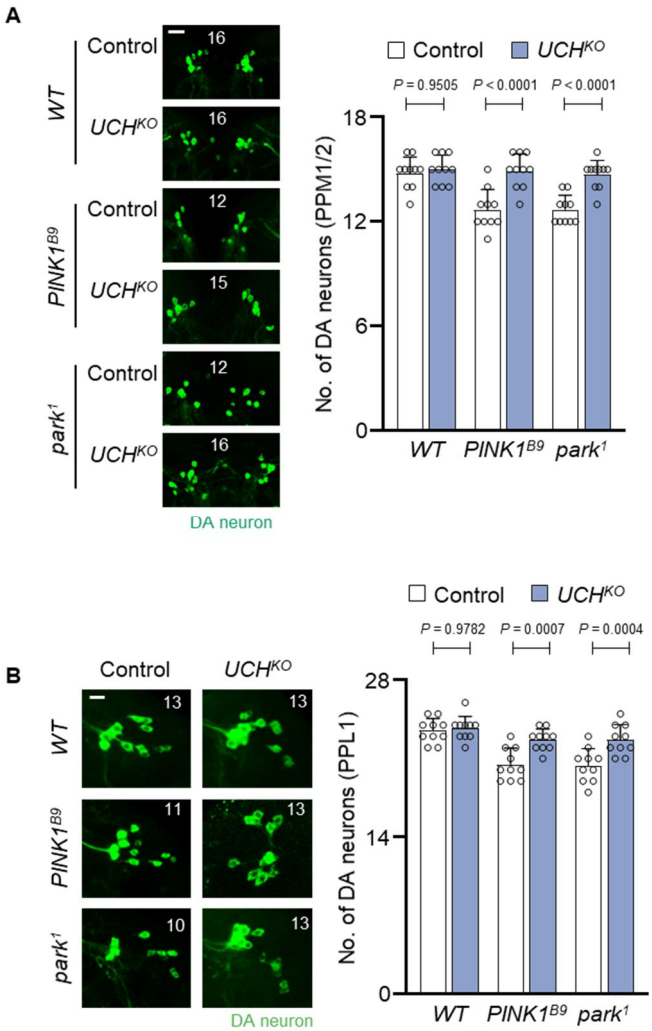

Figure 11. Loss of DA neurons in PPM1/2 and PPL1 regions of fly brains in PINK1 or Parkin mutants was rescued by *UCH^{KO}*.

(A) Confocal immunofluorescence images and numbers of DA neurons in PPM1/2 regions of adult fly brains. N = 10. Green indicates DA neuron. Scale bar, 20 μm. **(B)** Confocal immunofluorescence images and numbers of DA neurons in PPL1 regions of adult fly brains. The images were obtained from one of the left or right side of PPL1 regions. Numbers of the DA neurons in the PPL1 regions were counted from both hemispheres. Scale bar, 20 μm. The

number in panels indicates the number of DA neurons in each image. Two-way ANOVA with Sidak's multiple comparison test was used **(A and B)**. All data were presented as mean + SD.

Deubiquitinase (DUB) activity of UCHL1 was found to be negatively associated with the suppression of PD phenotypes

The three of point mutations, E7A, S18Y, and I93M, in UCHL1 have been known to be associated with neurodegeneration, especially PD. It has been reported that one German family was suffered from familial PD induced by I93M mutation of UCHL1 (Leroy et al., 1998). Also, motor neuron dysfunctions similar to PD were induced by UCHL1 E7A substitution (Bilguvar et al., 2013). On the contrary, S18Y polymorphism is known to reduce incidence of PD by several statistical studies (Carmine Belin et al., 2007; Lincoln et al., 1999; Maraganore et al., 2004a). Despite these findings, whether UCHL1 is directly related to PD pathogenesis is still controversial (Healy et al., 2006). Therefore, I tried to identify the correlations between UCHL1 mutations and PD.

Firstly, as UCHL1 serves as a DUB, I aligned the protein sequences of human UCHL1 and *Drosophila* UCH **(Fig. 12)** and examined the DUB activities of each protein. I measured the *in vitro* DUB activities of recombinant UCH proteins carrying E8A, H19Y, V96M, and C93S (a DUB dead form) mutations identical to human E7A, S18Y, I93M, and C90S, respectively **(Fig. 12)**. The DUB activities of UCH proteins bearing H19Y, V96M, E8A, and C93S were shown to be about 100, 50, 25, and 10 percent, each, compared to that of wild type (WT) UCH **(Fig. 13A)**. Similarly, the results from DUB activities of human UCHL1 proteins matched those of fly UCH proteins **(Fig. 13B)**.

For further investigation, I generated UCH KI flies having E8A, H19Y, V96M, and C93S mutations employing CRIPSR/Cas9 system **(Fig. 14)** and examined PD-like symptoms. However, there were no dramatic defects, including swollen mitochondria **(Fig. 15A)**, elevated apoptosis **(Fig. 15B)**, decreased climbing abilities **(Fig. 15C)**, and DA neuronal death **(Fig. 16)** among the KI flies.

To investigate the correlation of DUB activity of UCH and the PD pathogenesis developed by PINK1 or Parkin deficiency, I generated the flies having each KI alleles in PINK1 or Parkin KO backgrounds. Intriguingly, UCH^{E8A} and UCH^{C93S}, which have decreased DUB activities completely ameliorated the defects, abnormal mitochondria **(Fig. 17A, 17A', 18A, and 18A')**, increased apoptosis **(Fig. 17B, 17B', 18B, and 18B')**, impaired climbing abilities **(Fig. 17C and 18C)**, and DA neuronal death **(Fig. 19 and 20)**, related to PD developed in $PINK1^{B9}$ or $park^{1}$. UCH^{V96M} KI mutations partially rescued the phenotypes of PINK1 or Parkin null flies **(Fig. 17, 18, 19, and 20)**. However, flies expressing H19Y form of UCH proteins, which has similar DUB activity compared to UCH WT, did not mitigate PD-like symptoms of PINK1 or Parkin mutants **(Fig. 17, 18, 19, and 20)**. In conclusion, I found that the loss of UCH DUB activity protects the PD-like defects induced by PINK1 or Parkin deficiency.

Figure 12. Alignment of the protein sequences for UCHL1 from human, mouse, rat, and *Drosophila*.

Red arrows indicate E7, S18, C90S, and I93 residues, respectively.

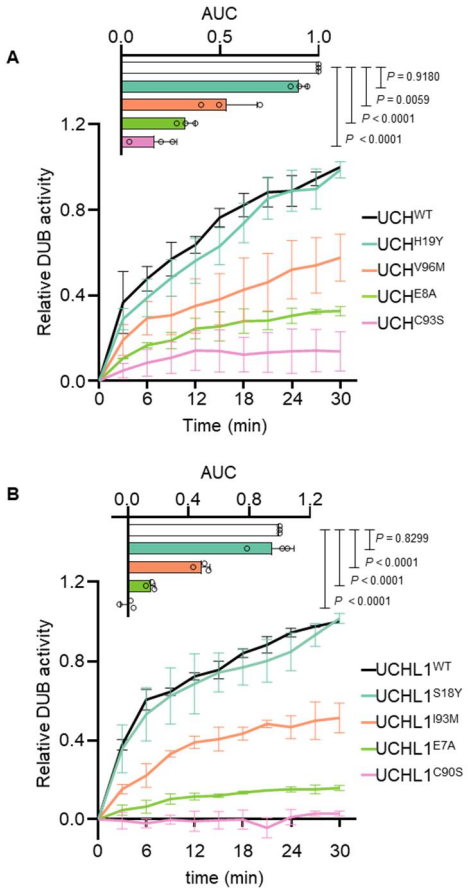

Figure 13. DUB activity of recombinant UCH and UCHL1 proteins carrying point mutations.

(A) Evaluation of the fly UCH DUB activities bearing H19Y, V96M, E8A, and C93S. Area under the curve (AUC) of each graph are quantified in the bar graphs normalized by the activity of UCH WT at 30 min. n = 3. **(B)** Evaluation of the human UCHL1 DUB activities bearing S18Y, I93M, E7A, and C90S. Area under the curve (AUC) of each graph are quantified in the bar graphs normalized by the activity of UCHL1 WT at 30 min. n = 3. One-way ANOVA with Dunnett's multiple comparison test was used **(A and B)**. Data were presented as mean + SD.

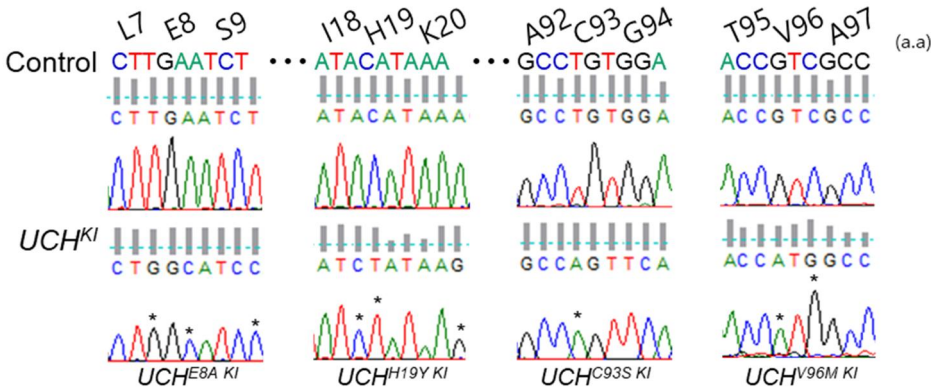

Figure 14. Generation of UCH knockin mutants using CRISPR/Cas9 system.

DNA sequence of UCH E8A, H19Y, C93S, and V96M from left to right. Asterisks indicate the knockin sequences compared to WT sequences.

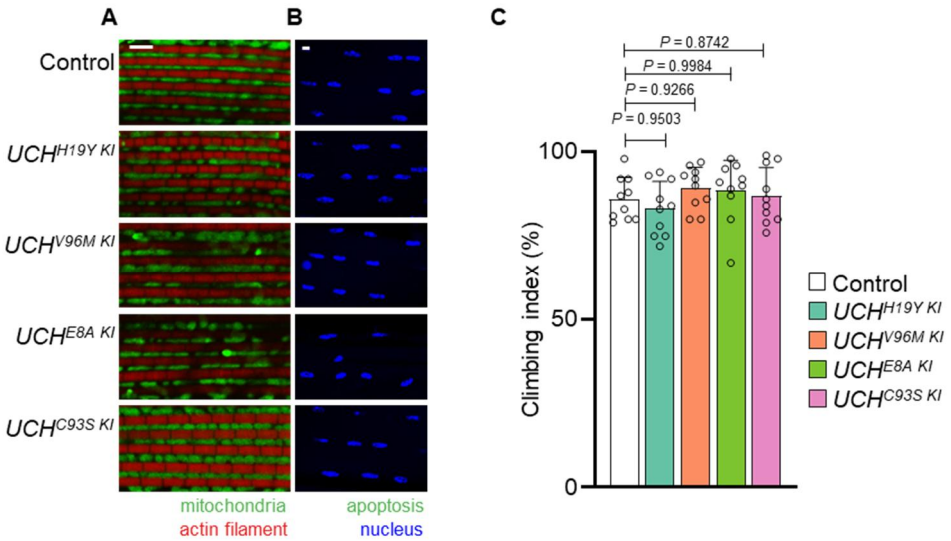

Figure 15. *UCH*^{KI} flies did not exhibit the defects related to PD.

(A) Confocal fluorescence images of the adult flight muscles of indicated genotypes. Green indicates mitochondria, and red indicates actin filament. Scale bar, 5 μm. **(B)** Confocal fluorescence images for TUNEL assays of the adult flight muscles in *Drosophila*. Green indicates apoptosis, and blue indicates nucleus. Scale bar, 20 μm. **(C)** Climbing abilities of the flies of indicated genotypes. One-way ANOVA with Dunnett's multiple comparison test was used **(C)**. Data were presented as mean + SD.

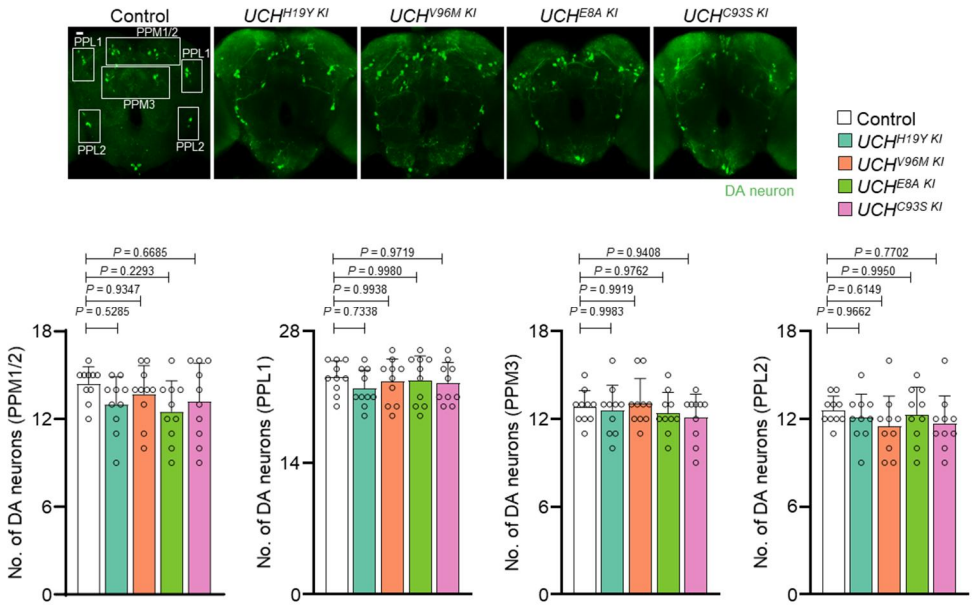

Figure 16. Knockin mutations of UCH did not provoke DA neuronal loss in fruit flies.

Confocal immunofluorescence images and the numbers of DA neurons in PPM1/2, PPL1, PPM3, and PPL2 regions of adult fly brains. n = 10. Green indicates DA neuron. Scale bar, 20 μm. One-way ANOVA with Dunnett's multiple comparison test was used. All data were presented as mean + SD.

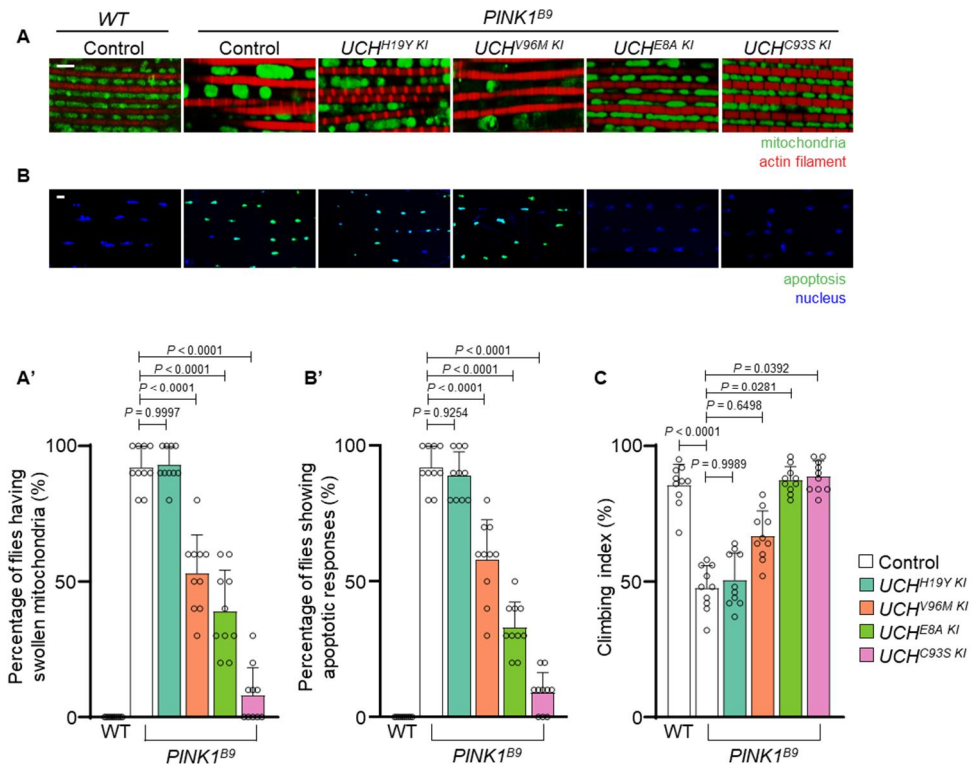

Figure 17. Loss of DUB activity of UCH alleviated the defects induced by PINK1 deficiency.

(A and A') Confocal fluorescence images of adult flight muscles in *Drosophila* **(A)**. Green indicates mitochondria, and red indicates actin filament. Scale bar, 5 μm. Percentages of the flies having swollen mitochondria **(A')**. n = 10. **(B and B')** Confocal fluorescence images for TUNEL assays of the adult flight muscles in *Drosophila* **(B)**. Green indicates apoptosis, and blue indicates nucleus. Scale bar, 20 μm. Percentages of the flies showing apoptotic responses **(B')**. n = 10. **(C)** Climbing abilities in the adult flies of indicated genotypes. n = 10. One-way ANOVA with Dunnett's multiple comparison test was used **(A', B', and C)**. Data were presented as mean + SD.

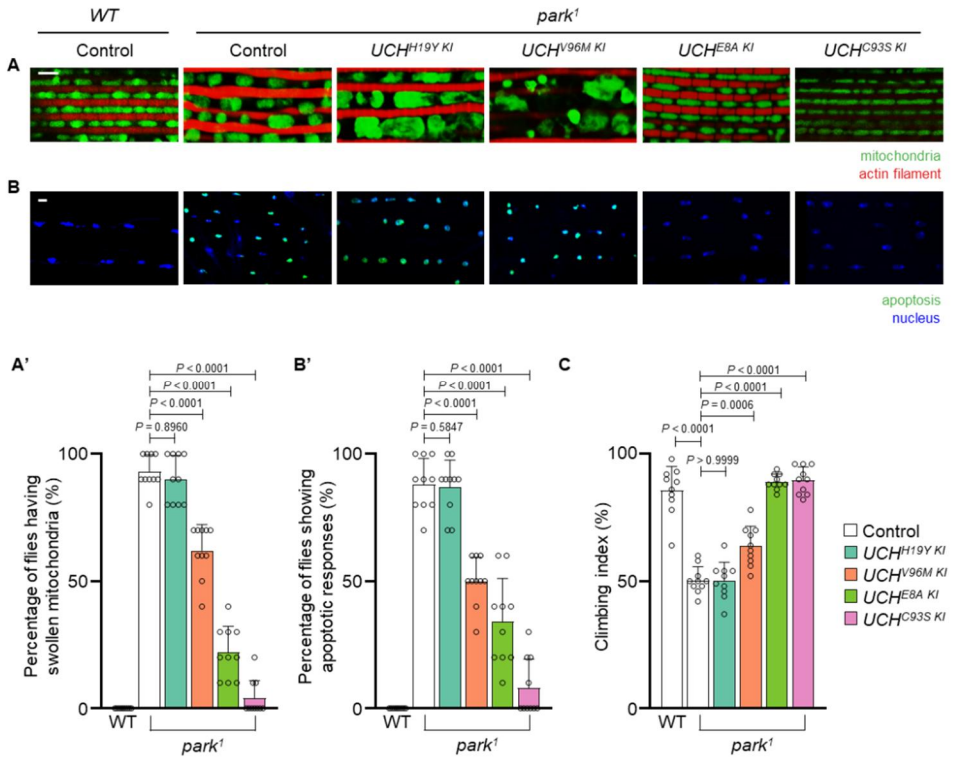

Figure 18. Loss of DUB activity of UCH alleviated the defects induced by Parkin deficiency.

(A and A') Confocal fluorescence images of adult flight muscles in *Drosophila* **(A)**. Green indicates mitochondria, and red indicates actin filament. Scale bar, 5 μm. Percentages of the flies having swollen mitochondria **(A')**. n = 10. **(B and B')** Confocal fluorescence images for TUNEL assays of the adult flight muscles in *Drosophila* **(B)**. Green indicates apoptosis, and blue indicates nucleus. Scale bar, 20 μm. Percentages of the flies showing apoptotic responses **(B')**. n = 10. **(C)** Climbing abilities in the adult flies of indicated genotypes. n = 10. One-way ANOVA with Dunnett's multiple comparison test was used **(A', B', and C)**. Data were presented as mean + SD.

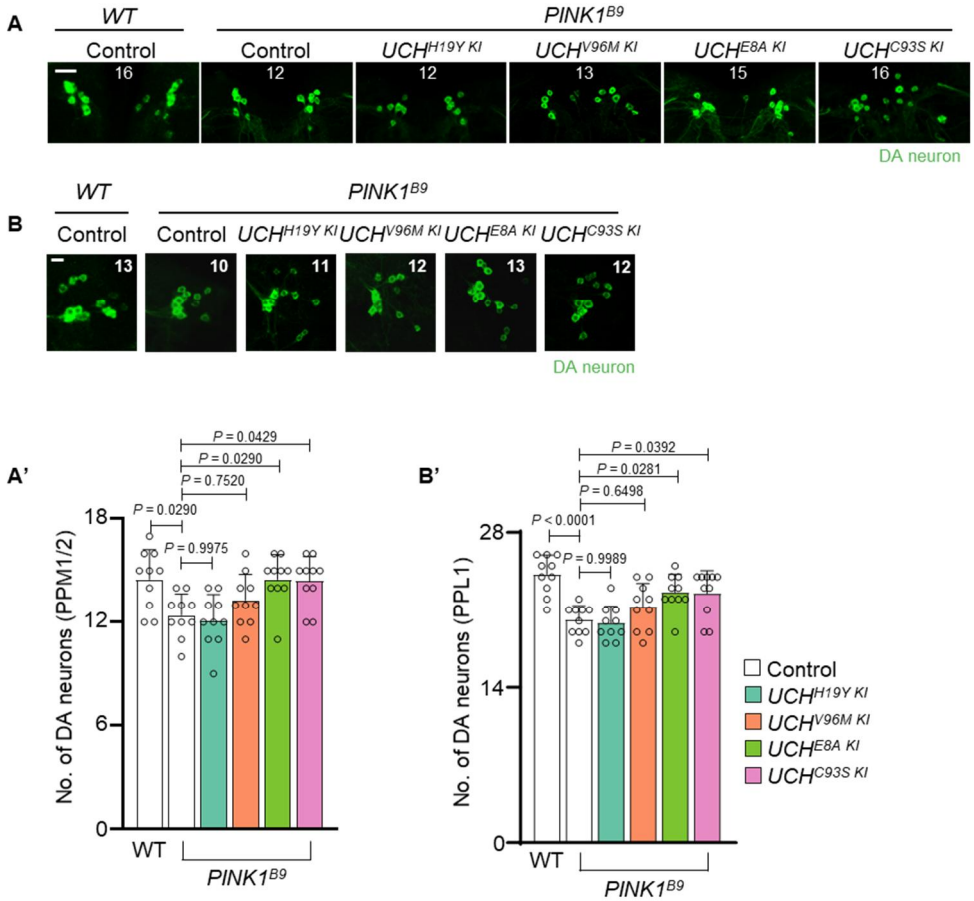

Figure 19. Loss of DUB activity of UCH rescued the death of DA neurons in PINK1 mutants.

(A and A') Confocal immunofluorescence images **(A)** and numbers **(A')** of DA neurons in PPM1/2 regions of adult fly brains. N = 10. Green indicates DA neuron. Scale bar, 20 μm. **(B and B')** Confocal immunofluorescence images **(B)** and numbers **(B')** of DA neurons in PPL1 regions of adult fly brains. The images were obtained from one of the left or right side of PPL1 regions. Numbers of the DA neurons in the PPL1 regions were counted from both hemispheres. Scale bar, 20 μm. The number in panels indicates the number of DA neurons in each image. Two-way ANOVA with Sidak's

multiple comparison test was used **(A' and B')**. All data were presented as mean + SD.

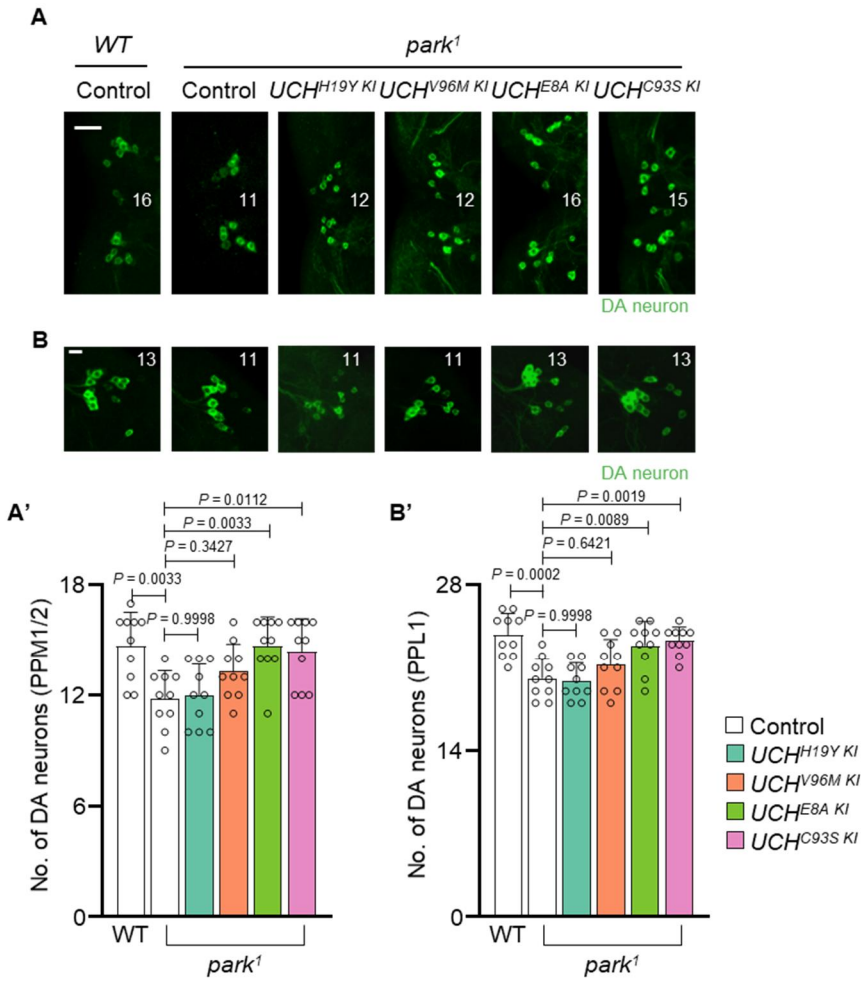

Figure 20. Loss of DUB activity of UCH rescued the death of DA neurons in Parkin mutants.

(A and A') Confocal immunofluorescence images **(A)** and numbers **(A')** of DA neurons in PPM1/2 regions of adult fly brains. N = 10. Green indicates DA neuron. Scale bar, 20 μm. **(B and B')** Confocal immunofluorescence images **(B)** and numbers **(B')** of DA neurons in PPL1 regions of adult fly brains. The images were obtained from one of the left or right side of PPL1 regions. Numbers of the DA neurons in the PPL1 regions were counted from both hemispheres. Scale bar, 20 μm. The number in panels indicates the

number of DA neurons in each image. Two-way ANOVA with Sidak's multiple comparison test was used **(A' and B')**. All data were presented as mean + SD.

Loss of UCHL1 elevated mitophagy

Since I have identified that the loss of UCH rescued the PD phenotypes in PINK1 or Parkin mutants, I employed mammalian cell lines to find the mechanism of this result. Therefore, I generated UCHL1 KO human embryonic kidney (HEK) 293 cell lines using CRISPR/Cas9 system **(Fig. 21)**. As PINK1 and Parkin is closely linked with mitophagy, I observed mitophagy by measuring the amounts of mitochondrial outer membrane (OM) proteins, mitofusin-1 (MFN1) and translocase of outer mitochondrial membrane 20 (TOM20), and mitochondrial inner membrane (IM) proteins, translocase of inner mitochondrial membrane 23 (TIM23) and cytochrome C oxidase subunit IV (COXIV) using UCHL1 KO HEK293 cell line. Under carbonyl cyanide *m*-chlorophenylhydrazone (CCCP) treatment, the amounts of both OM and IM proteins decreased more quickly and dramatically in UCHL1 KO cells compared to UCHL1 WT cells **(Fig. 22)**. Also, I used a dye for mitophagy (Mtphagy dye) for the visualization of mitophagy. Mtphagy dye stains mitochondria and produces red fluorescence under low mitochondrial pH by the translocation of lysosomes onto the mitochondria. The red fluorescence dots per cell in UCHL1 KO were similar to those in UCHL1 WT. However, when inducing mitophagy via CCCP treatment, the signals of red dots per cell were doubled in UCHL1 KO cells compared to UCHL1 WT cells **(Fig. 23)**.

Then, I determined to observe the relations between the DUB activity of UCHL1 and mitophagy. UCHL1 WT, E7A, S18Y, C90S, and I93M were

expressed in UCHL1 KO cells and mitophagy was measured by immunoblot analyses. Under CCCP stimulation, the amounts of mitochondrial proteins in UCHL1 KO cells expressing E7A and C90S were similar to those of UCHL1 KO cells. However, the mitophagy of UCHL1 KO cells with WT, S18Y, or I93M expression was not significantly decreased compared to that with E7A or C90S expression upon CCCP treatment **(Fig 24)**. In conclusion, reduced DUB activity of UCHL1 enhances mitophagy.

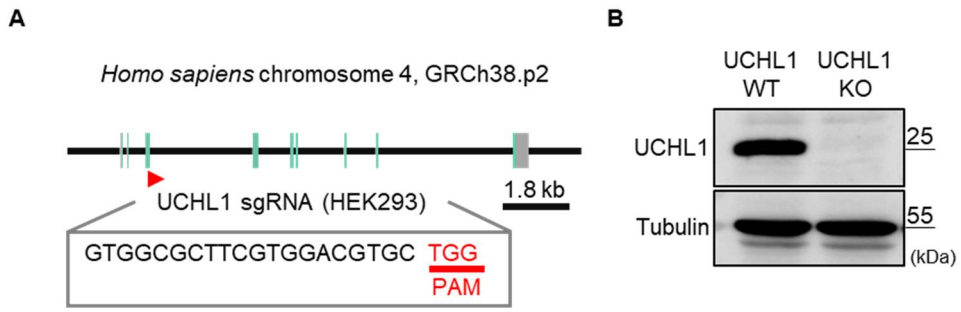

Figure 21. Generation of UCHL1 KO HEK293 cell lines using CRISPR/Cas9 system.

(A) A scheme for the generation of UCHL1 KO HEK293 cells. The sgRNA sequence to generate UCHL1 KO HEK293 cell lines is GTGGCGCTTCGTGGACGTGC and the PAM sequence is TGG. **(B)** Immunoblot analysis of UCHL1 in UCHL1 WT and UCHL1 KO HEK293 cells.

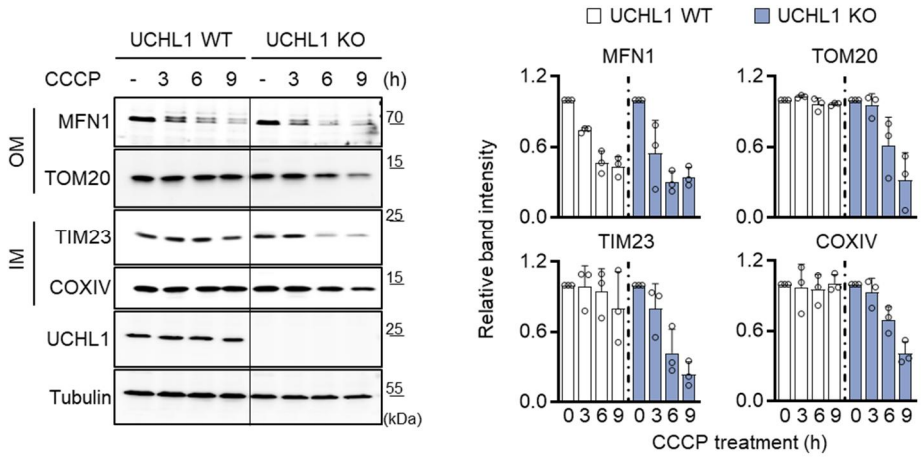

Figure 22. Elevated mitophagy was shown in UCHL1 KO cells.

Left, immunoblot analysis of OM (MFN1 and TOM20) and IM (TIM23 and COXIV) proteins upon 20 μM CCCP treatment. Right, quantification of immunoblot band intensity of indicated proteins normalized by first lane. *n* = 3. Data were presented as mean + SD.

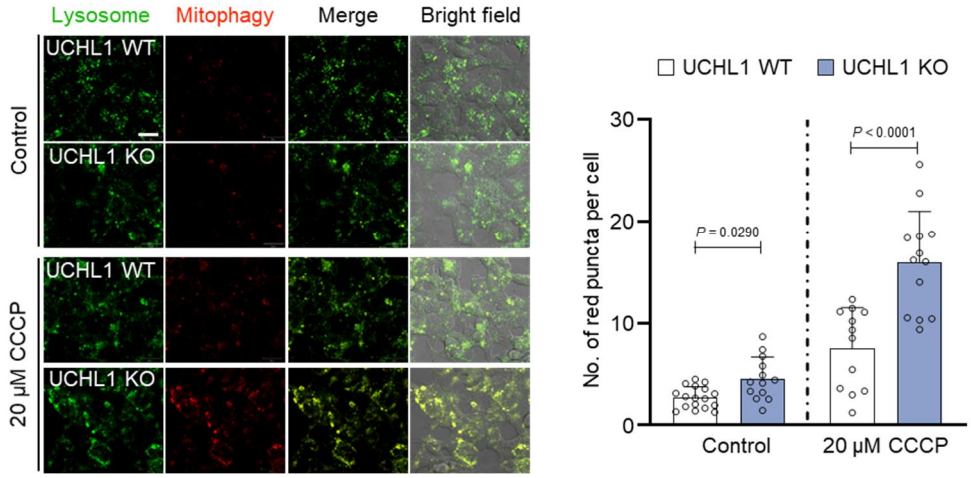

Figure 23. Increased mitophagic signals were exhibited in UCHL1 KO cells.

Left, confocal fluorescence images stained with Mtphagy dye in UCHL1 WT and KO HEK293 cells upon 20 μM CCCP treatment. Right, number of red dots per cell. n = 17, 13, 12, and 13 (UCHL1 WT without CCCP, UCHL1 KO without CCCP, UCHL1 WT with CCCP, and UCHL1 KO with CCCP, respectively). Two-way ANOVA with Sidak's multiple comparison test was used. Data were presented as mean + SD.

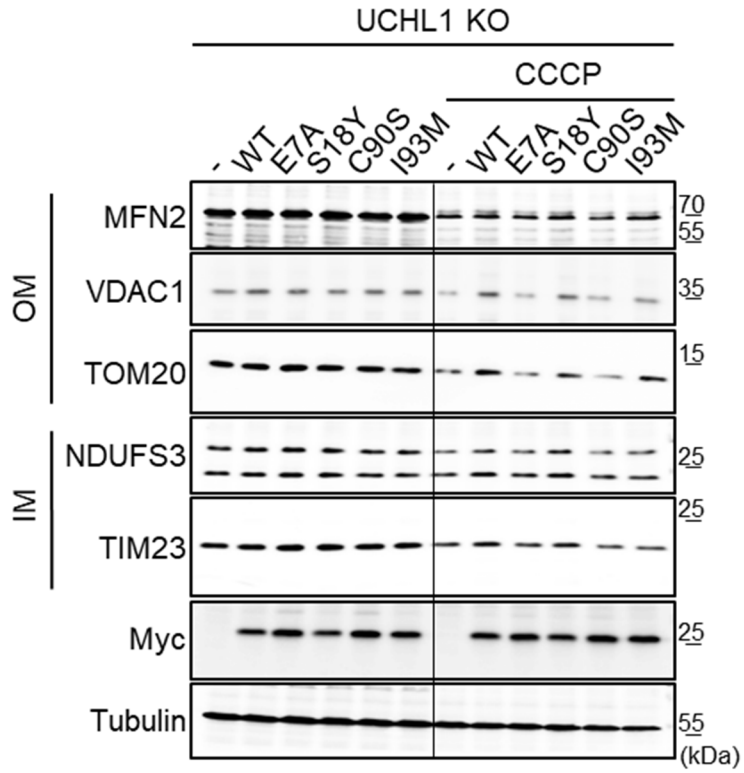

Figure 24. Loss of DUB activity of UCHL1 increased mitophagy.

Immunoblot analysis of OM (mitofusin-2 (MFN2), voltage dependent anion channel 1 (VDAC1), TOM20) and IM (NADH dehydrogenase [ubiquinone] iron-sulfur protein 3 (NDUFS3), TIM23) upon 20 μM CCCP treatment in UCHL1 KO cells expressing UCHL1 WT or mutants.

A genetic screen to find the mitophagy receptor of UCHL1-mediated mitophagy

After identifying that loss of UCHL1 activated mitophagy, I sought to determine which mitophagy receptor is associated with UCHL1-mediated mitophagy. Therefore, I performed again a small-scale genetic screen using flies among well-known mitophagy receptors, zonda (zda) (Bhujabal et al., 2017; Lim and Lim, 2017), Bcl-2/adenovirus E1B 19-kDa interacting protein 3 (Bnip3) (Hanna et al., 2012), sequestosome 1 (p62) (Pankiv et al., 2007), and FUN14 domain-containing 1 (FUNDC1) (Liu et al., 2012). I expressed RNAi against each of these four genes using *heat-shock* (*hs*)-GAL4 in UCH and PINK1 double knockout (DKO) and observed the morphology of mitochondria in the flight muscles. Knockdown of zda, Bnip3, or p62 did not modify the mitochondrial morphology of PINK1 and UCH DKO flies, but knockdown of FUNDC1 blocked the effects of UCH^{KO} and showed the impaired mitochondria **(Fig. 25)**.

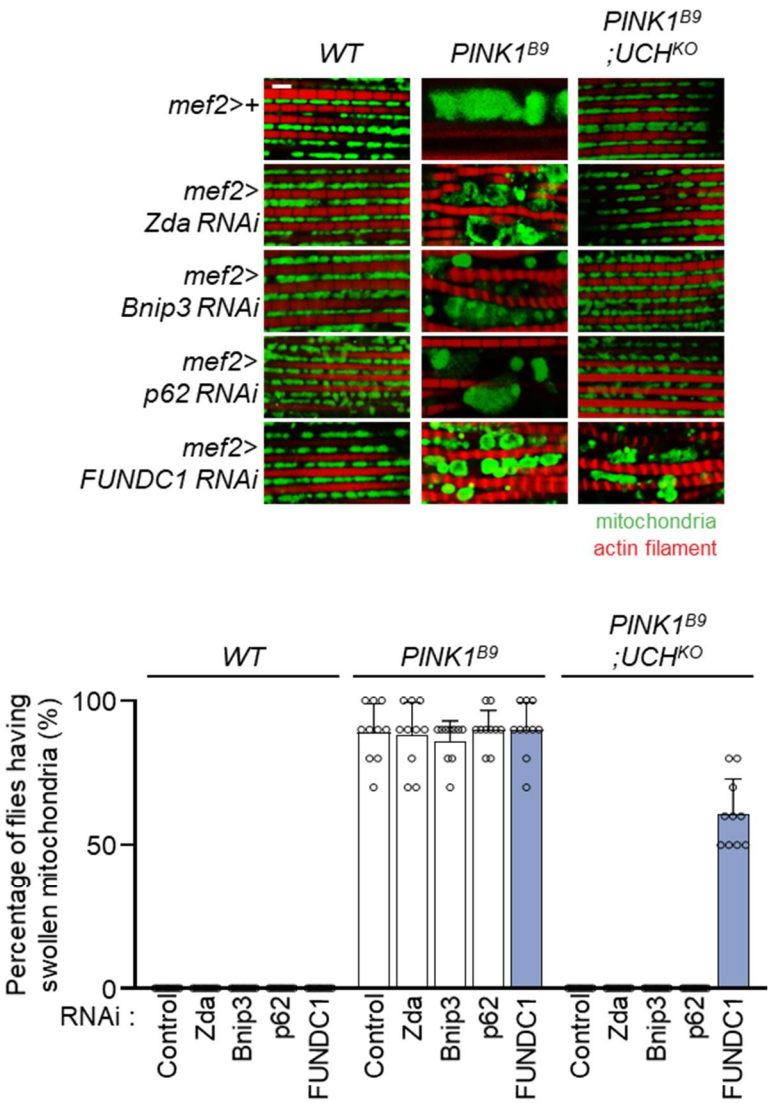

Figure 25. Loss of UCH rescued the impaired mitochondrial morphology of *PINK1^{B9}* through FUNDC1.

Top, confocal fluorescence images of adult flight muscles in *Drosophila*. Green indicates mitochondria, and red indicates actin filament. Scale bar, 5 μm. Bottom, percentages of the flies having swollen mitochondria. n = 10. Data were presented as mean + SD.

PD-rescuing effects of UCHL1 deficiency were blocked by FUNDC1 knockdown

Furthermore, FUNDC1 knockdown blocked the PD-rescuing phenotypes, including decreased climbing abilities **(Fig. 26A)**, increased apoptosis **(Fig. 26B and 26B')**, and DA neuronal degeneration **(Fig. 27)**, of UCH deletion in PINK1 mutant backgrounds. Similarly, in *park*^{1} flies, the effects of UCH deficiency were blocked by FUNDC1 knockdown **(Fig. 26 and 27)**. In mammalian cells, I also measured mitophagy whether UCHL1 interacts with FUNDC1. Like the results from *Drosophila*, the boosted mitophagy under CCCP treatment in UCHL1 KO HEK293 cells was hindered by FUNDC1 knockdown **(Fig. 28)**. Therefore, I ascertained that FUNDC1-mediated mitophagy was induced by the loss of UCHL1.

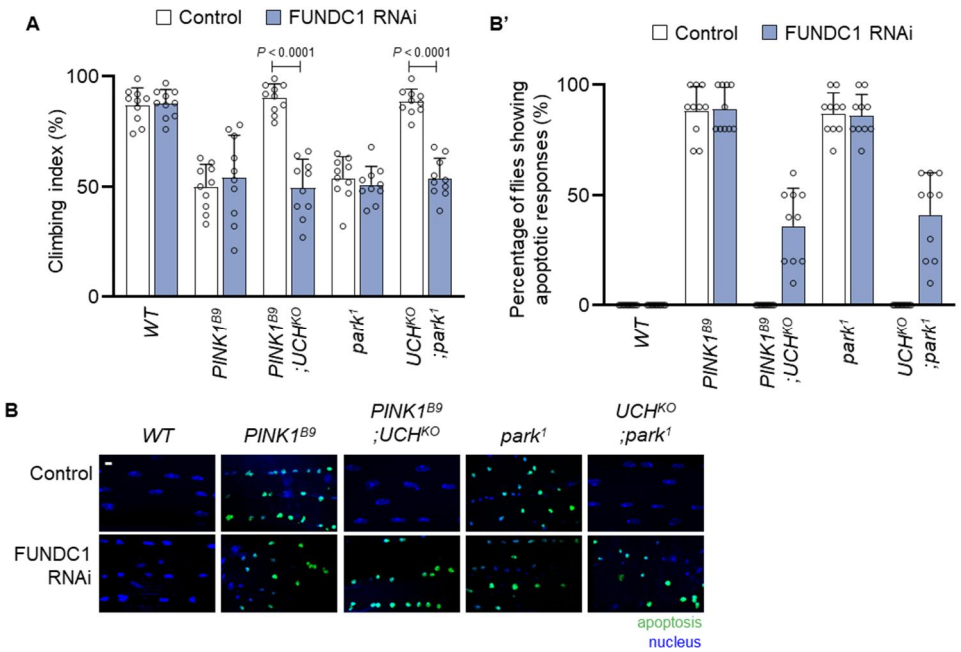

Figure 26. Loss of UCH rescued impaired climbing abilities and increased apoptosis of PINK1 or Parkin mutants via FUNDC1.

(A) Climbing abilities in the adult flies of indicated genotypes. $n = 10$. **(B and B')** Confocal fluorescence images for TUNEL assays of the adult flight muscles in *Drosophila* **(B)**. Green indicates apoptosis, and blue indicates nucleus. Scale bar, 20 μm. Percentages of the flies showing apoptotic responses **(B')**. $n = 10$. Genotype, control (*Hs>+*) and FUNDC1 RNAi (*Hs>FUNDC1 RNAi*). Two-way ANOVA with Sidak's multiple comparison test was used **(A)**. Data were presented as mean + SD.

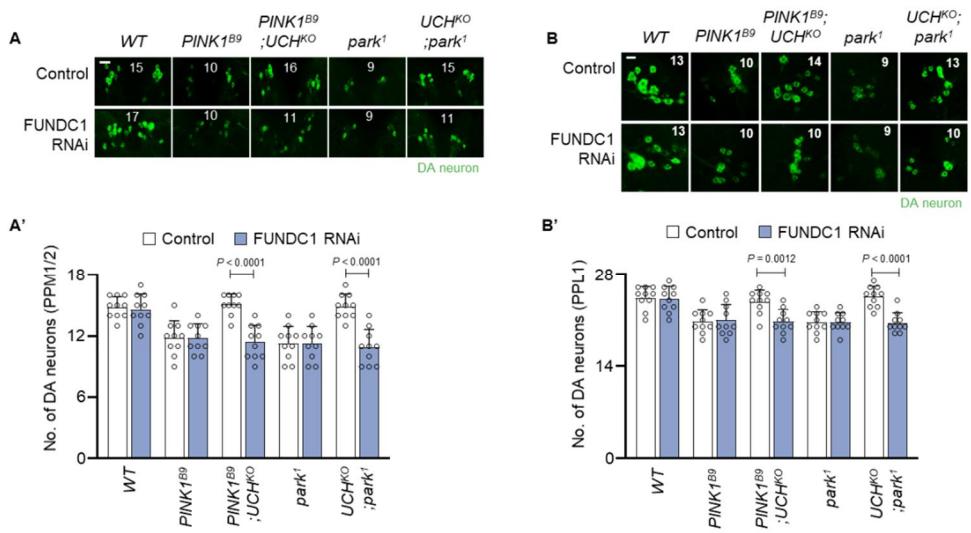

Figure 27. Loss of UCH rescued DA neuronal degeneration of PINK1 or Parkin mutants via FUNDC1.

(A and A') Confocal immunofluorescence images **(A)** and numbers **(A')** of DA neurons in PPM1/2 regions of adult fly brains. *n* = 10. Green indicates DA neuron. Scale bar, 20 μm. **(B and B')** Confocal immunofluorescence images **(B)** and numbers **(B')** of DA neurons in PPL1 regions of adult fly brains. The images were obtained from one of the left or right side of PPL1 regions. Numbers of the DA neurons in the PPL1 regions were counted from both hemispheres. Scale bar, 20 μm. The number in panels indicates the number of DA neurons in each image. Genotype, control (*Hs>+*) and FUNDC1 RNAi (*Hs>FUNDC1 RNAi*). Two-way ANOVA with Sidak's multiple comparison test was used **(A' and B')**. All data were presented as mean + SD.

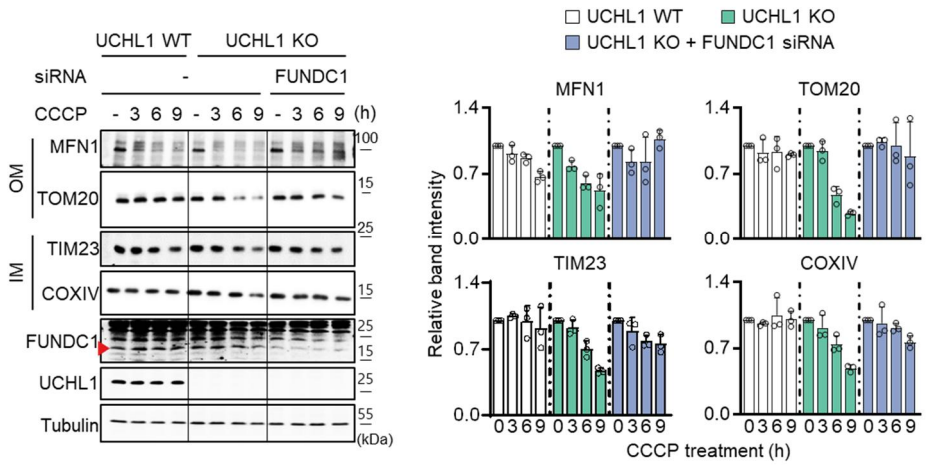

Figure 28. Mitophagy induced by UCHL1 deletion was mediated by FUNDC1.

Left, immunoblot analysis of OM (MFN1 and TOM20) and IM (TIM23 and COXIV) proteins upon 20 μM CCCP and FUNDC1 siRNA treatment. Right, quantification of immunoblot band intensity of indicated proteins normalized by first lane. n = 3. Data were presented as mean + SD.

AMPK and ULK1 were activated by UCHL1 inhibition

In the former studies, it has been reported that AMPK phosphorylates 555th serine residue of ULK1, which phosphorylates FUNDC1 and triggers FUNDC1-mediated mitophagy (Laker et al., 2017; Tian et al., 2015; Wu et al., 2014). To test the relevance of AMPK or ULK1 with UCHL1, I analyzed the phosphorylation of AMPK and ULK1 in UCHL1 KO cells. The phosphorylation at T172 of AMPK and S555 of ULK1 was increased in UCHL1 KO cells compared to UCHL1 WT cells **(Fig. 29)**. Also, as treating compound C, an inhibitor of AMPK, blocked the elevated phosphorylation of AMPK and ULK1 in UCHL1 KO, I identified that the phosphorylation of ULK1 was resulted from AMPK activation **(Fig. 29)**. Then, I investigated whether the mitophagy induced by the loss of UCHL1 is via AMPK and ULK1. Therefore, I transfected small interfering RNA (siRNA) of AMPK and ULK1 in UCHL1 KO cells and measured the amounts of mitochondrial proteins under CCCP treatment. I found that elevated mitophagy in UCHL1 KO cells was decreased by AMPK **(Fig. 30A)** or ULK1 knockdown **(Fig. 30B)**.

To investigate that UCH interacts with AMPK and ULK1 also in fruit flies, I generated flies expressing AMPK and ULK1 RNAi lines in UCH and PINK1 or Parkin double KO backgrounds. As AMPK and ULK1 knockdown in the whole body or muscles caused developmental lethality, I used tyrosine hydrolase (*th*)-GAL4, a DA neuron specific driver, for expressing AMPK or ULK1 RNAi lines and observed the DA neuronal phenotypes. UCH^{KO} still

rescued the loss of DA neurons in PINK1 or Parkin mutants, but the concurrent knockdown of AMPK or ULK1 blocked these effects of UCH deletion **(Fig. 31)**. Therefore, I suggest that AMPK and ULK1 are the downstream of UCHL1 in both human and *Drosophila*.

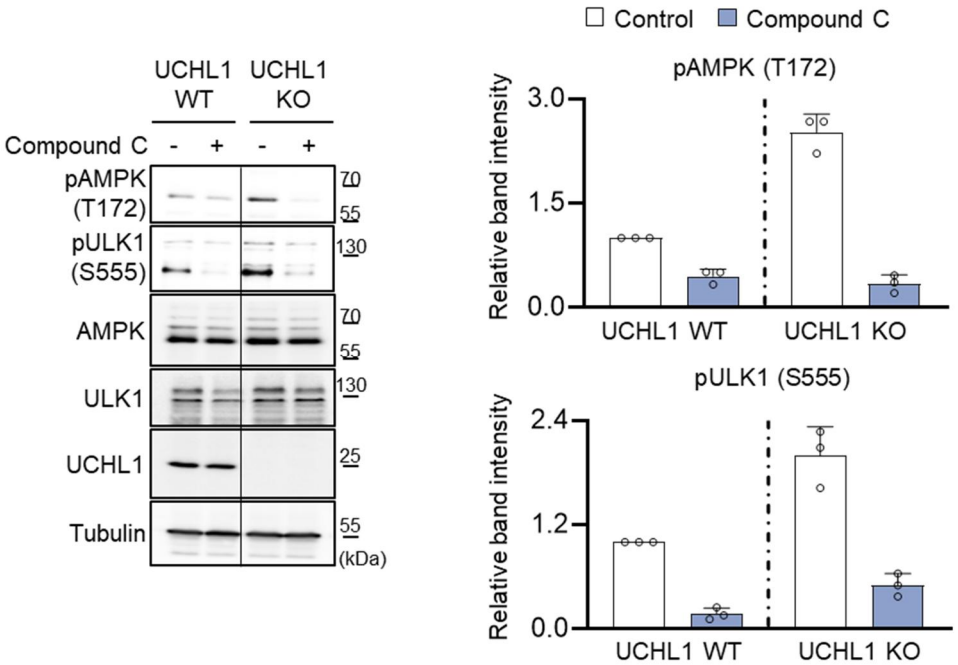

Figure 29. The phosphorylation of AMPK and ULK1 was increased in UCHL1 KO cells.

Left, immunoblot analysis of AMPK and ULK1 phosphorylation in UCHL1 WT and KO HEK293 cell lines upon compound C 10 μM treatment. Right, quantification of immunoblot band intensity of indicated proteins normalized by first lane. n = 3. Data were presented as mean + SD.

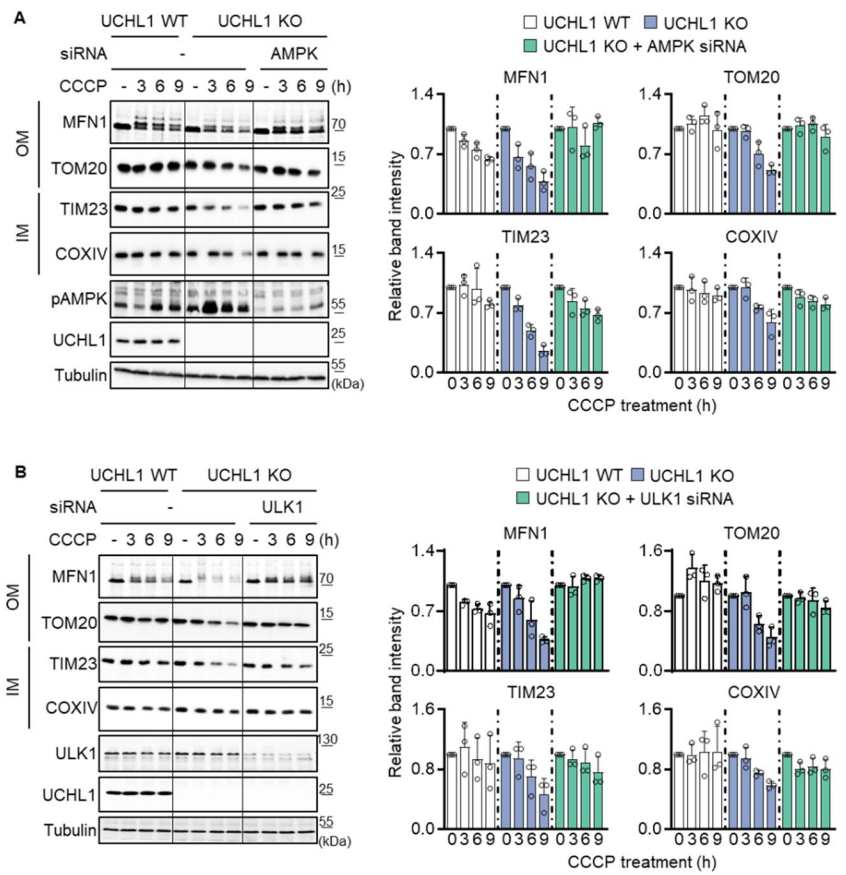

Figure 30. Increased mitophagy in UCHL1 KO cells was reduced by AMPK or ULK1 knockdown.

(A) Left, immunoblot analysis of OM (MFN1 and TOM20) and IM (TIM23 and COXIV) proteins upon 20 μM CCCP and AMPK siRNA treatment. Right, quantification of immunoblot band intensity of indicated proteins normalized by first lane. *n* = 3. **(B)** Left, immunoblot analysis of OM (MFN1 and TOM20) and IM (TIM23 and COXIV) proteins upon 20 μM CCCP and ULK1 siRNA treatment. Right, quantification of immunoblot band intensity of indicated proteins normalized by first lane. *n* = 3. Data were presented as mean + SD.

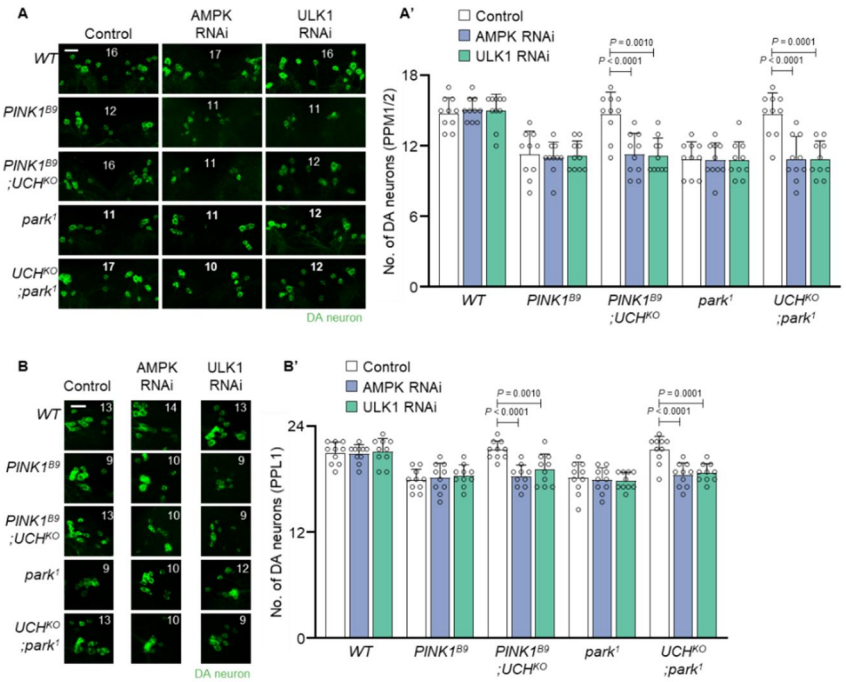

Figure 31. AMPK or ULK1 knockdown blocked the DA neuronal effects of UCH deletion.

(A and A') Confocal immunofluorescence images **(A)** and numbers **(A')** of DA neurons in PPM1/2 regions of adult fly brains. N = 10. Green indicates DA neuron. Scale bar, 20 μm. **(B and B')** Confocal immunofluorescence images **(B)** and numbers **(B')** of DA neurons in PPL1 regions of adult fly brains. The images were obtained from one of the left or right side of PPL1 regions. Numbers of the DA neurons in the PPL1 regions were counted from both hemispheres. Scale bar, 20 μm. The number in panels indicates the number of DA neurons in each image. Genotype, control (*th*>+), AMPK RNAi (*th*>*AMPK RNAi*), and ULK1 RNAi (*th*>*ULK1 RNAi*). Two-way ANOVA with Sidak's multiple comparison test was used **(A' and B')**. All data were presented as mean + SD.

AMPK activation ameliorated PINK1 or Parkin deficiency through FUNDC1

I tested if AMPK and ULK1 also interact with FUNDC1 in *Drosophila*. I found that overexpressing constitutively active form of AMPK ($AMPK^{CA}$) rescued the PD-related defects in $PINK^{B9}$ and $park^{1}$ similar to previous studies (Lee et al., 2007; Ng et al., 2012). Similarly, FUNDC1 overexpression rescued the PD-like pathologies of PINK1 or Parkin mutants, proposing a possibility that AMPK and FUNDC1 might be in the same axis. Then, I generated the flies expressing $AMPK^{CA}$ and FUNDC1 RNAi and observed several phenotypes. Surprisingly, the rescued phenotypes of $AMPK^{CA}$ were blocked by concurrent expression of FUNDC1 RNAi **(Fig. 32, 33, and 34)**. I also would like to examine the interactions between ULK1 and FUNDC1, but overexpressing ULK1 was all lethal.

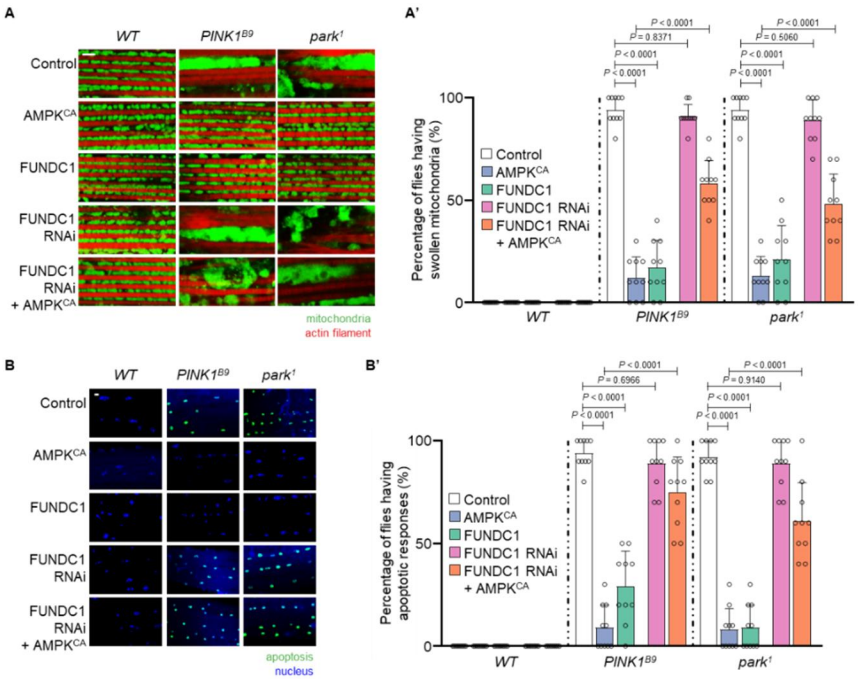

Figure 32. AMPK^{CA} overexpression rescued abnormal mitochondria and elevated apoptosis of PINK1 and Parkin mutants via FUNDC1.

(A and A') Confocal fluorescence images of adult flight muscles in *Drosophila* **(A)**. Green indicates mitochondria, and red indicates actin filament. Scale bar, 5 μm. Percentages of the flies having swollen mitochondria **(A')**. n = 10. **(B and B')** Confocal fluorescence images for TUNEL assays of the adult flight muscles in *Drosophila* **(B)**. Green indicates apoptosis, and blue indicates nucleus. Scale bar, 20 μm. Percentages of the flies showing apoptotic responses **(B')**. n = 10. Genotype, control (*Hs>+*), AMPK^{CA} (*Hs>AMPK^{CA}*), FUNDC1 (*Hs>FUNDC1*), FUNDC1 RNAi (*Hs>FUNDC1 RNAi*), and FUNDC1 RNAi + AMPK^{CA} (*Hs>FUNDC1 RNAi, AMPK^{CA}*). Two-way ANOVA with Sidak's multiple comparison test was used **(A' and B')**. Data were presented as mean + SD.

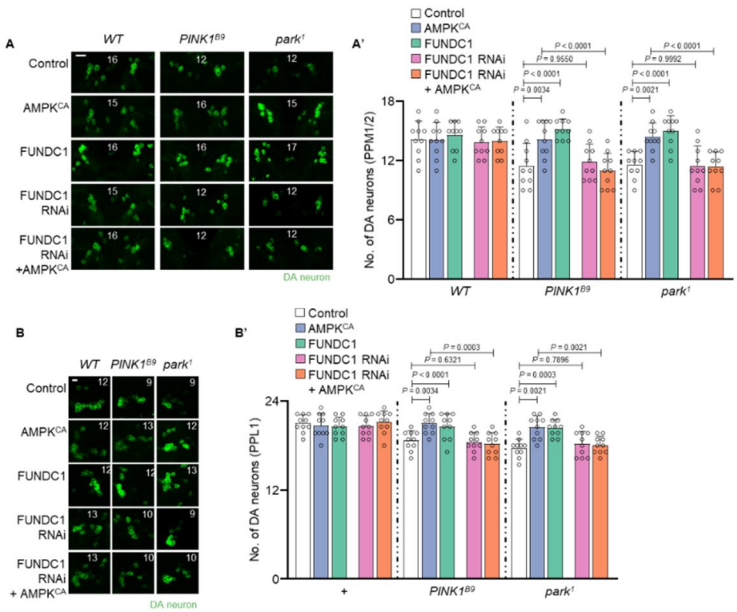

Figure 33. AMPK^{CA} overexpression rescued DA neuronal degeneration of PINK1 and Parkin mutants via FUNDC1.

(A and A') Confocal immunofluorescence images **(A)** and numbers **(A')** of DA neurons in PPM1/2 regions of adult fly brains. N = 10. Green indicates DA neuron. Scale bar, 20 μm. **(B and B')** Confocal immunofluorescence images **(B)** and numbers **(B')** of DA neurons in PPL1 regions of adult fly brains. The images were obtained from one of the left or right side of PPL1 regions. Numbers of the DA neurons in the PPL1 regions were counted from both hemispheres. Scale bar, 20 μm. The number in panels indicates the number of DA neurons in each image. Genotype, control (*Hs>+*), AMPK^{CA} (*Hs>AMPK^{CA}*), FUNDC1 (*Hs>FUNDC1*), FUNDC1 RNAi (*Hs>FUNDC1 RNAi*), and FUNDC1 RNAi + AMPK^{CA} (*Hs>FUNDC1 RNAi, AMPK^{CA}*). Two-way ANOVA with Sidak's multiple comparison test was used **(A' and B')**. All data were presented as mean + SD.

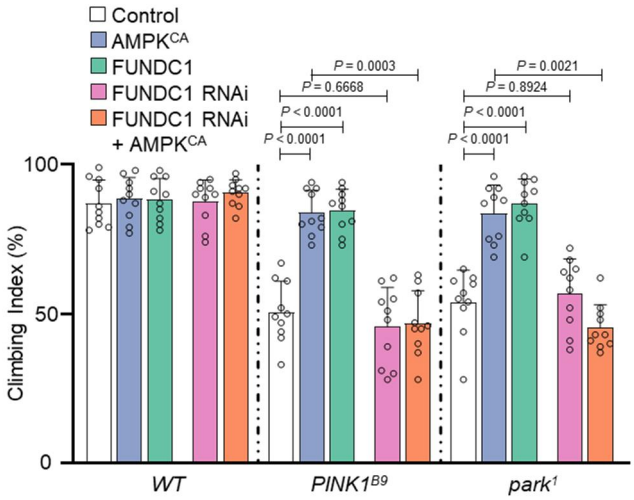

Figure 34. AMPK^{CA} overexpression rescued impaired climbing abilities of PINK1 and Parkin mutants via FUNDC1.

Climbing abilities in the adult flies of indicated genotypes. n = 10. Genotype, control (*Hs>+*), AMPK^{CA} (*Hs>AMPK^{CA}*), FUNDC1 (*Hs>FUNDC1*), FUNDC1 RNAi (*Hs>FUNDC1 RNAi*), and FUNDC1 RNAi + AMPK^{CA} (*Hs>FUNDC1 RNAi, AMPK^{CA}*). Two-way ANOVA with Sidak's multiple comparison test was used. Data were presented as mean + SD.

Loss of UCHL1 exhibited decreased ATP levels resulted from diminished glycolysis

Since AMPK plays a key role for energy sensor by recognizing AMP/adenosine 5'-triphosphate (ATP) levels, I hypothesized that UCHL1 deficiency can affect cellular energy levels. Therefore, I measured the ATP levels in UCHL1 WT and KO cells. UCHL1 KO cells had reduced ATP compared to UCHL1 WT cells **(Fig. 35A)**. For further investigation, I tested if the effect of UCHL1 KO is associated with the main pathways of ATP production, including glycolysis and oxidative phosphorylation (OXPHOS). I treated 2-deoxy-D-glucose (2-DG), rotenone, or oligomycin to UCHL1 WT and KO cells. 2-DG is an inhibitor of glycolysis (Wick et al., 1957), and both rotenone and oligomycin are inhibitors of OXPHOS (Jastroch et al., 2010). Halved ATP levels in UCHL1 KO cells compared to UCHL1 WT cells were proportionally reduced by treating rotenone or oligomycin. However, there were no differences in ATP levels between UCHL1 WT and KO cells upon 2-DG treatment.

I also repeated these experiments in *Drosophila*. UCH^{KO} mutants exhibited decreased ATP levels. However, the differences between WT and UCH^{KO} were blocked by feeding 2-DG, not rotenone or oligomycin. Therefore, I determined that glycolysis decreases by UCHL1 inhibition **(Fig. 35B)**. To identify these results genetically, I expressed RNAi against glucose transporter 1 (GLUT1), NDUFS3, or ATP synthase subunit β (ATPsynβ) in UCH deletion backgrounds. Consistent to the pharmacological data, the ATP

levels of UCH deletion mutants with GLUT1 knockdown were similar to those of WT flies with GLUT1 knockdown. However, NDUFS3 or ATPsynβ did not alter the relative differences of ATP levels between WT and UCH^{KO} **(Fig. 36)**.

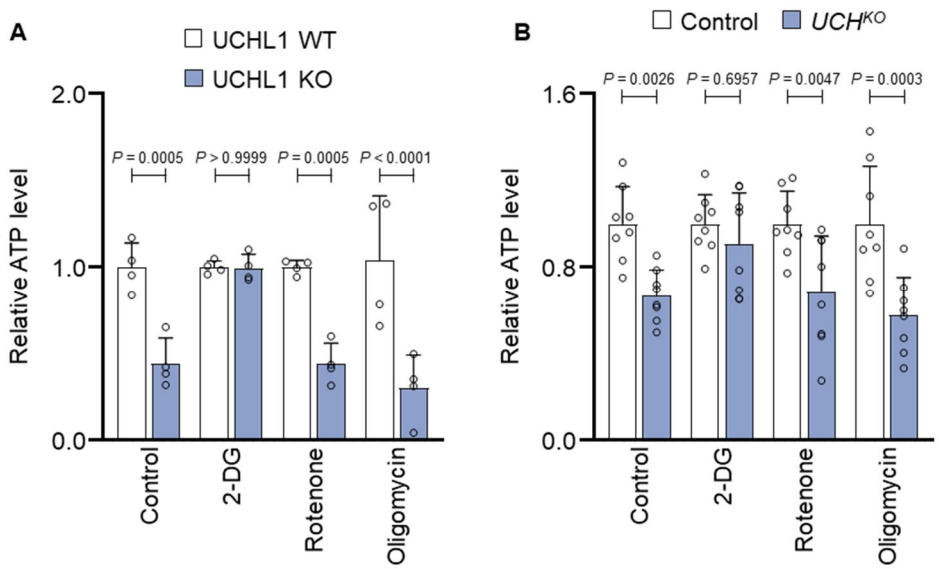

Figure 35. UCHL1 deficiency reduced cellular ATP levels, which was blocked by 2-DG.

(A) Measurement of ATP levels in UCHL1 WT and KO HEK293 cells upon 25 mM 2-DG, 1 μM rotenone, or 10 μM oligomycin. $n = 4$. **(B)** Measurement of ATP levels in WT and UCH KO flies fed with 400 mM 2-DG, 500 μM rotenone, or 300 μM oligomycin. $n = 8$. Two-way ANOVA with Sidak's multiple comparison test was used **(A and B)**. All data were presented as mean + SD.

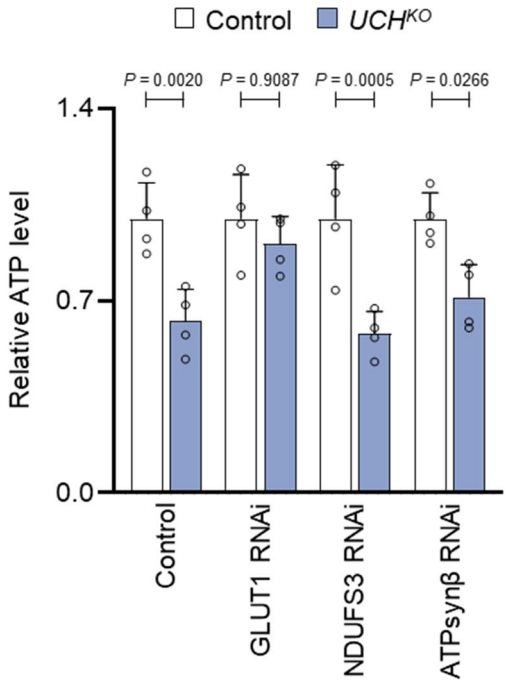

Figure 36. UCHL1 deficiency reduced cellular ATP levels, which was blocked by GLUT1 knockdown.

Measurement of ATP levels in the flies of indicated genotypes. n = 4. Two-way ANOVA with Sidak's multiple comparison test was used. Data were presented as mean + SD.

Pyruvate kinase (PKM) is a direct target of UCHL1

For finding a specific target of UCHL1, which can regulate glycolysis, I cultured cells with ^{13}C-labeled glucose and analyzed the amounts of glycolytic metabolites **(Table 2)**. Surprisingly, the pyruvate levels were dramatically reduced in UCHL1 KO cells compared to UCHL1 WT cells. However, most of other glycolytic metabolites generated before the pyruvate production step were increased by UCHL1 deletion **(Fig. 37A)**. As pyruvate kinase (PKM) converts phosphoenolpyruvate (PEP) into pyruvate **(Fig. 37B)** I hypothesized that PKM is the target of UCHL1. Thus, I measured the ubiquitination of PKM in HEK293 cells while expressing UCHL1 WT, C90S, or R178Q, a hyperactive form of UCHL1 under MG132, an inhibitor of proteasomal degradation, treatment. The PKM ubiquitination decreased by the expression of UCHL1 WT or R178Q, but did not change when expressing UCHL1 C90S **(Fig. 38)**. Furthermore, I observed the stability of PKM while suppressing UCHL1. The endogenous amount of PKM proteins was decreased in UCHL1 KO cells compared to UCHL1 WT **(Fig. 39)**.

^{12}C-labeled metabolite	m/z	^{13}C-labeled metabolite	m/z	Retention time (min)
^{12}C-G6P	259.02267	^{13}C-G6P	265.04294	9.1
^{12}C-F1,6P	338.98907	^{13}C-F1,6P	345.00928	9.6
^{12}C-3PG	184.98485	^{13}C-3PG	187.99492	9.2
^{12}C-PEP	166.97420	^{13}C-PEP	169.98429	9.5
^{12}C-Pyruvate	87.00736	^{13}C-Pyruvate	90.01747	2.3
^{12}C-Lactate	89.02304	^{13}C-Lactate	92.03300	3.3

Table 2. Retention times and m/z values of the ^{13}C-labeled metabolites.

^{13}C-labeled metabolites were separated on the ZIC-pHILIC column ran at flow rate 0.2 ml/min with water/acetonitrile solvent system based on ammonium carbonate additive, and were detected by Thermo Scientific Orbitrap-based mass spectrometer. G6P, glucose-6-phosphate. F1,6P, fructose-1,6-bisphosphate. 3PG, 3-phosphoglycerate. PEP, phosphoenolpyruvate.

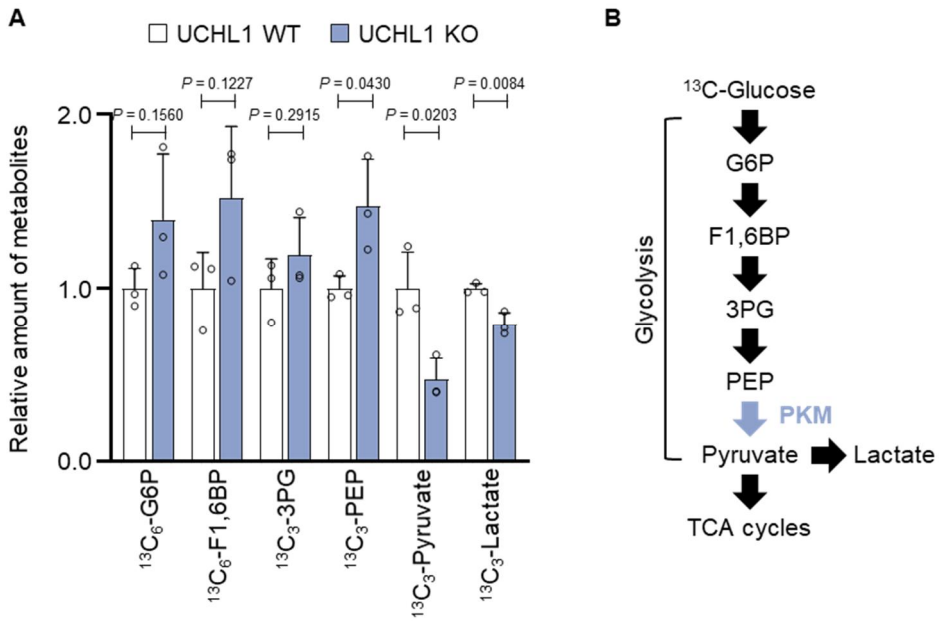

Figure 37. Pyruvate productions were decreased in UCHL1 KO cells.

(A) Measurement of metabolites produced by glycolysis in HEK293 UCHL1 WT and KO cells cultured in media with ^{13}C-glucose. n = 3. **(B)** Schematic diagram of glycolysis pathway. PEP is converted into pyruvate by PKM. Data were presented as mean + SD.

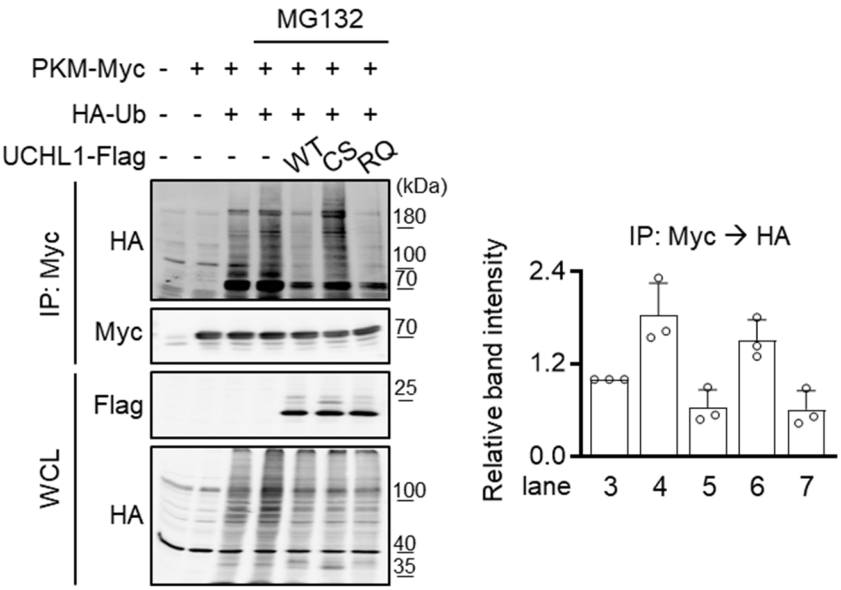

Figure 38. Ubiquitination of PKM was decreased dramatically by expressing UCHL1.

(A) Left, immunoblot analysis of PKM ubiquitination in HEK293 cells. The cells were co-transfected with Myc-tagged PKM, hemagglutinin (HA)-tagged ubiquitin, and Flag-tagged UCHL1 WT, C90S, or R178Q upon 20 μM MG132 for 4 hours. IP: immunoprecipitation. WCL: whole-cell lysate. Right, quantification of immunoblot band intensity of HA immunoprecipitated by Myc antibody normalized by third lane. n = 3. Data were presented as mean + SD.

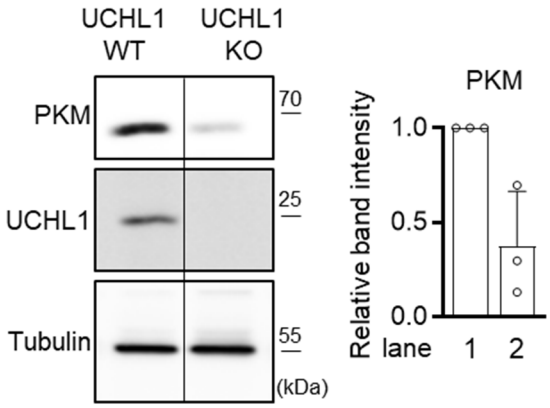

Figure 39. PKM levels were reduced in UCHL1 KO cells.

Left, immunoblot analysis of PKM in UCHL1 WT and KO HEK293 cells. Right, quantification of immunoblot band intensity of PKM normalized by first lane. *n* = 3. Data were presented as mean + SD.

Loss of UCHL1 enhanced mitophagy via PKM destabilization

As UCHL1 inhibition destabilized PKM, I sought to identify the increased mitophagy by the loss of UCHL1 is caused by PKM destabilization. Therefore, I used MG132 to stop proteasomal degradation of ubiquitinated PKM and PKM siRNA not to translate PKM proteins, and measured mitophagy. In UCHL1 WT cells, mitophagy was not changed by MG132 treatment since UCHL1 deubiquitinated PKM. Treating MG132 and PKM siRNA to UCHL1 WT cells enhanced the mitophagy **(Fig. 40A)**. However, MG132 treatment blocked the elevation of mitophagy in UCHL1 KO cells. Intriguingly, mitophagy was induced by treating both MG132 and PKM siRNA to UCHL1 KO cells, which suggested that the quantity of PKM protein plays a key role in UCHL1-mediated mitophagy **(Fig. 40B)**. Furthermore, I observed that the enhanced mitophagy in UCHL1 KO cells was blocked by expressing PKM **(Fig. 41)**.

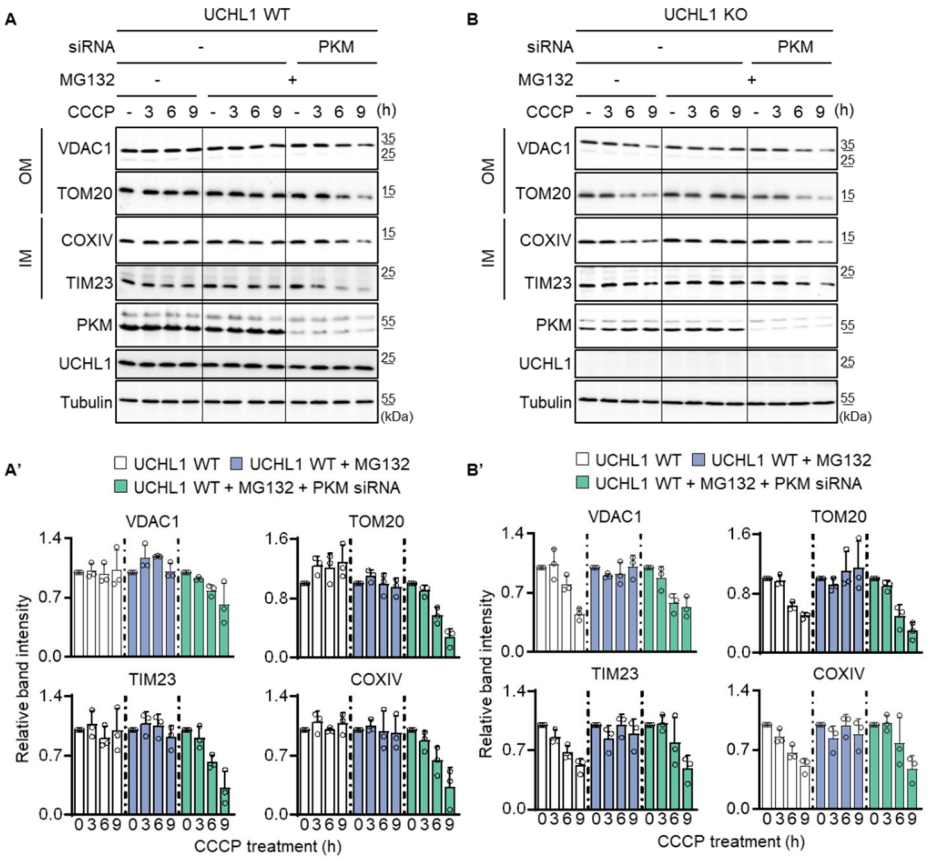

Figure 40. PKM protein stability was important for UCHL1-mediated mitophagy.

(A) Left, immunoblot analysis of OM (VDAC11 and TOM20) and IM (TIM23 and COXIV) proteins upon 20 μM MG132 treatment and PKM expression in UCHL1 WT HEK293 cells. Right, immunoblot analysis of OM (VDAC11 and TOM20) and IM (TIM23 and COXIV) proteins upon 20 μM MG132 treatment and PKM expression in UCHL1 KO HEK293 cells. **(A')** Quantification of immunoblot band intensity of indicated proteins normalized by first lane. $n = 3$. Data were presented as mean + SD.

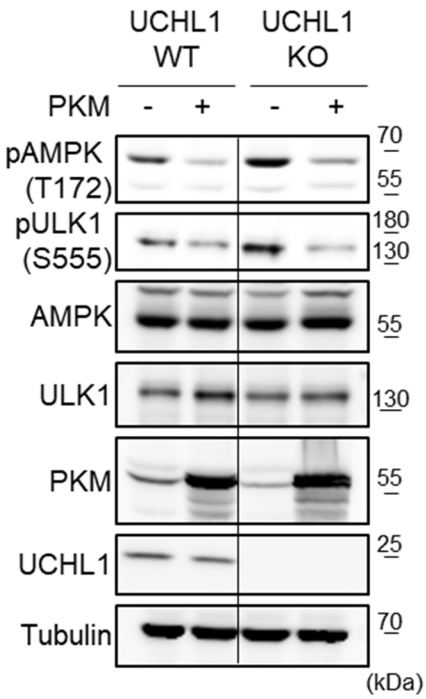

Figure 41. Elevated phosphorylation of AMPK and ULK1 was reduced by PKM expression in UCHL1 KO cells.

Immunoblot analysis of AMPK and ULK1 phosphorylation in UCHL1 WT and KO HEK293 cell lines with or without PKM expression.

Tripartite motif-containing 63 (TRIM63) played an antagonistic role of UCHL1

For finding an E3 ligase whose role is antagonistic toward UCHL1, I used the Biological General Repository for Interaction Datasets (BioGRID) (Oughtred et al., 2019) and found seven E3 ligases, Parkin, mouse double minute 2 homolog (MDM2), TRIM63, HECT and RLD domain-containing E3 ubiquitin ligase family member 1 (HERC1), HECT, UBA, and WWE domain-containing E3 ubiquitin ligase 1 (HUWE1), ligand of numb-protein X 1 (LNX1), and STIP homology and U-box-containing protein 1 (STUB1) which can interact with PKM. The ubiquitination of PKM was elevated by expressing TRIM63 among these candidates **(Fig. 42)**.

I wondered whether TRIM63 shows antagonistic interactions with UCHL1. The increased ubiquitination of PKM proteins induced by expressing TRIM63 was reduced by the concurrent expression of UCHL1 WT, not C90S **(Fig. 43)**. In addition, I measured the stability of PKM proteins and mitophagy in UCHL1 KO cells with TRIM63 siRNA. Under TRIM63 siRNA treatment, the decreased stability of PKM proteins in UCHL1 knockout cell lines was increased as much as that in UCHL1 WT cell lines **(Fig. 44)**. Increased mitophagy in UCHL1 KO cells was reduced by knocking down TRIM63 **(Fig. 45)**.

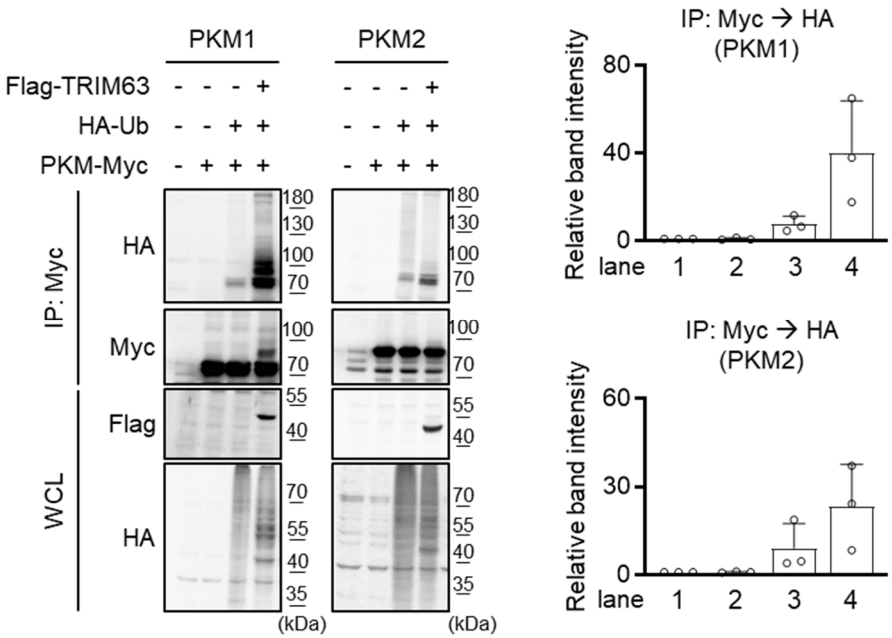

Figure 42. Ubiquitination of PKM was elevated by TRIM63 expression.

Left, immunoblot analysis of PKM ubiquitination in HEK293 cell lines expressing Flag-tagged TRIM63, HA-tagged ubiquitin, and Myc-tagged PKM1/2. Right, quantification of immunoblot band intensity of HA immunoprecipitated by Myc antibody normalized by first lane. n = 3. Data were presented as mean + SD.

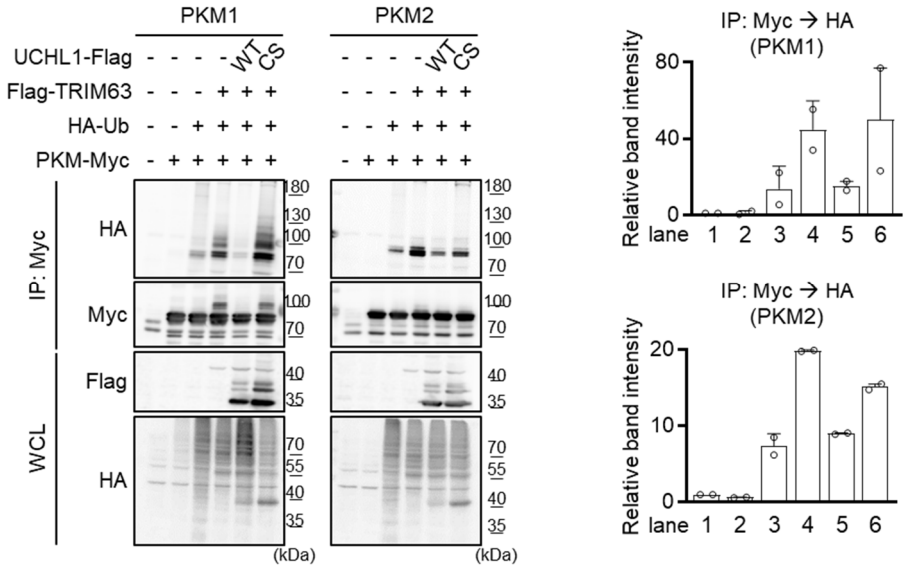

Figure. 43. Increased ubiquitination of PKM by TRIM63 expression was virginfemalereduced by UCHL1 expression.

Left, immunoblot analysis of PKM ubiquitination in HEK293 cell lines expressing Flag-tagged UCHL1 (WT or C90S), Flag-tagged TRIM63, HA-tagged ubiquitin, and Myc-tagged PKM1/2. Right, quantification of immunoblot band intensity of HA immunoprecipitated by Myc antibody normalized by first lane. n = 2. Data were presented as mean + SD.

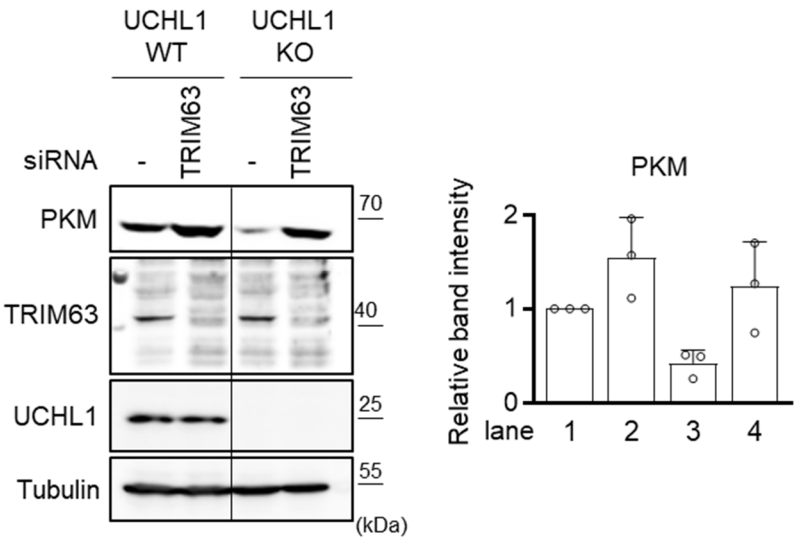

Figure 44. Decreased stability of PKM by UCHL1 KO was blocked by TRIM63 knockdown.

Left, immunoblot analysis of PKM in UCHL1 WT and KO HEK293 cells with or without TRIM63 siRNA. Right, quantification of immunoblot band intensity of PKM normalized by first lane. $n = 3$. Data were presented as mean + SD.

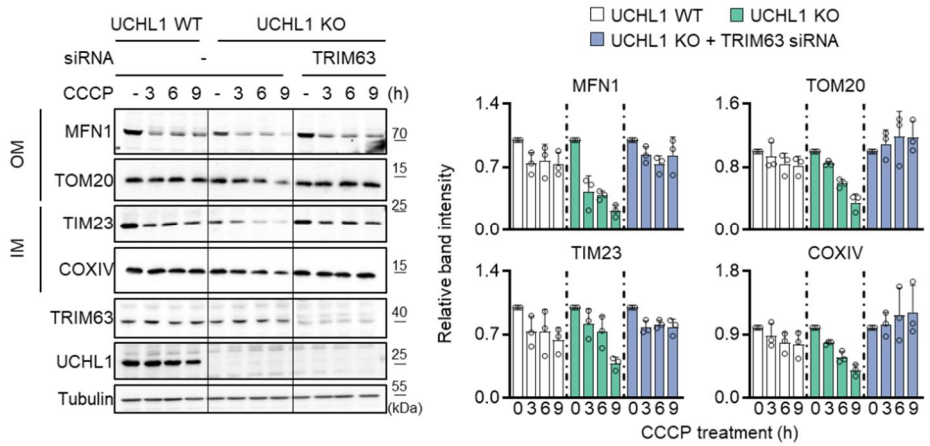

Figure 45. Increased mitophagy in UCHL1 KO cells was reduced by TRIM63 knockdown.

Left, immunoblot analysis of OM (MFN1 and TOM20) and IM (TIM23 and COXIV) proteins upon 20 μM CCCP and TRIM63 siRNA treatment. Right, quantification of immunoblot band intensity of indicated proteins normalized by first lane. *n* = 3. Data were presented as mean + SD.

Loss of UCHL1 exhibited anti-Parkinsonian effects via PKM destabilization

Using mammalian cell lines, I identified that UCHL1 interacts with PKM and TRIM63. Therefore, I sought to find that these results are also conserved in fruit flies. First, I observed that PKM (*cg7070*) knockdown or TRIM9 (*cg31721*, ortholog of human TRIM63) overexpression under *hs*-GAL4 drivers ameliorated PD-related phenotypes, including impaired mitochondria, increased apoptosis, DA neuronal death, and decreased climbing abilities, of PINK1 or Parkin mutants similar to UCHL1 **(Fig. 46, 47, and 48)**. Therefore, I hypothesized that the anti-Parkinsonian effects of UCH deletion might be blocked by PKM overexpression or TRIM9 knockdown. I generated flies with overexpressing PKM or knocking down TRIM9 in PINK1 and UCH DKO or Parkin and UCH DKO backgrounds. By PKM expressing or TRIM9 knockdown, the effects of UCH^{KO}, rescuing the defects in PINK1 or Parkin mutants, were all blocked **(Fig. 49, 50, and 51)**. Finally, I would like to observe the interaction between PKM and AMPK-ULK1-FUNDC1 signaling in *Drosophila*. Thus, I generated PKM knockdown flies in PINK1 or Parkin KO backgrounds while expressing AMPK, ULK1, or FUNDC1 RNAi. I found that PKM knockdown rescued the DA neuronal degeneration in $PINK1^{B9}$ or $park^{1}$, but concurrent expression of AMPK, ULK1, or FUNDC1 knockdown blocked these effects **(Fig. 52 and 53)**. In conclusion, I proved that the loss of UCHL1 exhibited anti-

Parkinsonian effect against PINK1 or Parkin mutants via PKM-AMPK-ULK1-FUNDC1 pathway in fruit flies.

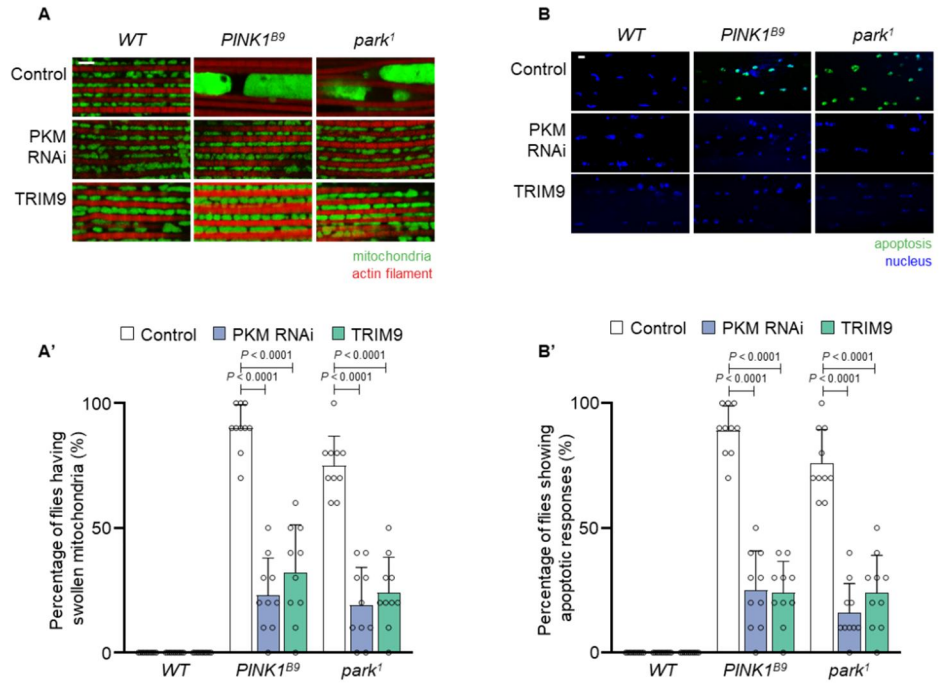

Figure 46. PKM knockdown or TRIM9 overexpression rescued abnormal mitochondria and elevated apoptosis of PINK1 and Parkin mutants.

(A and A') Confocal fluorescence images of adult flight muscles in *Drosophila* **(A)**. Green indicates mitochondria, and red indicates actin filament. Scale bar, 5 μm. Percentages of the flies having swollen mitochondria **(A')**. n = 10. **(B and B')** Confocal fluorescence images for TUNEL assays of the adult flight muscles in *Drosophila* **(B)**. Green indicates apoptosis, and blue indicates nucleus. Scale bar, 20 μm. Percentages of the flies showing apoptotic responses **(B')**. n = 10. Genotype, control (*Hs>+*), PKM RNAi (*Hs>PKM RNAi*), and TRIM9 (*Hs>TRIM9*). Two-way ANOVA with Sidak's multiple comparison test was used **(A' and B')**. Data were presented as mean + SD.

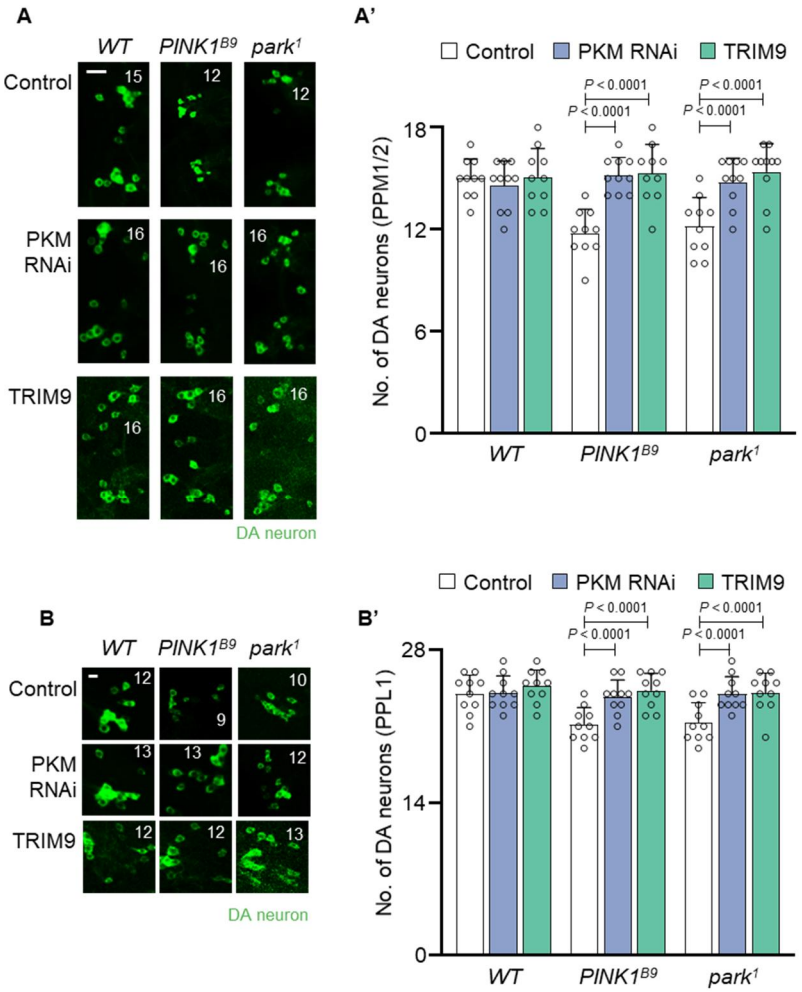

Figure 47. PKM knockdown or TRIM9 overexpression rescued DA neuronal degeneration of PINK1 and Parkin mutants.

(A and A') Confocal immunofluorescence images **(A)** and numbers **(A')** of DA neurons in PPM1/2 regions of adult fly brains. N = 10. Green indicates DA neuron. Scale bar, 20 μm. **(B and B')** Confocal immunofluorescence images **(B)** and numbers **(B')** of DA neurons in PPL1 regions of adult fly brains. The images were obtained from one of the left or right side of PPL1 regions. Numbers of the DA neurons in the PPL1 regions were counted from

both hemispheres. Scale bar, 20 μm. The number in panels indicates the number of DA neurons in each image. Genotype, control (*Hs*>+), PKM RNAi (*Hs>PKM RNAi*), and TRIM9 (*Hs>TRIM9*). Two-way ANOVA with Sidak's multiple comparison test was used **(A' and B')**. All data were presented as mean + SD.

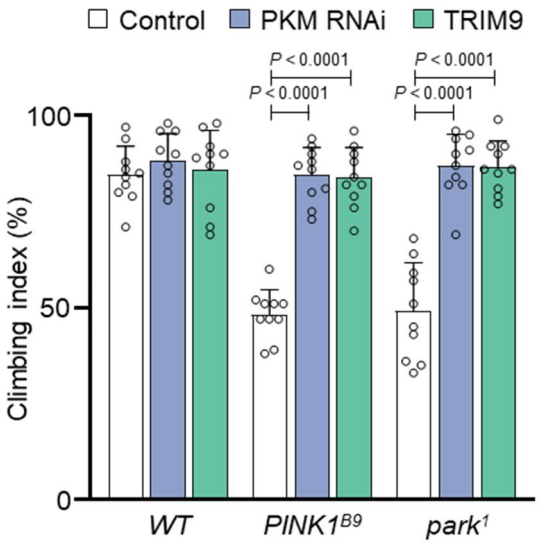

Figure 48. PKM knockdown or TRIM9 overexpression rescued impaired climbing abilities of PINK1 and Parkin mutants.

Climbing abilities in the adult flies of indicated genotypes. $n = 10$. Genotype, control (*Hs>+*), PKM RNAi (*Hs>PKM RNAi*), and TRIM9 (*Hs>TRIM9*). Two-way ANOVA with Sidak's multiple comparison test was used. Data were presented as mean + SD.

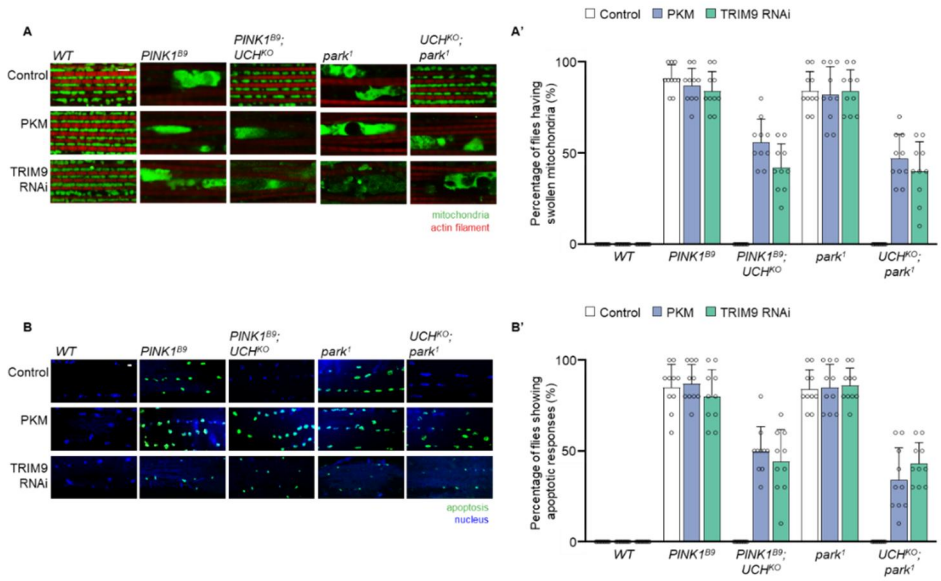

Figure 49. PKM overexpression or TRIM9 knockdown blocked the rescuing effects of mitochondrial morphology and apoptosis by UCHL1 deletion in PINK1 or Parkin mutants.

(A and A') Confocal fluorescence images of adult flight muscles in *Drosophila* **(A)**. Green indicates mitochondria, and red indicates actin filament. Scale bar, 5 μm. Percentages of the flies having swollen mitochondria **(A')**. n = 10. **(B and B')** Confocal fluorescence images for TUNEL assays of the adult flight muscles in *Drosophila* **(B)**. Green indicates apoptosis, and blue indicates nucleus. Scale bar, 20 μm. Percentages of the flies showing apoptotic responses **(B')**. n = 10. Genotype, control (*Hs>+*), PKM(*Hs>PKM*), and TRIM9 RNAi (*Hs>TRIM9 RNAi*). Data were presented as mean + SD.

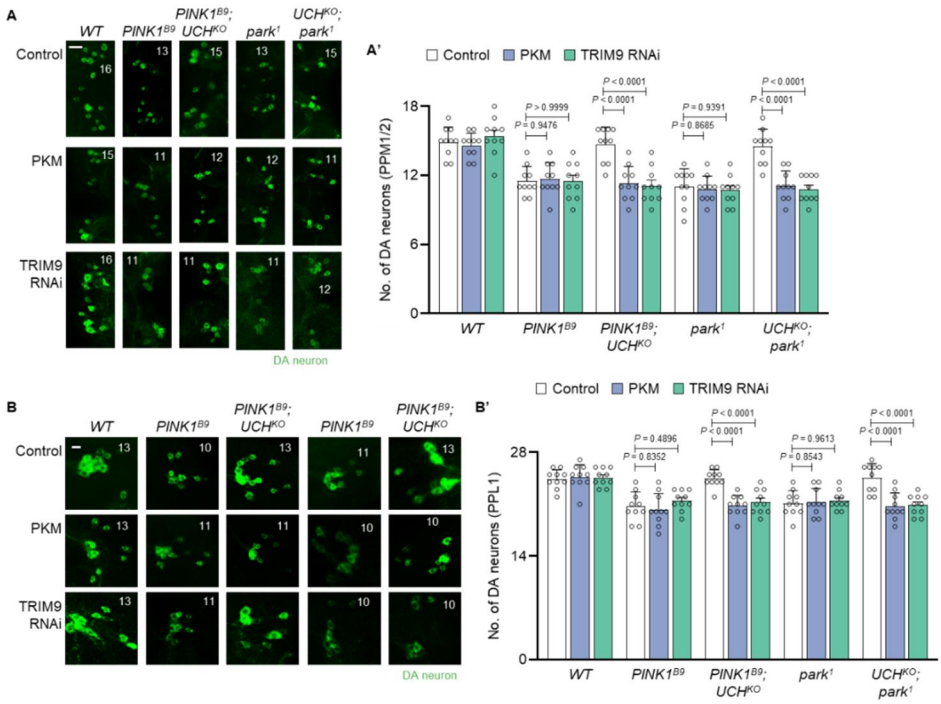

Figure 50. PKM overexpression or TRIM9 knockdown blocked the DA neuronal protections by UCHL1 deletion in PINK1 or Parkin mutants.

(A and A') Confocal immunofluorescence images **(A)** and numbers **(A')** of DA neurons in PPM1/2 regions of adult fly brains. N = 10. Green indicates DA neuron. Scale bar, 20 μm. **(B and B')** Confocal immunofluorescence images **(B)** and numbers **(B')** of DA neurons in PPL1 regions of adult fly brains. The images were obtained from one of the left or right side of PPL1 regions. Numbers of the DA neurons in the PPL1 regions were counted from both hemispheres. Scale bar, 20 μm. The number in panels indicates the number of DA neurons in each image. Genotype, control (*Hs>+*), PKM(*Hs>PKM*), and TRIM9 RNAi (*Hs>TRIM9 RNAi*). Two-way ANOVA with Sidak's multiple comparison test was used **(A' and B')**. All data were presented as mean + SD.

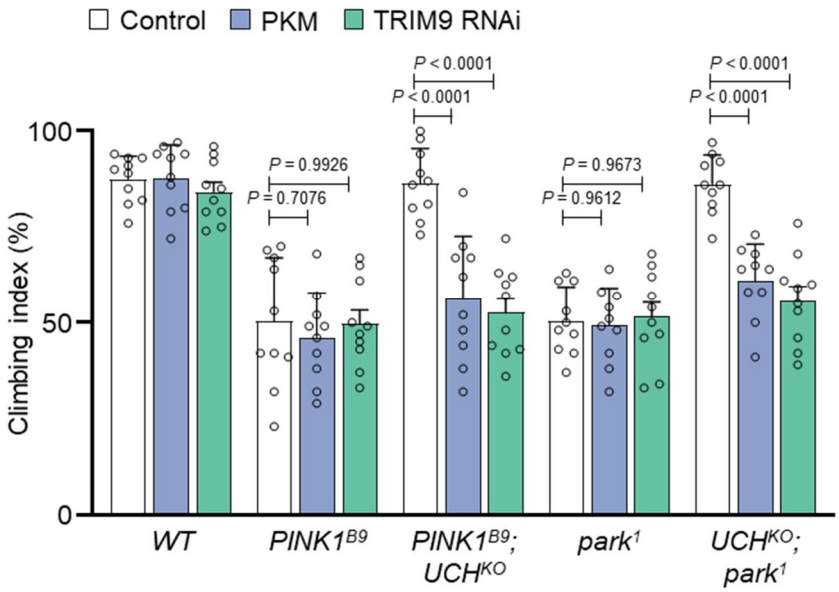

Figure 51. PKM overexpression or TRIM9 knockdown blocked the rescuing effects of climbing abilities by UCHL1 deletion in PINK1 or Parkin mutants.

Climbing abilities in the adult flies of indicated genotypes. *n* = 10. Genotype, control (*Hs>+*), PKM(*Hs>PKM*), and TRIM9 RNAi (*Hs>TRIM9 RNAi*). Two-way ANOVA with Sidak's multiple comparison test was used. Data were presented as mean + SD.

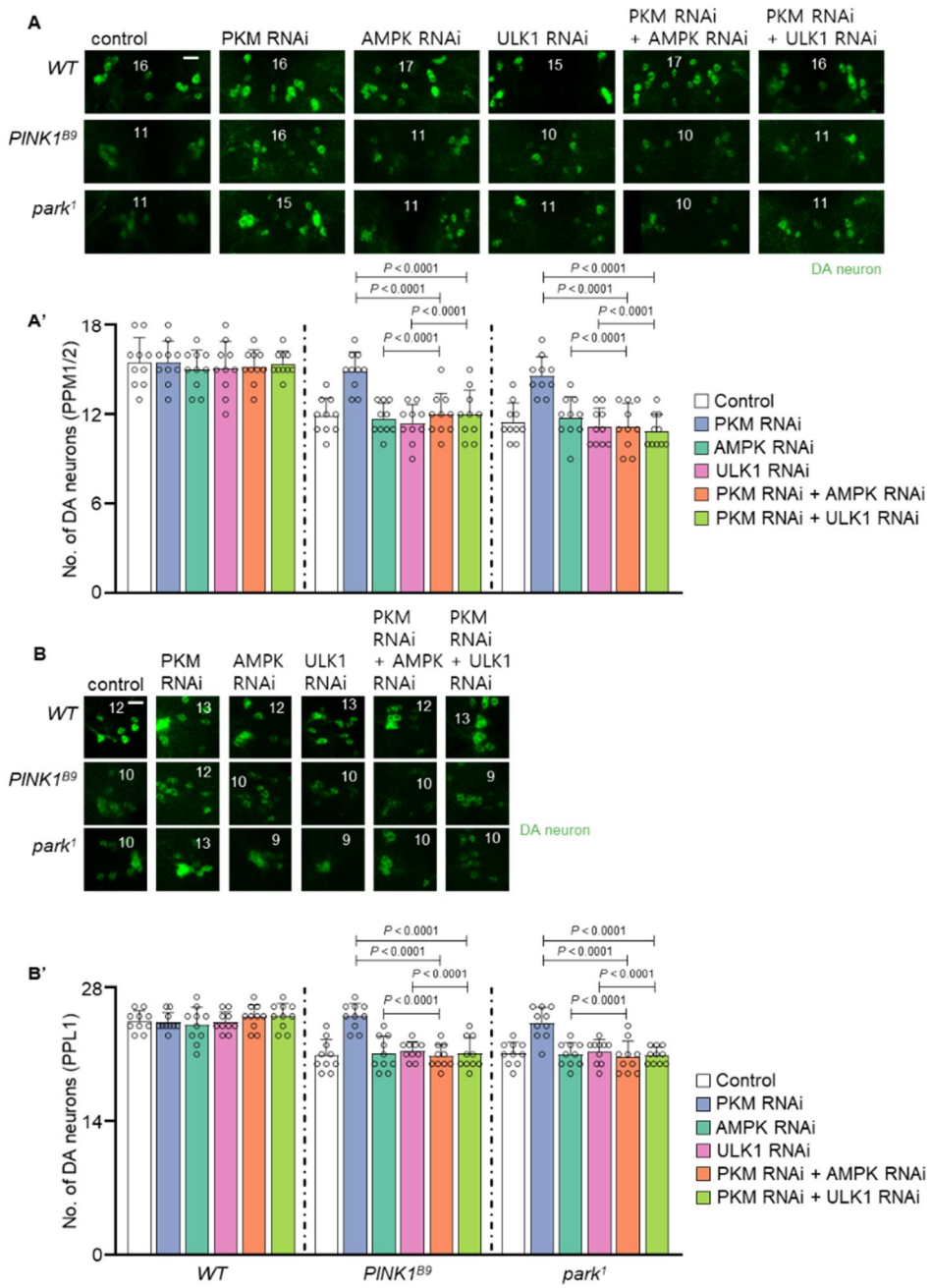

Figure 52. AMPK or ULK1 knockdown blocked the DA neuronal protections by PKM knockdown in PINK1 or Parkin mutants.

(A and A') Confocal immunofluorescence images **(A)** and numbers **(A')** of DA neurons in PPM1/2 regions of adult fly brains. N = 10. Green indicates

DA neuron. Scale bar, 20 μm. **(B and B')** Confocal immunofluorescence images **(B)** and numbers **(B')** of DA neurons in PPL1 regions of adult fly brains. The images were obtained from one of the left or right side of PPL1 regions. Numbers of the DA neurons in the PPL1 regions were counted from both hemispheres. Scale bar, 20 μm. The number in panels indicates the number of DA neurons in each image. Genotype, control (*th*>+), PKM RNAi (*th>PKM RNAi*), AMPK RNAi (*th>AMPK RNAi*), ULK1 RNAi (*th>ULK1 RNAi*), PKM RNAi + AMPK RNAi (*th>PKM RNAi, AMPK RNAi*), and PKM RNAi + ULK1 RNAi (*th>PKM RNAi, ULK1 RNAi*). Two-way ANOVA with Sidak's multiple comparison test was used **(A' and B')**. All data were presented as mean + SD.

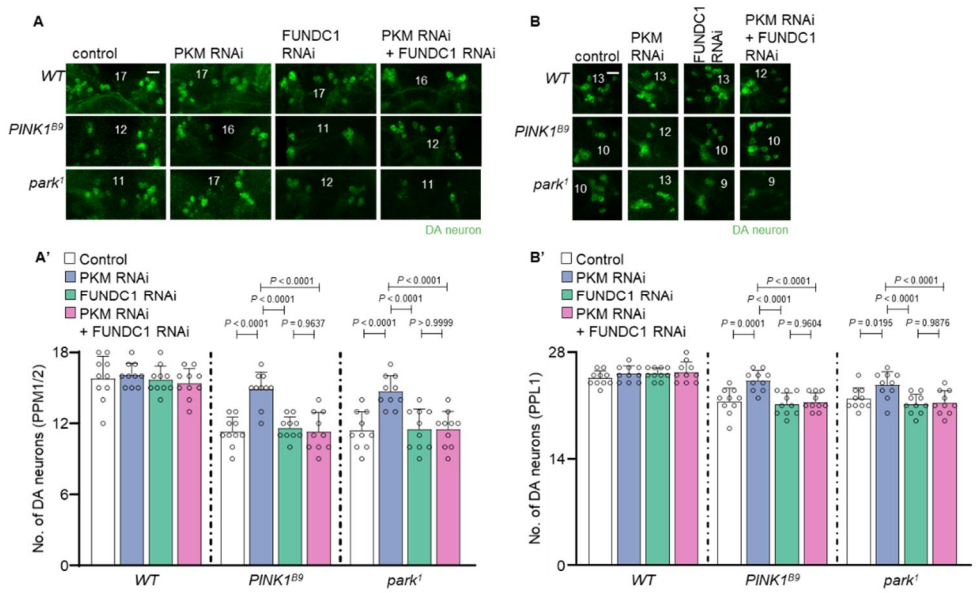

Figure 53. FUNDC1 knockdown blocked the DA neuronal protections by PKM knockdown in PINK1 or Parkin mutants.

(A and A') Confocal immunofluorescence images **(A)** and numbers **(A')** of DA neurons in PPM1/2 regions of adult fly brains. N = 10. Green indicates DA neuron. Scale bar, 20 μm. **(B and B')** Confocal immunofluorescence images **(B)** and numbers **(B')** of DA neurons in PPL1 regions of adult fly brains. The images were obtained from one of the left or right side of PPL1 regions. Numbers of the DA neurons in the PPL1 regions were counted from both hemispheres. Scale bar, 20 μm. The number in panels indicates the number of DA neurons in each image. Genotype, control (th>+), PKM RNAi (*th>PKM RNAi*), FUNDC1 RNAi (*th>FUNDC1 RNAi*), and PKM RNAi + FUNDC1 RNAi (*th>PKM RNAi, FUNDC1 RNAi*). Two-way ANOVA with Sidak's multiple comparison test was used **(A' and B')**. All data were presented as mean + SD.

Discussion

Summary

In PART 1, I have established that UCHL1 regulates glycolysis and energy-dependent mitophagy pathway by deubiquitinating pyruvate kinase. In addition, UCHL1 mutations which reduced DUB activity alleviated PD pathogenesis by elevating mitophagy via sequential activation of AMPK, ULK1, and FUNDC1. It has been controversial whether loss-of function mutations of UCHL1 induces PD, but I observed that UCHL1 mutations rather ameliorated PD pathologies in PINK1 or Parkin deficient *Drosophila* models. Also, these effects were regulated by TRIM63, a novel E3 ligase for pyruvate kinase. Therefore, I proposed UCHL1 as an integrative molecule between glycolysis and PD pathogenesis **(Fig. 54)**.

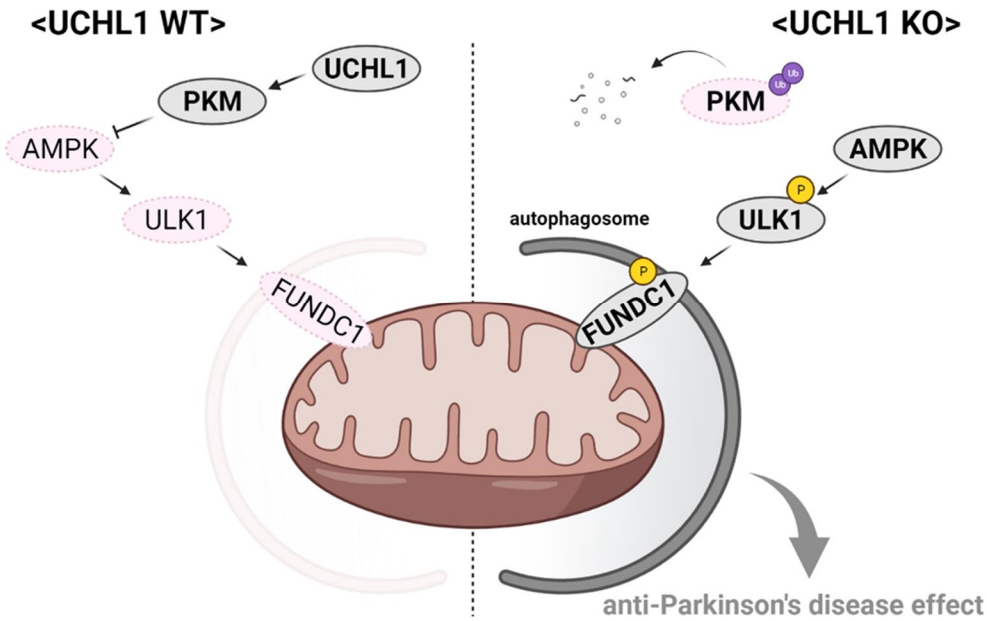

Figure 54. A proposed model for the roles of UCHL1 in mitophagy and PD.

Image was generated from Biorender.

Pyruvate and PD

In this study, I revealed that PKM is a compelling factor for mitophagy and PD pathogenesis. Likewise, several studies have been reported that PKM or pyruvate is linked with PD. In astrocyte cancer cell lines, Parkin ubiquitinates PKM and decreases its activity, which is strengthened by glucose starvation (Liu et al., 2016). However, I observed that PD phenotypes in Parkin KO mutants were completely rescued by UCHL1 KO. As the ubiquitination of PKM by Parkin was absent in Parkin mutants, the deubiquitination sites of PKM by UCHL1 is separate from the ubiquitination site of PKM by Parkin. It implies that there is a novel E3 ligase which plays an antagonistic role of UCHL1. Therefore, I identified that TRIM63 as the E3 ligase and TRIM63 also was able to control mitophagy or PD pathogenesis. Additionally, it has been considered important that that pyruvate metabolism is associated with PD. In the blood of PD patients, pyruvate concentration was elevated and the expressions of pyruvate dehydrogenase E1 subunit β were reduced (Ahmed et al., 2009). Also, chemical inhibition of mitochondrial pyruvate carrier (MPC), which transports pyruvate into mitochondrial matrix, showed neuroprotective effects in neurodegeneration models. Especially, inhibition of MPC by MSDC-160 increases the survival rate of DA neurons in substantia nigra and the dopamine productions by DA neurons in MPTP-treated mice and Lund human mesencephalic (LUHMES) cell lines (Ghosh et al., 2016). In conclusion, the increased activity of PKM

or elevating pyruvate levels are closely connected to PD pathogenesis. Therefore, regulating these can be potential remedies for treating PD.

UCHL1 inhibitor as a drug for PD

Based on the data from this study, pharmacological inhibition of UCHL1 might be able to rescue PD symptoms. It has been known that 5-Chloro-1-[(2,5-dichlorophenyl) methyl]-1*H*-indole-2,3-dione (LDN-57444) can inhibit the DUB activity of UCHL1 (Liu et al., 2003). Also, I observed that LDN-57444 inhibits both human UCHL1 and *Drosophila* UCH **(Fig. 55)**. As UCHL1 inhibition elevated mitophagy, I measured mitophagy in PINK1 or Parkin KO mouse embryonic fibroblast (MEF) cell lines under LDN-57444 treatment. Surprisingly, decreased mitophagy in PINK1 and Parkin KO cells was resumed by LDN-57444 treatment **(Fig. 56)**. Furthermore, LDN-57444 treatment elevated the phosphorylation of AMPK **(Fig. 57)**. Finally, I tried to observe whether the administration of LDN-57444 can mitigate PD-like pathologies in fruit flies. However, since LDN-57444 is very unstable under our experimental conditions and dimethyl sulfoxide (DMSO), the solvent of LDN-57444, are toxic to flies, I couldn't feed LDN-57444 to *Drosophila*. Therefore, I am currently screening to find a novel UCHL1 inhibitor with less toxicity and better physical and chemical properties.

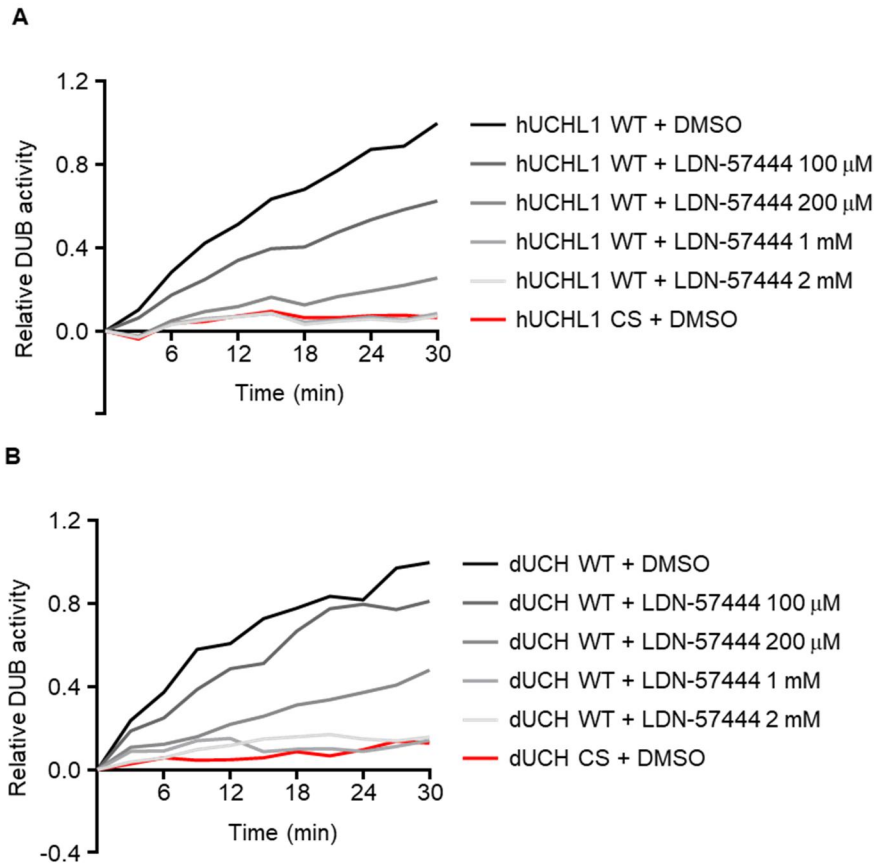

Figure 55. LDN-57444 treatment decreased the activity of UCHL1 from human and *Drosophila*.

(A) Evaluation of the human UCHL1 DUB activities under LDN-57444 treatment. The values were normalized by the activity of UCHL1 WT under DMSO treatment at 30 min. **(B)** Evaluation of the *Drosophila* UCH DUB activities under LDN-57444 treatment. The values were normalized by the activity of dUCH WT under DMSO treatment at 30 min.

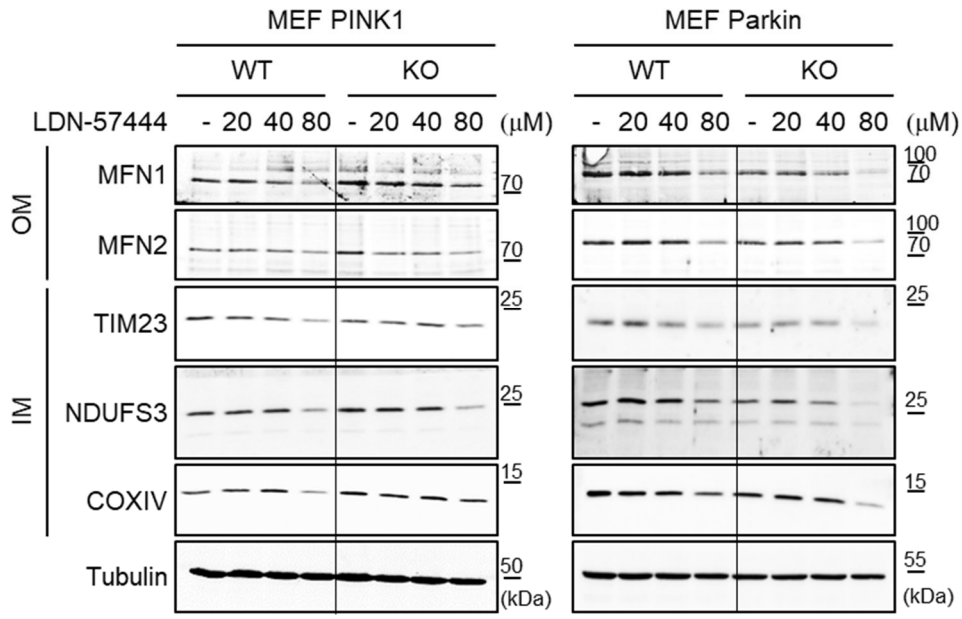

Figure 56. Decreased mitophagy in PINK1 or Parkin KO cells was increased by treating LDN-57444.

Immunoblot analysis of OM (MFN1 and MFN2) and IM (TIM23, NDUFS3 and COXIV) proteins in MEF PINK1 WT or KO, MEF Parkin WT or KO while treating LDN-57444.

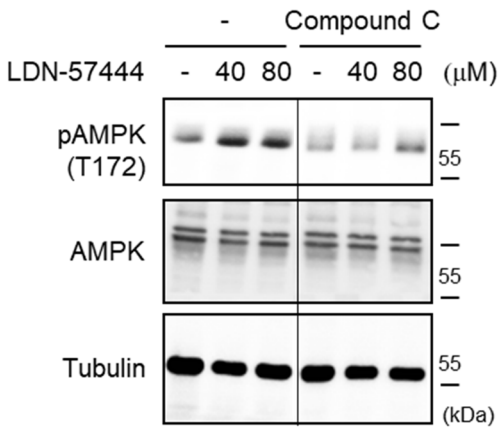

Figure 57. LDN-57444 treatment activated AMPK.

Immunoblot analysis of AMPK phosphorylation upon LDN-57444 treatment.

Induction of mitophagy reflecting cytosolic energy levels

The PINK1/Parkin pathway detects the damages of mitochondria. Then, the pathway labels the proteins of damaged mitochondria with ubiquitin and initiates mitophagy. However, I found that the mitophagy controlled by UCHL1 deficiency is triggered via PKM destabilization, which inhibits glycolysis. As glycolysis occurs in and mainly linked with cytosol, UCHL1-controlled mitophagy do not determine between damaged and undamaged mitochondria unlike PINK1/Parkin pathway. Therefore, I propose that the mitophagy induced by the loss of UCHL1 plays a house-keeping role for mitochondrial homeostasis depending on cytosolic energy status.

PART 2

UCHL1 regulates insulin signaling through IRS1 deubiquitination

Results

It has been reported that the treatment for PD is closely linked with type 2 diabetes pathogenesis. Since I observed that UCHL1 knockout flies completely rescued the pathologies related to PD in PART 1, I determined to observe the T2D-related phenotypes in UCHL1 KO flies.

Type 2 diabetic phenotypes were shown in UCHL1 mutant flies

I employed UCH KO (UCH^{KO}) and UCH C93S ($UCH^{C93S\ KI}$), which expresses the activity dead form of UCH, mutants for identifying T2D-like symptoms in *Drosophila*. Surprisingly, the glucose levels in hemolymph of UCH^{KO} and $UCH^{C93S\ KI}$ were increased by approximately 50 percent compared to those of wild-type (WT) flies at 3rd-instar larval, 3-day (young) adult, and 30-day (old) adult stages **(Fig. 58A)**. Also, the levels of trehalose **(Fig. 58B)**, triacylglyceride (TAG) **(Fig 59A)**, and glycogen **(Fig. 59B)** were elevated at the larval and adult stages by these two types of UCH mutations. Therefore, I sought to measure the levels of insulin in UCH mutant flies if these diabetic phenotypes were developed by insulin depletion. I observed that all the *Drosophila* insulin-like peptides (DILPs), the homologs of human insulin, were slightly increased in UCH^{KO} and $UCH^{C93S\ KI}$ **(Fig. 60)**.

Therefore, I ascertained that the loss-of-function mutations of UCH showed T2D-like phenotypes, not type 1 diabetes (T1D)-like phenotypes. Since T2D patients diagnose insulin resistance by glucose tolerance test (GTT), I applied the method of GTT to fruit flies and measured the glycemia of UCH^{KO} and $UCH^{C93S\ KI}$. After fasting for 24 hours, the glycemia of WT, UCH^{KO}, and $UCH^{C93S\ KI}$ was all decreased, but it was dramatically increased after feeding glucose food for 1 hour. Then, the elevated blood glucose in WT flies was decreased by the normal level in the 3 hours after the feeding start. However, the high glucose levels in UCH^{KO} and $UCH^{C93S\ KI}$ were not decreased as quickly as those in WT flies **(Fig. 61)**. For further investigation,

I also performed an insulin tolerance test (ITT) and observed the insulin sensitivity of UCH mutants. Although I couldn't inject insulin into *Drosophila*, I decided to make flies expressing insulin genetically. Thus, I generated flies which expressed DILP2 exogenously (UAS-DILP2) in dilp2 neurons (*DILP2*-GAL4) at 29 ℃ using $GAL80^{TS}$. While expressing DILP2, UCH^{KO} and $UCH^{C93S\ KI}$ flies showed higher glycemia compared to WT flies **(Fig. 62)**. Therefore, I suggested that the flies with UCH mutations were resistant to insulin.

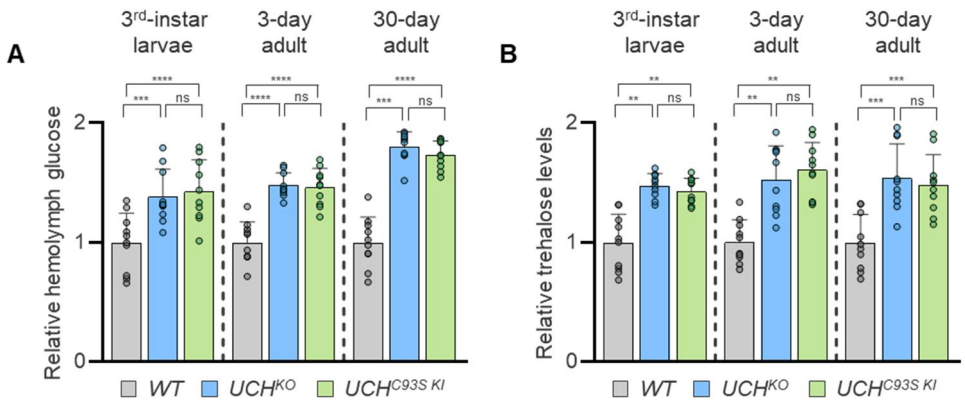

Figure 58. Increased glucose and trehalose levels were developed by the loss-of-function mutations in UCH.

(A) Relative levels of hemolymph glucose normalized to wildtype at each stage. *n* = 10. **(B)** Relative levels of trehalose normalized to wildtype at each stage. *n* = 10. Two-way ANOVA with Sidak's multiple comparison test was used **(A and B)**. **p < 0.01, ***p < 0.001, ****p < 0.0001, and ns (p > 0.05). All data were presented as mean + SD.

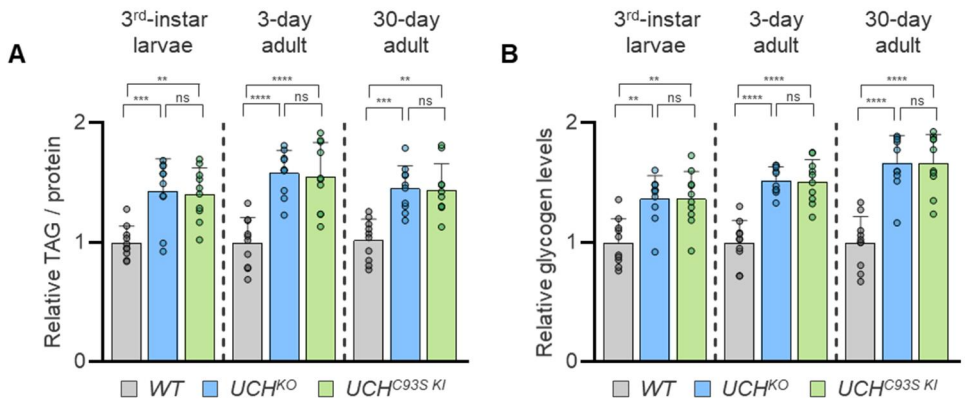

Figure 59. Increased triacylglyceride and glycogen levels were induced by the loss-of-function mutations in UCH.

(A) Relative levels of TAG per protein levels normalized to wildtype at each stage. $n = 10$. **(B)** Relative levels of glycogen normalized to wildtype at each stage. $n = 10$. Two-way ANOVA with Sidak's multiple comparison test was used **(A and B)**. **$p < 0.01$, ***$p < 0.001$, ****$p < 0.0001$, and ns ($p > 0.05$). All data were presented as mean + SD.

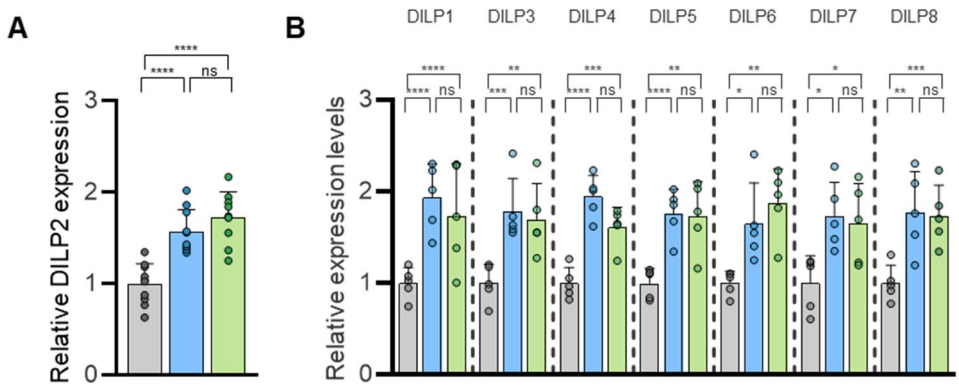

Figure 60. Expression of *Drosophila* insulin homologs was elevated in UCH^{KO} and $UCH^{C93S\ KI}$.

(A) Relative expressions of DILP2 normalized to rp49. $n = 10$. **(B)** Relative expressions of DILP1, 3, 4, 5, 6, 7, and 8 normalized to rp49. $n = 5$. Two-way ANOVA with Sidak's multiple comparison test was used **(A and B)**. *$p < 0.05$ **$p < 0.01$, ***$p < 0.001$, ****$p < 0.0001$, and ns ($p > 0.05$). All data were presented as mean + SD.

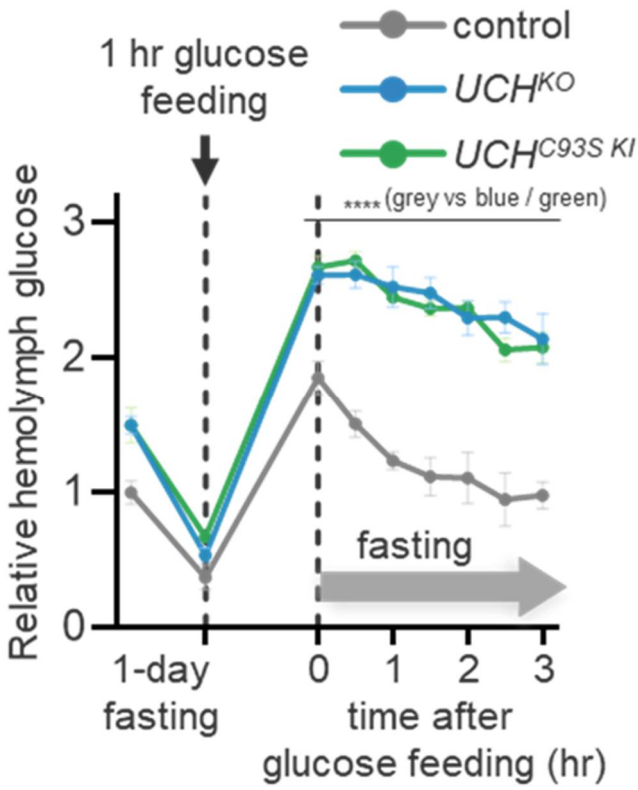

Figure 61. *UCH*^{KO} and *UCH*$^{C93S\ KI}$ showed impaired glucose tolerance.

Relative levels of hemolymph glucose normalized to the glycemia of control before 1-day fasting. Flies fasted for 1 day, and then they ate glucose containing food for 1 hour. After feeding, the flies fasted again. $n = 3$. One-way ANOVA with Dunnett's multiple comparison test was used. ****$p < 0.0001$. All data were presented as mean ± SD.

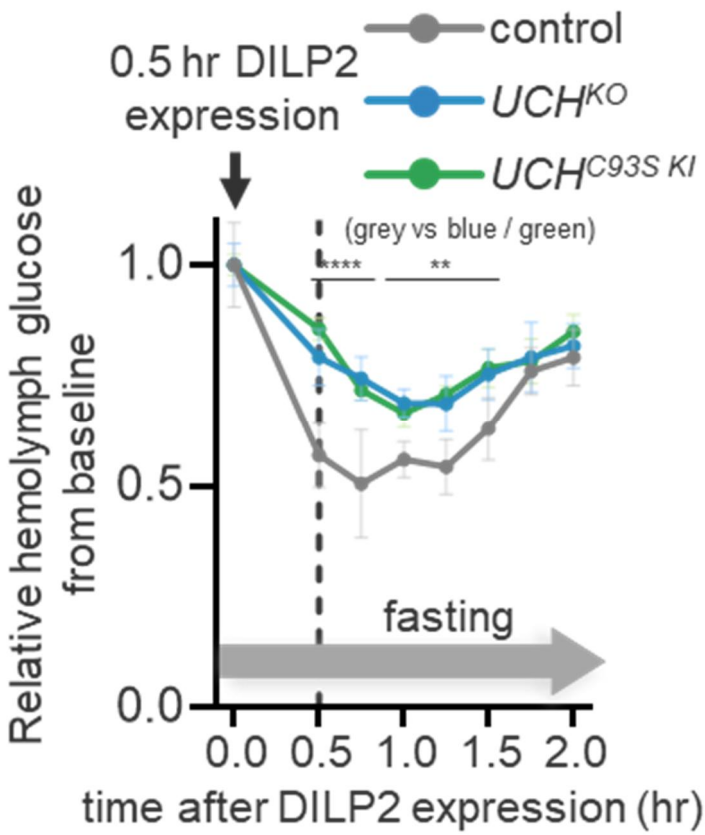

Figure 62. *UCH*^{KO} and *UCH*$^{C93S\ KI}$ showed resistance to insulin.

Relative levels of hemolymph glucose normalized to the glycemia right before the DILP2 expression of each genotype. Flies fasted during 6 hours before DILP2 expression. Dilp2 was expressed for 30 minutes and the flies were kept fasting during the expression and after the expression. $n = 3$. One-way ANOVA with Dunnett's multiple comparison test was used. **$p < 0.005$, ****$p < 0.0001$. All data were presented as mean ± SD.

UCHL1 KO induced insulin resistance in *Drosophila* brains

For further investigation, I expressed RNAi against UCH using collagen (*cg*)-GAL4, *mef2*-GAL4, and *elav*-GAL4 for knocking down UCH in the fat body, muscle, and brain, respectively. Interestingly, only brain-specific knockdown of UCH showed hyperglycemia similar to UCH^{KO} **(Fig. 63)**. In addition, I observed that UCH expression was abundant in the fly head compared to that in the thorax or abdomen **(Fig. 64)**. In conclusion, as UCH was highly expressed in the fly brain, UCH deficiency induced brain-specific insulin resistance, which developed into hyperglycemia in UCH mutant flies.

Similar to these results, I found that the brains of UCH^{KO} or $UCH^{C93S\ KI}$ were larger than those of control flies **(Fig. 65)**. Furthermore, one of the diabetic phenotypes, feeding behavior, was increased by UCH mutations **(Fig. 66)**.

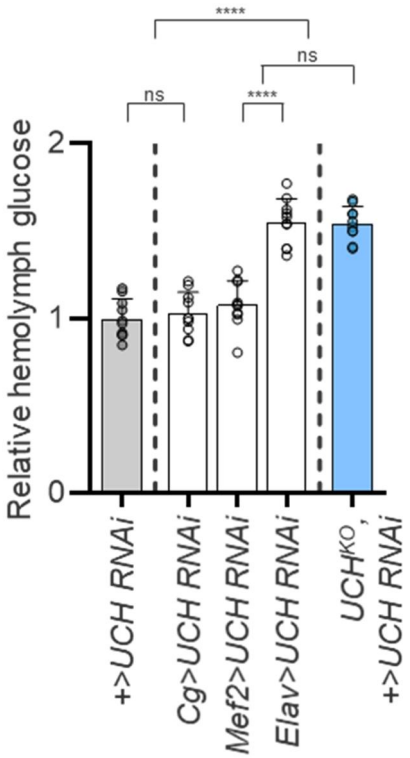

Figure 63. Neuron-specific knockdown of UCH elevated glycemia.

Relative levels of hemolymph glucose normalized to the glycemia of control (+>*UCH RNAi*). $n = 10$. Two-way ANOVA with Sidak's multiple comparison test was used. ****$p < 0.001$, and ns ($p > 0.05$). All data were presented as mean + SD.

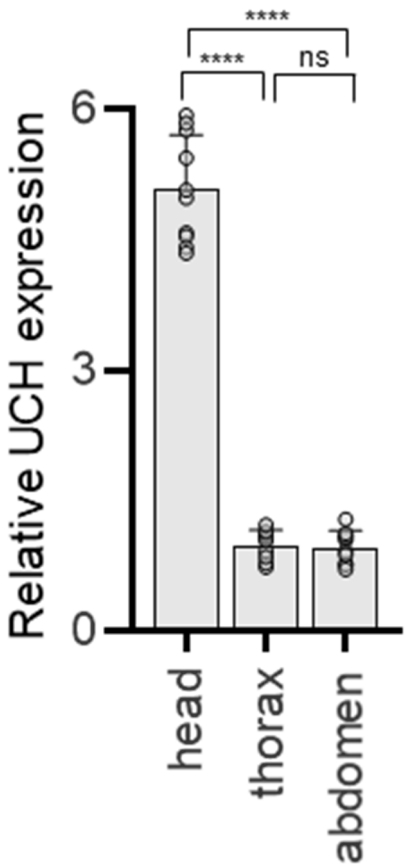

Figure 64. UCH was mainly expressed in fly heads.

Relative expressions of UCH in the fly head, thorax, or abdomen normalized to ribosomal protein 49 (rp49) expression. *n* = 10. One-way ANOVA with Dunnett's multiple comparison test was used. ****$p < 0.0001$, and ns ($p > 0.05$). All data were presented as mean + SD.

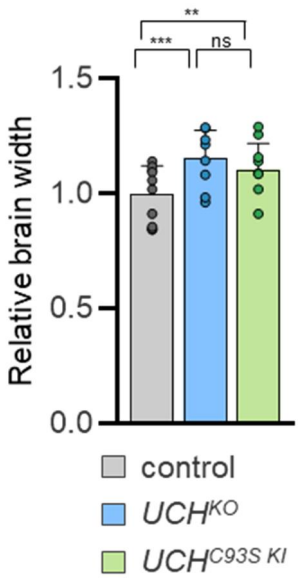

Figure 65. The brains of UCH mutant flies were larger than those of control flies.

Relative width of the fly brains normalized to control. *n* = 10. One-way ANOVA with Dunnett's multiple comparison test was used. **p < 0.01, ***p < 0.001, and ns (p > 0.05). All data were presented as mean + SD.

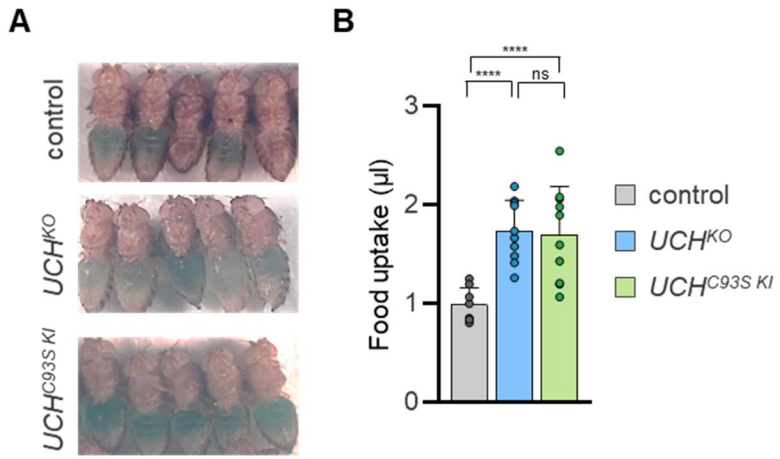

Figure 66. Food uptake of *UCH^{KO}* and *UCH$^{C93S\ KI}$* was increased at older ages.

(A) Visualized food uptake of the 30-day-old flies of indicated genotypes by the accumulation of green-dyed food in the stomach. **(B)** Measurement of 30-day-old fly food uptake by CAFÉ assay. n = 10. One-way ANOVA with Dunnett's multiple comparison test was used **(B)**. ****$p < 0.0001$, and ns ($p > 0.05$). All data were presented as mean + SD.

Insulin sensitivity was elevated by UCH overexpression in various tissues of *Drosophila*

Since UCH dysfunctions caused insulin resistance, I hypothesized that UCH overexpression could elevate insulin sensitivity. Therefore, I generated T2D model flies by high sugar diet (HSD) and expressed UCH in these flies. As expected, UCH overexpression by brain-specific GAL4 driver, *elav*-GAL4, decreased the hyperglycemia in HSD flies. Surprisingly, UCH overexpression using other tissue gal4 drivers, *mef2*- or *cg*-GAL4, also reduced the increased glycemia induced by HSD. Expressing UCH exogenously by whole body GAL4 driver, *hs*-GAL4, completely rescued the glycemia by the normal glycemic levels **(Fig. 67)**. Furthermore, the impaired glucose tolerance from HSD flies was rescued by UCH expression **(Fig. 68)**. These results suggested that insulin resistance was improved by UCH overexpression in any tissues. However, as the endogenous expression of UCH was abundant only in *Drosophila* head, UCH mutant flies showed neuron-specific insulin resistance. In conclusion, UCH might play critical role in keeping insulin sensitivity.

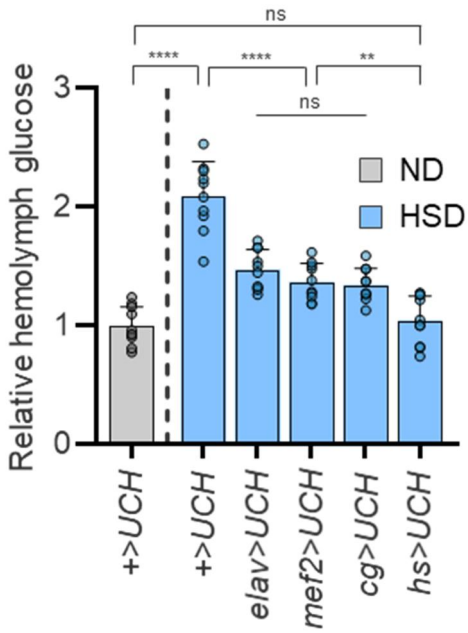

Figure 67. Hyperglycemia induced by HSD was decreased by UCH expression.

Relative levels of hemolymph glucose normalized to the glycemia of control (+>*UCH*) with normal diet (ND). n = 10. Two-way ANOVA with Sidak's multiple comparison test was used. **p < 0.01, ****p < 0.0001, and ns (p > 0.05). All data were presented as mean + SD.

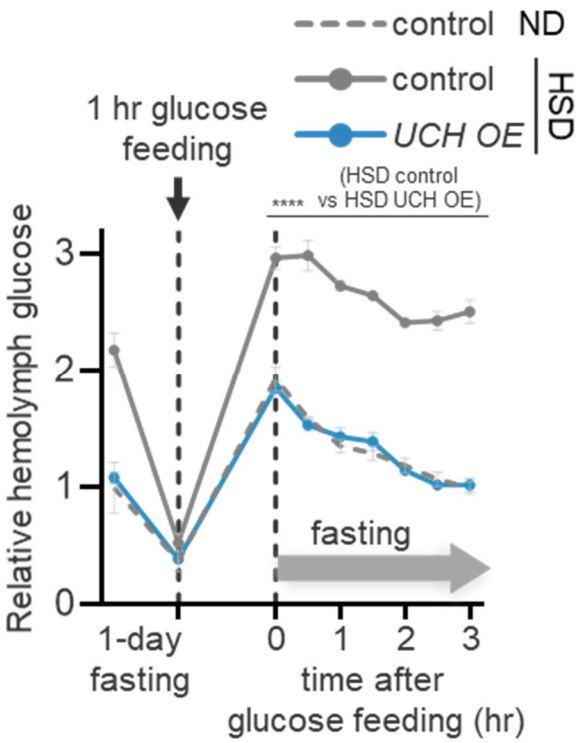

Figure 68. Impaired glucose tolerance by HSD was alleviated by UCH overexpression.

Relative levels of hemolymph glucose normalized to the glycemia of control with ND before 1-day fasting. Flies fasted for 1 day, and then they ate glucose containing food for 1 hour. After feeding, the flies fasted again. n = 3. Genotype, control (*hs*>+), and UCH OE (*hs*>*UCH*). One-way ANOVA with Dunnett's multiple comparison test was used. ****$p < 0.0001$. All data were presented as mean ± SD.

UCHL1 deficiency progressively caused death of sensory neurons and numbness to noxious stimuli with age

As UCH expression is important for maintaining insulin sensitivity, I thought that the cells or tissues in which the endogenous UCH expression is highly elevated might be vulnerable in UCH mutant flies. According to human and mouse gene expression data from all RNA-sequencing and chromatin immunoprecipitation-sequencing sample and signature search (ARCHS4) (Lachmann et al., 2018), UCHL1 is mainly expressed in the nervous system, especially in sensory neurons **(fig. 69)**. Also, one of the diabetic complications, neuropathy, is developed by the loss of sensory neurons. Therefore, I ascertained that diabetic neuropathy (DN)-like phenotypes might be developed in UCH mutants.

Since the death of leg sensory neurons are the main symptoms of DN, I observed the sensory neurons in the front leg tarsus segment using *OK371*-GAL4, a glutamatergic neuronal driver which can target sensory neurons **(Fig. 70)**. I also used UAS-nuclear localization signal (NLS)-tagged GFP which could visualize the sensory nucleus for measuring the number of sensory neurons. The number of sensory neurons in UCH^{KO} and $UCH^{C93S\ KI}$ flies had no differences compared to WT flies when they were young. However, the number of sensory neurons was significantly decreased in UCH^{KO} and $UCH^{C93S\ KI}$ at older ages **(Fig. 71)**. Thus, I concluded that the loss of plantar sensory neurons was induced by UCH malfunction in *Drosophila*.

Also, I examined pain escape responses of UCH mutants under virulent stimuli, similar to DN symptoms from T2D patients. I mounted flies on a 43℃ plate to conduct noxious heat stimuli to flies and measured the time when the flies started jumping (pain escape). The two fly lines carrying UCH KO or C93S KI mutations showed similar escape responses compared to WT flies when they are young (3-day flies). However, the nociception to the physical stimulation decreased with age in UCH^{KO} and $UCH^{C93S\ KI}$ flies **(Fig. 72A)**. In addition to the decreased responses to heat stimulation, I decided to measure pain escape upon chemical responses. I placed flies on the plate filled with 12% sulfuric acid and investigated the jumping responses. Consistent with the heat stimuli results, the flies with UCH dysfunction showed normal pain escape responses compared with control flies at young ages. However, at their old ages, the two types of UCH mutant flies reacted to the chemical stimulation less than WT flies **(Fig. 72B)**. Furthermore, I observed that the locomotor activities of UCH^{KO} or $UCH^{C93S\ KI}$ were similar to those of control flies **(Fig. 73)**.

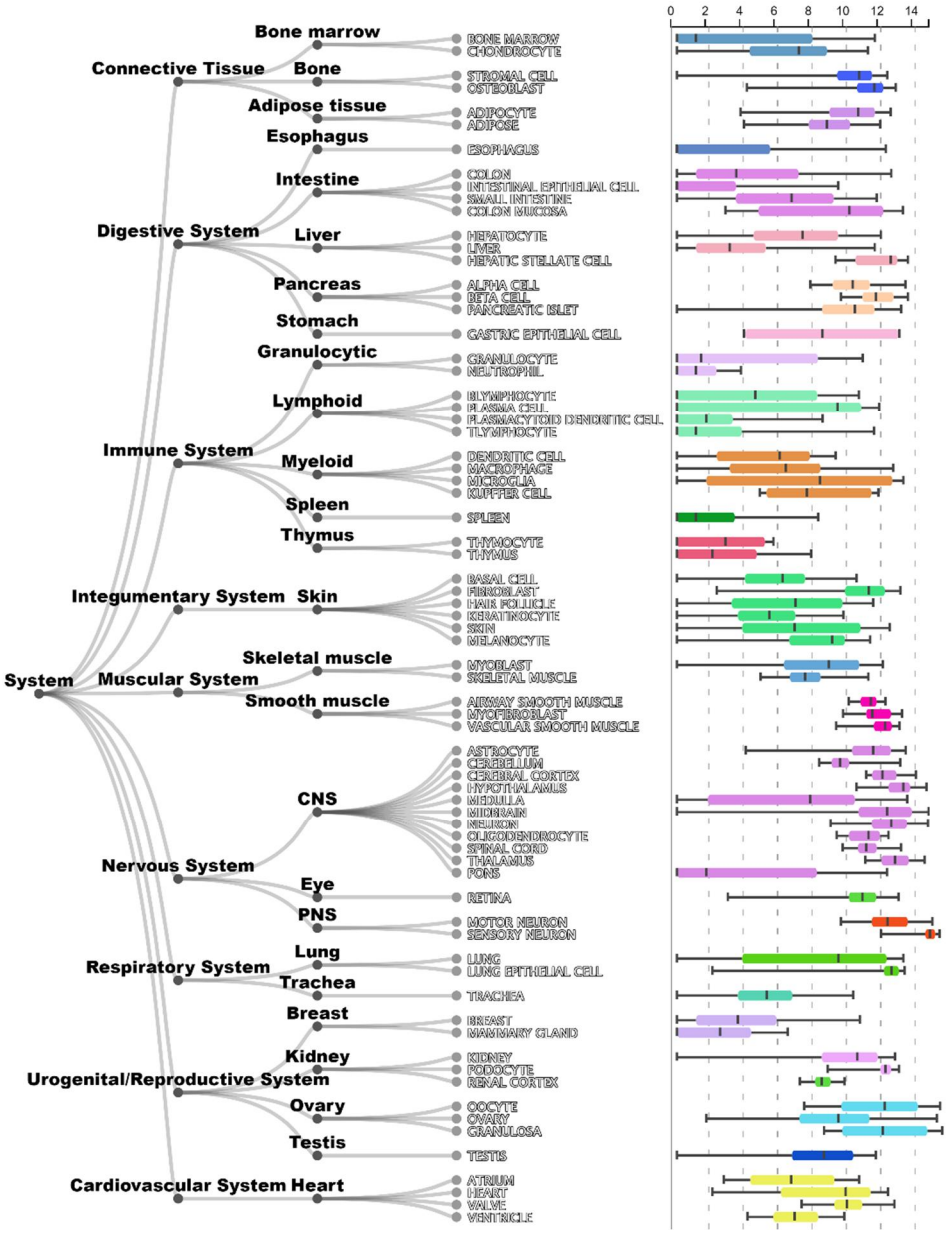

Figure 69. UCHL1 is highly expressed in sensory neurons.

Images are obtained from ARCHS4.

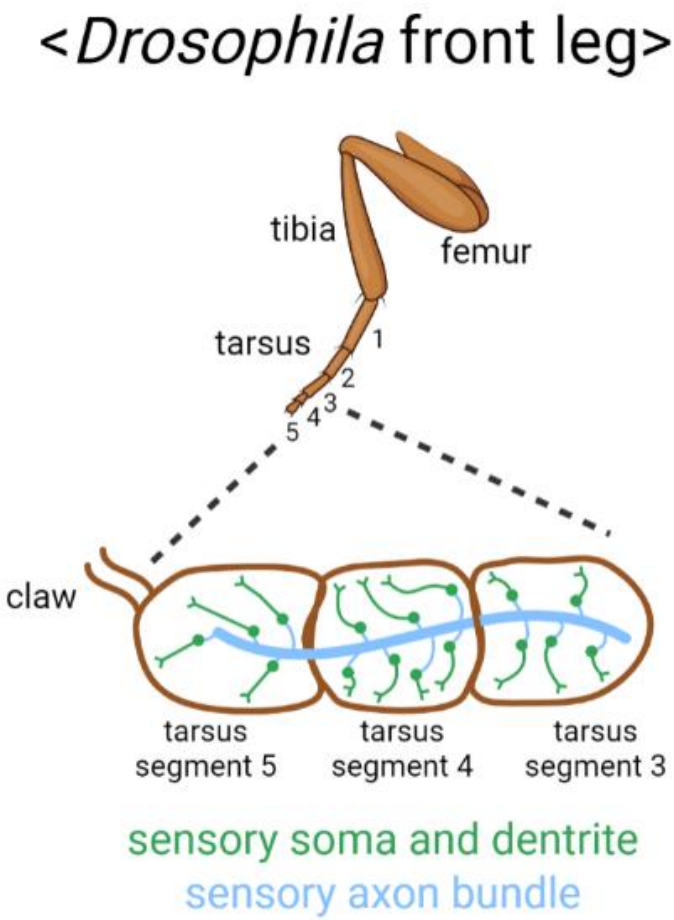

Figure 70. Illustration depicting a front leg of *Drosophila*.

Image was generated from Biorender.

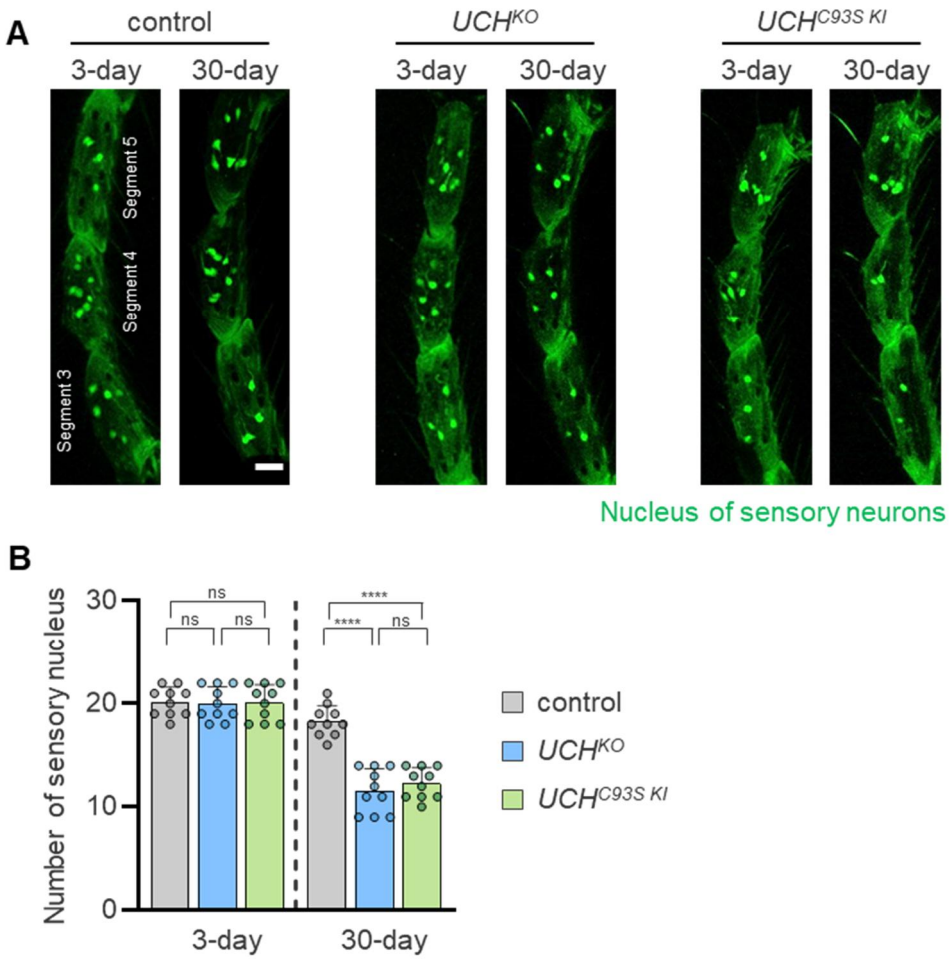

Figure 71. Sensory neurons in the fly tarsus segments were decreased by UCH mutations.

(A) Confocal fluorescence images of tarsus segment 3, 4, and 5 in 3-day-old or 30-day-old adult *Drosophila*. Green indicates nucleus of sensory neurons. Scale bar, 20 μm. **(B)** Numbers of sensory nucleus in tarsus segment 3, 4, and 5. $n = 10$. Two-way ANOVA with Sidak's multiple comparison test was used **(B)**. ****$p < 0.0001$, ns ($p > 0.05$). All data were presented as mean + SD.

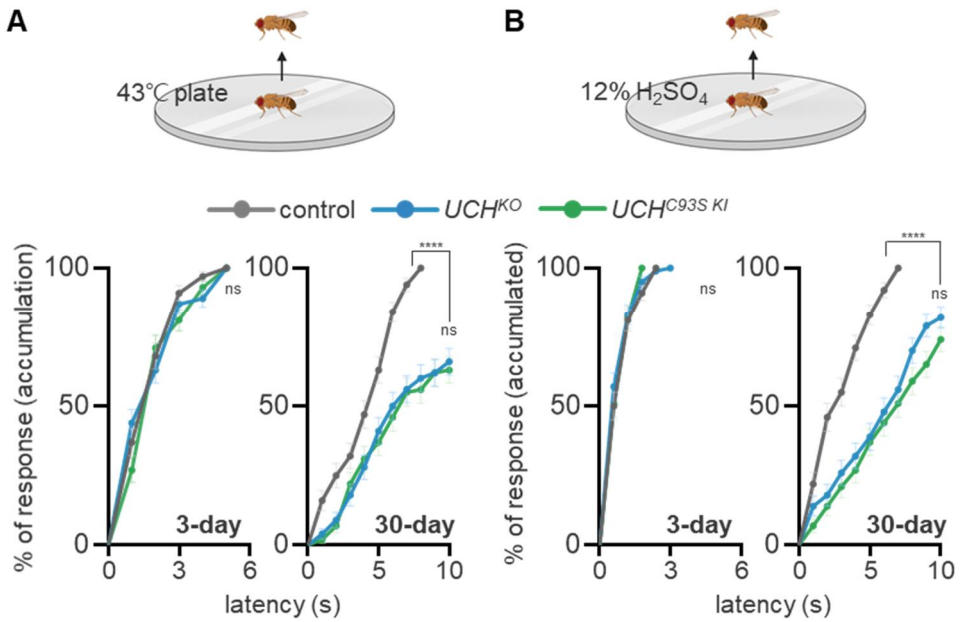

Figure 72. Pain escape responses were reduced by the loss-of-function mutations of UCH.

(A) Measurement of jumping responses upon 43℃ heat stimuli of 3-day- or 30-day-old flies. *n* = 100. **(B)** Measurement of jumping responses upon 43℃ heat stimuli of 3-day- or 30-day-old flies. *n* = 100. Log-rank (Mantel-Cox) tests were used to identify statistical significance between different groups **(A and B)**. ****p < 0.0001, and ns (p > 0.05). All data were presented as mean ± SD.

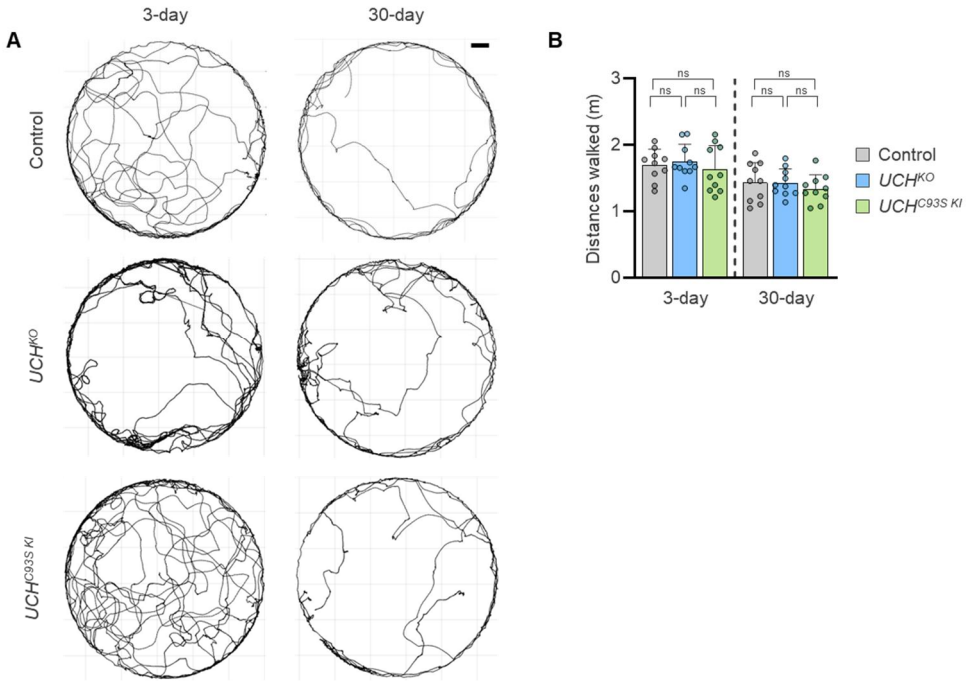

Figure 73. Locomotion of *UCH*^{KO} and *UCH*$^{C93S\ KI}$ flies was similar to control flies at both young and old ages.

(A) Walking trajectories of 3 flies of indicated genotype for 5 minutes. The flies were 3-day-old or 30-day-old. Scale bar, 10 mm. **(B)** Measurement of the distances fly walked for 5 minutes. $n = 10$. Two-way ANOVA with Sidak's multiple comparison test was used. ns ($p > 0.05$). All data were presented as mean + SD.

UCHL1 overexpression rescued the neuropathy-like phenotypes induced by high sugar diet (HSD)

I sought to identify that UCH overexpression could rescue DN-like phenotypes as well as insulin resistance or hyperglycemia. Firstly, I observed that DN-like phenotypes, sensory neuronal death, and numbness to the stimulations, were induced by HSD **(Fig. 74)**. Intriguingly, the reduced number of sensory neurons developed by HSD was rescued by overexpressing UCH in sensory neurons **(Fig. 74)**. I also found that the flies with HSD showed numbness to the heat and acid stimuli progressively with age. When the flies were 30-day old, the decreased nociception to the heat and acid stimulation in WT flies was mitigated by the sensory neuronal overexpression of UCH **(Fig. 75)**.

For further investigation, I tried to observe the correlations between sensory neuronal death and increased glycemia. I knocked down UCH in sensory neurons using *OK371*-GAL4. The sensory neuronal knockdown of UCH was not enough to elevate glycemia of flies, but developed into sensory neuronal degeneration **(Fig. 76A and 76B)**. Also, sensory neuronal UCH overexpression did not decrease the hyperglycemia in UCH KO flies, but rescued the sensory neuronal death in UCH mutant flies **(Fig. 76C and 76D)**. Therefore, I proposed that the sensory neuronal death in UCH mutant flies or HSD flies was caused by insulin resistance in sensory neurons, not the elevated glycemia near sensory neurons.

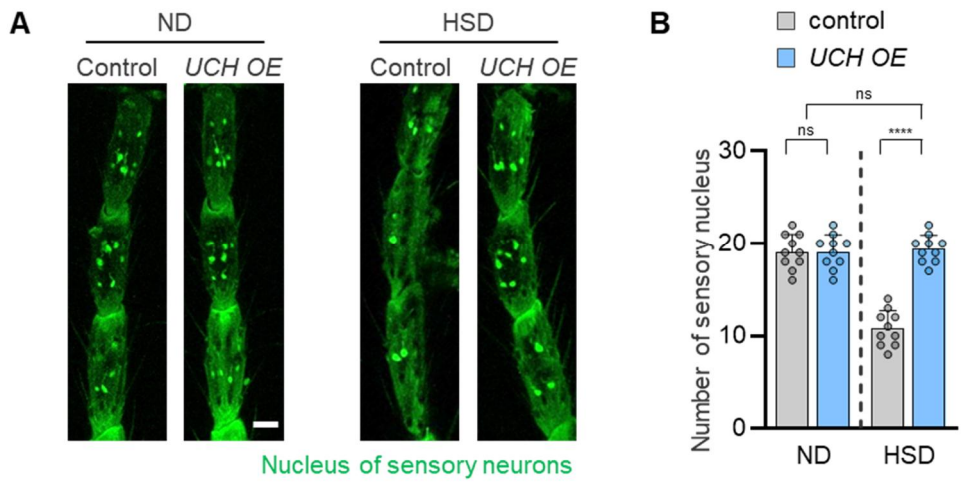

Figure 74. HSD-induced loss of sensory neurons in the fly tarsus segments was rescued by UCH expression.

(A) Confocal fluorescence images of tarsus segment 3, 4, and 5 in 30-day-old adult flies with ND or HSD. Green indicates nucleus of sensory neurons. Scale bar, 20 μm. **(B)** Numbers of sensory nucleus in tarsus segment 3, 4, and 5. n = 10. Genotype, control (*OK371>+*), and UCH OE (*OK371>UCH*). Two-way ANOVA with Sidak's multiple comparison test was used **(B)**. ****p < 0.0001, ns (p > 0.05). All data were presented as mean + SD.

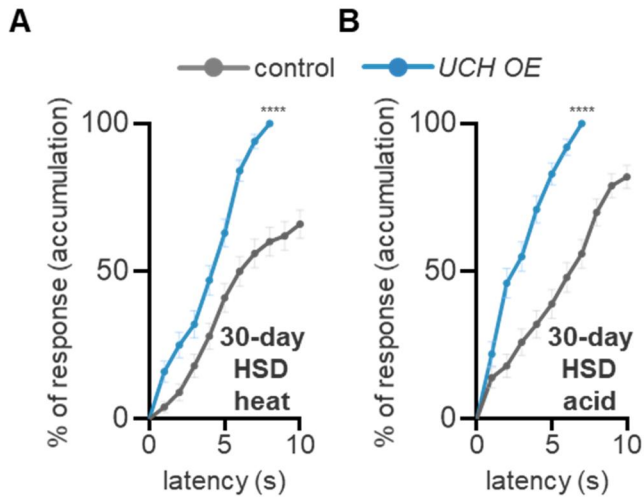

Figure 75. Decreased nociception developed by HSD was rescued by overexpressing UCH.

(A) Measurement of jumping responses upon 43°C heat stimuli of 30-day-old flies with HSD. n = 100. **(B)** Measurement of jumping responses upon 43°C heat stimuli of 3-day- or 30-day-old flies. n = 100. Genotype, control (*OK371>+*), and UCH OE (*OK371>UCH*). Log-rank (Mantel-Cox) tests were used to identify statistical significance between different groups **(A and B)**. ****$p < 0.0001$. All data were presented as mean ± SD.

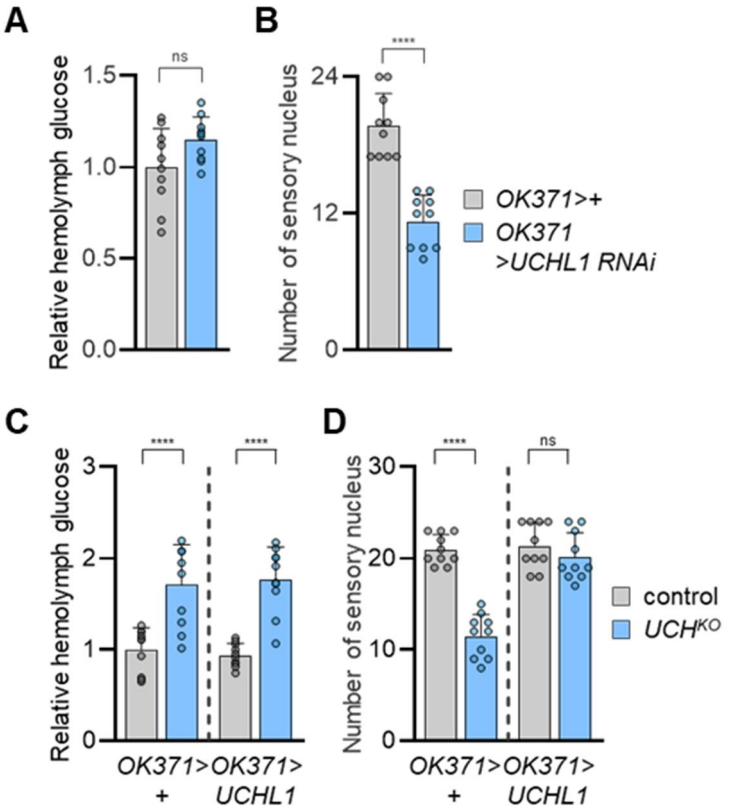

Figure 76. The degeneration of sensory neurons was induced autonomously regardless of hyperglycemia.

(A) Relative levels of hemolymph glucose normalized to the glycemia of control (*OK371*>+). *n* = 10. **(B)** Numbers of sensory nucleus in tarsus segment 3, 4, and 5. *n* = 10. **(C)** Relative levels of hemolymph glucose normalized to the glycemia of control (*OK371*>+). *n* = 10. **(D)** Numbers of sensory nucleus in tarsus segment 3, 4, and 5. *n* = 10. Two-way ANOVA with Sidak's multiple comparison test was used **(A, B, C, and D)**. ****p < 0.0001, and ns (p > 0.05). All data were presented as mean + SD.

Insulin signaling was downregulated in UCHL1 KO cells

It has been reported that decreased insulin signaling is one of the main causes of T2D development (Boucher et al., 2014). Therefore, I measured the phosphorylation of ribosomal protein S6 kinase (S6K) and AKT in UCHL1 KO cell lines to identify insulin signaling. As expected, the insulin signaling was decreased in UCHL1 KO cells **(Fig. 77)**.

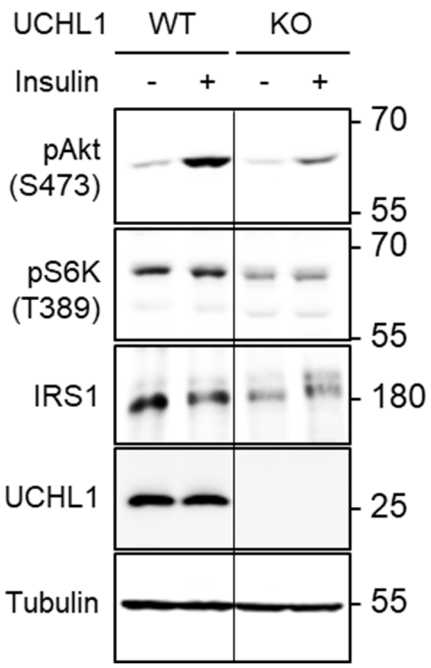

Figure 77. Downregulated insulin signaling and decreased amount of IRS1 were exhibited in UCHL1 KO cells.

Immunoblot analysis of the AKT and S6K phosphorylation in UCHL1 WT and KO HEK293E cell lines with or without 200 nM insulin treatment for 30 min.

UCHL1 regulated insulin signaling through IRS1

I determined to find a specific target of UCHL1 which can regulate insulin signaling. First of all, I tested if the well-known components of the insulin pathway can control hyperglycemia in UCH^{KO} flies. I expressed a constitutively active form of insulin receptor (InR^{CA}), insulin receptor substrate 1 (IRS1), constitutively active form of phosphoinositide 3-kinases ($PI3K^{CAAX}$), and constitutively active form of AKT (myrAKT) in UCH^{KO} flies using *elav*-GAL4 and measured the glycemia of each fly. Though the expression of InR^{CA} did not alter the hyperglycemia of UCH^{KO}, the flies with overexpression of IRS1, $PI3K^{CAAX}$, or myrAKT rescued the elevated hemolymph glucose levels of UCH^{KO} flies **(Fig. 78)**. Therefore, I hypothesized that UCHL1 might interact with IRS1 and tested if UCHL1 could deubiquitinate IRS1. Astonishingly, the ubiquitination of IRS1 was reduced by expressing UCHL1 WT or UCHL1 RQ in HEK293 cell lines. However, expressing a catalytic dead form of UCHL1 did not decrease the IRS1 ubiquitination **(Fig. 79)**. Also, the amount of IRS1 was decreased in UCHL1 KO cells **(Fig. 77)**.

Furthermore, I observed that the diabetic phenotypes in UCH^{KO} could be ameliorated by IRS1 overexpression. In the glucose tolerance test, elevated glucose tolerance induced by UCH deletion was mitigated by exogenous expression of IRS1 **(Fig. 80)**. Also, the decreased pain responses to the heat stimulus of 30-day-old UCH^{KO} flies were dramatically rescued by IRS1

expression **(Fig 81)**. The loss of sensory neurons was improved by overexpressing IRS1 **(Fig. 82)**.

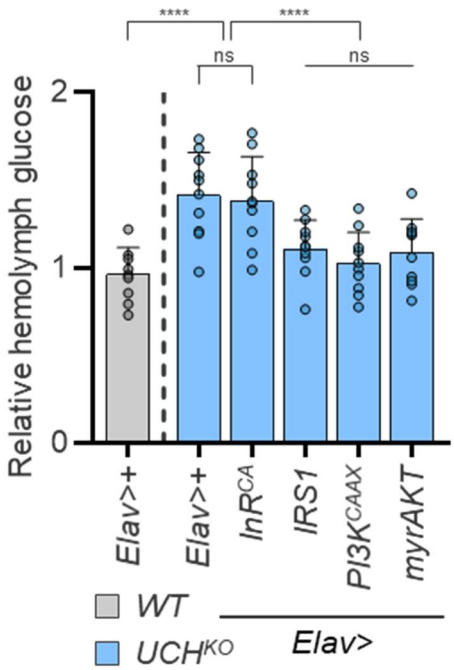

Figure 78. Hyperglycemia of *UCH*^{KO} flies was rescued by expressing IRS1, PI3K^{CAAX}, or myrAKT.

(A) Relative levels of hemolymph glucose normalized to the glycemia of control in WT background. *n* = 10. Two-way ANOVA with Sidak's multiple comparison test was used. ****p < 0.0001, and ns (p > 0.05). All data were presented as mean + SD.

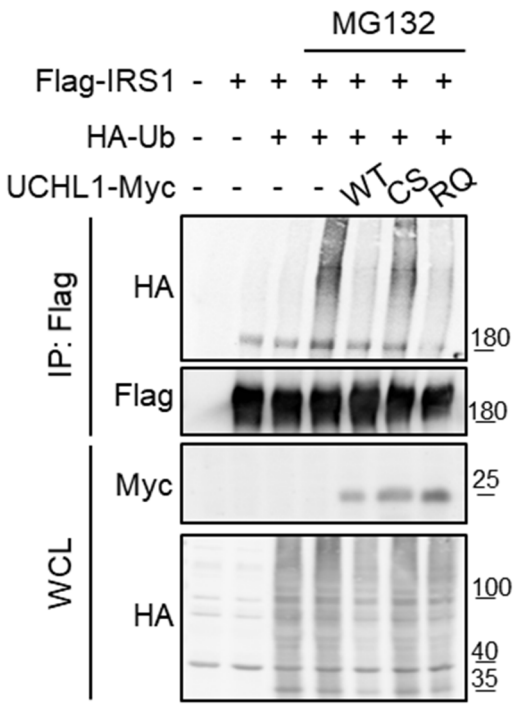

Figure 79. Ubiquitination of IRS1 was decreased by UCHL1 overexpression.

Immunoblot analysis of IRS1 ubiquitination in HEK293 cells. The cells were co-transfected with Flag-tagged IRS1, HA-tagged ubiquitin, and Myc-tagged UCHL1 WT, C90S, or R178Q upon 20 μM MG132 for 4 hours. IP: immunoprecipitation. WCL: whole-cell lysate.

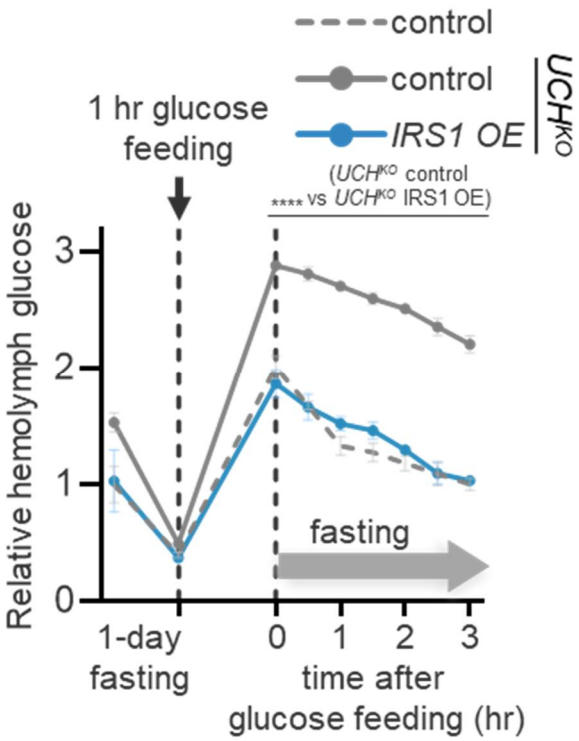

Figure 80. Impaired glucose tolerance of *UCH^{KO}* was mitigated by IRS1 overexpression in neurons.

Relative levels of hemolymph glucose normalized to the glycemia of control in WT background before 1-day fasting. Flies fasted for 1 day, and then they ate glucose containing food for 1 hour. After feeding, the flies fasted again. *n* = 3. Genotype, control (*elav*>+), and IRS1 OE (*elav*>*IRS1*). One-way ANOVA with Dunnett's multiple comparison test was used. ****$p < 0.0001$. All data were presented as mean ± SD.

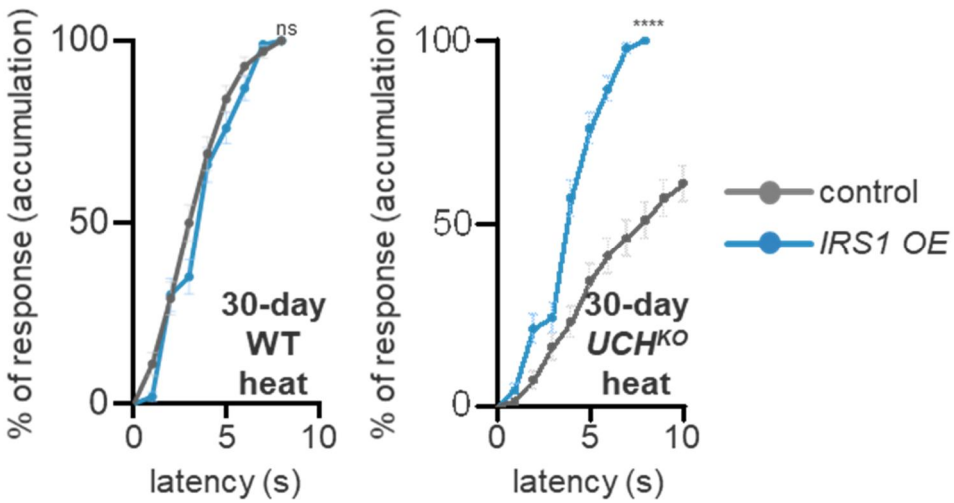

Figure 81. Decreased nociception developed by UCH deletion was rescued by overexpressing IRS1.

Measurement of jumping responses upon 43℃ heat stimuli of 30-day-old flies in WT or UCH^{KO} background. n = 100. Genotype, control (*OK371>+*), and IRS1 OE (*OK371>IRS1*). Log-rank (Mantel-Cox) tests were used to identify statistical significance between different groups. ****$p < 0.0001$. All data were presented as mean ± SD.

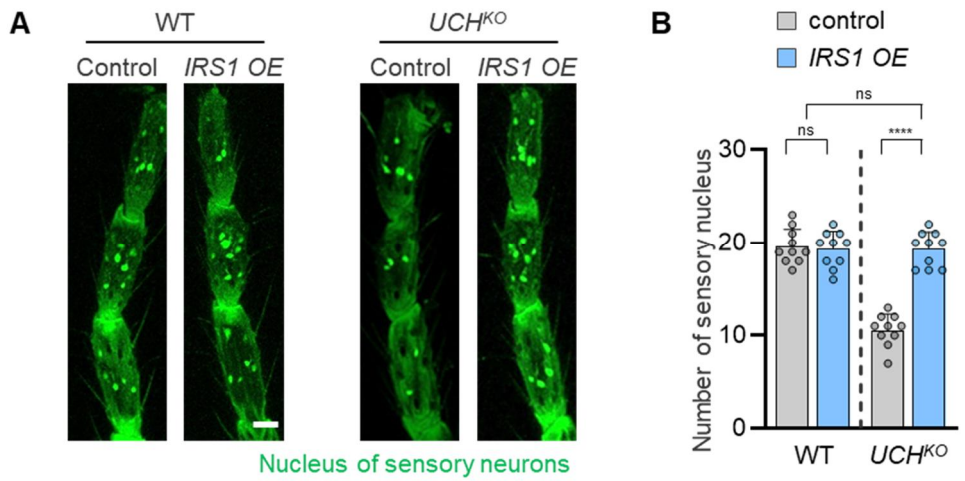

Figure 82. Loss of sensory neurons in *UCH^{KO}* tarsus segments was rescued by IRS1 expression.

(A) Confocal fluorescence images of tarsus segment 3, 4, and 5 in 30-day-old adult flies in WT or *UCH^{KO}* background. Green indicates nucleus of sensory neurons. Scale bar, 20 μm. **(B)** Numbers of sensory nucleus in tarsus segment 3, 4, and 5. n = 10. Genotype, control (*OK371>+*), and IRS1 OE (*OK371>IRS1*). Two-way ANOVA with Sidak's multiple comparison test was used **(B)**. ****$p < 0.0001$, ns ($p > 0.05$). All data were presented as mean + SD.

The E3 ligase CUL1 played an antagonistic role of UCHL1

Since UCHL1 reduced the ubiquitination levels of IRS1, I sought to find an enzyme that can ubiquitinate IRS1 while playing an antagonistic role of UCHL1. It has been reported that the six E3 ligases including Cbl proto-oncogene (CBL) (Nakao et al., 2009), Cullin-1 (CUL1) (Chen et al., 2022), Cullin-7 (CUL7) (Xu et al., 2008), MDM2 proto-oncogene (MDM2) (Li et al., 2021), tripartite motif containing 72 (TRIM72) (Lee et al., 2010), and TNF receptor associated factor 4 (TRAF4) ubiquitinates IRS1 and regulates its stability (Yu et al., 2021). However, as MDM2 and TRIM72 are not conserved in *Drosophila*, I used the four RNAi lines. I tested if UCHL1 could interact with these four E3 ligases and control the diabetic phenotypes in UCH^{KO} flies. I expressed the RNAi lines against each E3 ligase gene in UCH mutant flies using *elav*-GAL4 and measured the glycemia. Surprisingly, only CUL1 knockdown rescued the increased glycemia of UCH KO mutant flies **(Fig. 83)**. Furthermore, all the diabetic phenotypes of UCH^{KO}, including decreased pain responses to the heat stimulation **(Fig. 84)**, the impairments of sensory neurons in the tarsus segment **(Fig. 85)** were alleviated by CUL1 knockdown.

Furthermore, I sought to identify if the diabetic phenotypes were induced by CUL1 overexpression. Surprisingly, CUL1 overexpression in any tissues, including neurons, muscles, fat body, or whole-body, elevated glycemia **(Fig. 86)**. On the contrary to the results that UCH expression kept insulin sensitivity by stabilizing IRS1, I proposed that CUL1 expression

destroyed insulin resistance by destabilizing IRS1. Then, I tested if the diabetic phenotypes by CUL1 overexpression could be mitigated by overexpressing UCH. I found that the hyperglycemia induced by expressing CUL1 in *Drosophila* whole body was rescued by the concurrent expression of UCH **(Fig. 87)**. Also, the decreased pain responses against heat stimuli and the defects in the sensory neurons in the tarsus segments observed from CUL1 overexpression flies were rescued by UCH overexpression **(Fig. 88 and 89)**.

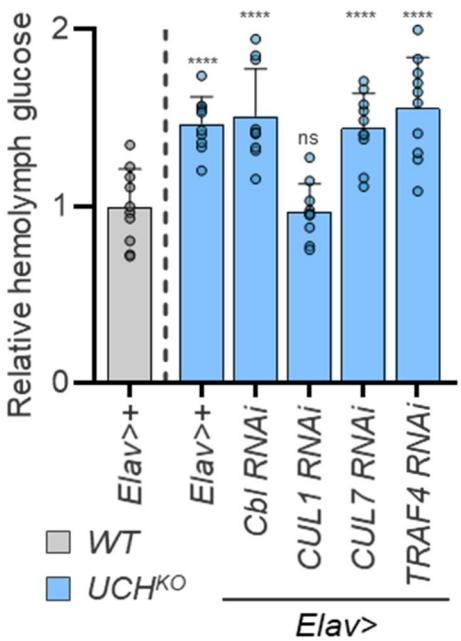

Figure 83. Hyperglycemia of *UCH^{KO}* flies was alleviated by CUL1 knockdown.

Relative levels of hemolymph glucose normalized to the glycemia of control in WT background. n = 10. Two-way ANOVA with Sidak's multiple comparison test was used. ****$p < 0.0001$, and ns ($p > 0.05$). All data were presented as mean + SD.

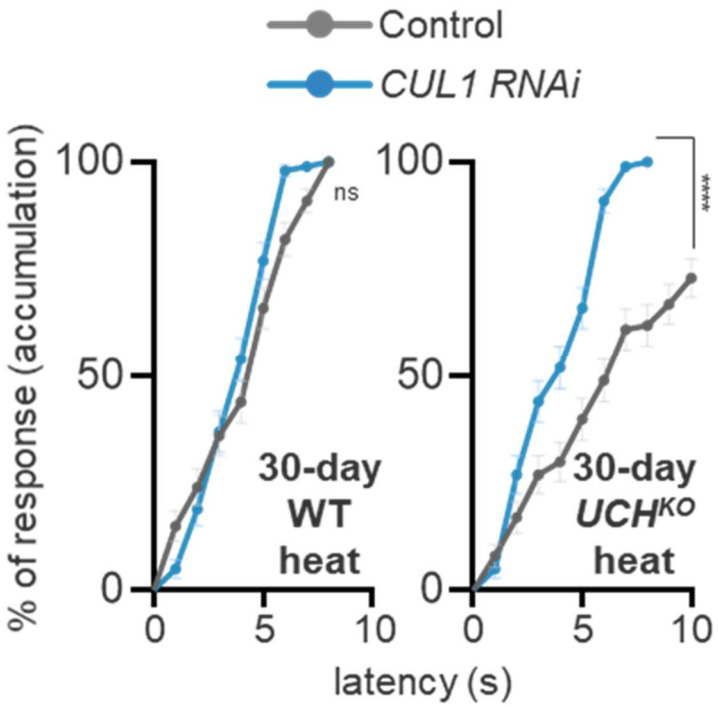

Figure 84. Decreased pain responses to the heat stimulation in UCH KO flies were improved by CUL1 knockdown.

Measurement of jumping responses upon 43℃ heat stimuli of 30-day-old WT or UCH^{KO} flies. n = 100. Genotype, control (*OK371*>+), and CUL1 RNAi (*OK371*>*CUL1 RNAi*). Log-rank (Mantel-Cox) tests were used to identify statistical significance between different groups. ****$p < 0.0001$, and ns ($p > 0.05$). All data were presented as mean ± SD.

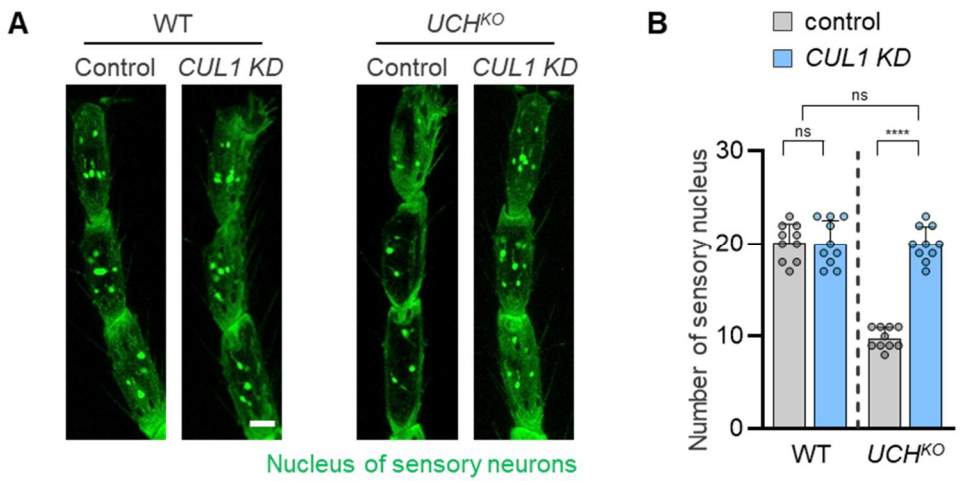

Figure 85. Loss of sensory neurons of *UCH^{KO}* tarsus segments was rescued by knocking down CUL1.

(A) Confocal fluorescence images of tarsus segment 3, 4, and 5 in 30-day-old adult *Drosophila*. Green indicates nucleus of sensory neurons. Scale bar, 20 μm. **(B)** Numbers of sensory nucleus in tarsus segment 3, 4, and 5. n = 10. Genotype, control (*OK371>+*), and CUL1 RNAi (*OK371>CUL1 RNAi*). Two-way ANOVA with Sidak's multiple comparison test was used **(B)**. ****p < 0.0001, ns (p > 0.05). All data were presented as mean + SD.

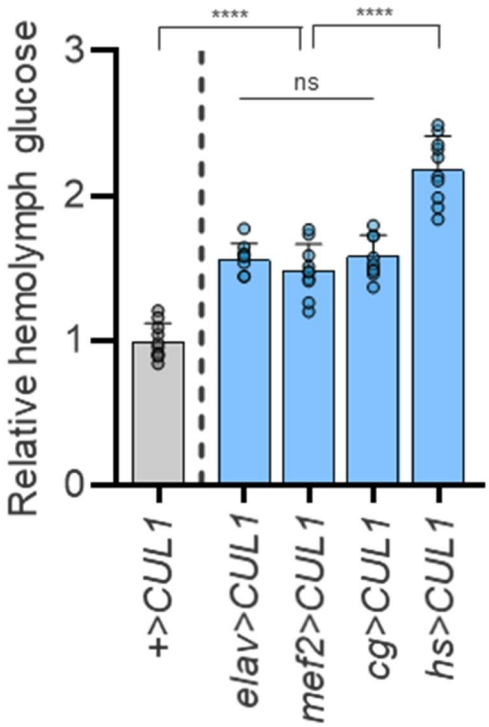

Figure 86. Increased glycemia was induced by CUL1 overexpression.

Relative levels of hemolymph glucose normalized to the glycemia of control (+>*CUL1*). $n = 10$. One-way ANOVA with Sidak's multiple comparison test was used. ****$p < 0.0001$, and ns ($p > 0.05$). All data were presented as mean + SD.

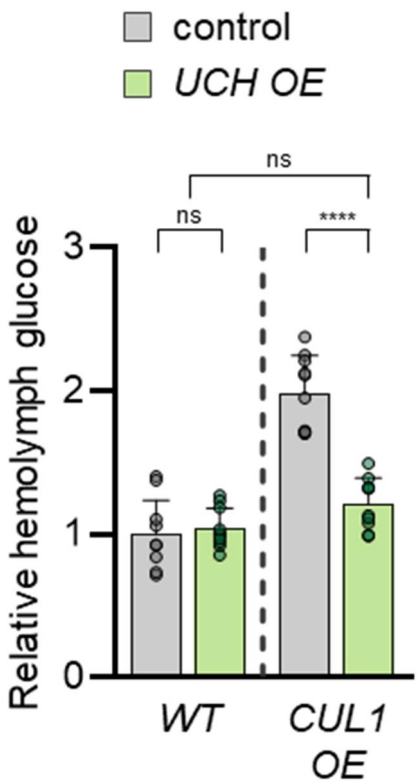

Figure 87. Hyperglycemia induced by CUL1 overexpression was decreased by overexpressing UCH.

Relative levels of hemolymph glucose normalized to the glycemia of control in WT background. n = 10. Genotype, control (*hs*>+), and UCH OE (*hs*>*UCH*). Two-way ANOVA with Sidak's multiple comparison test was used. ****$p < 0.0001$, and ns ($p > 0.05$). All data were presented as mean + SD.

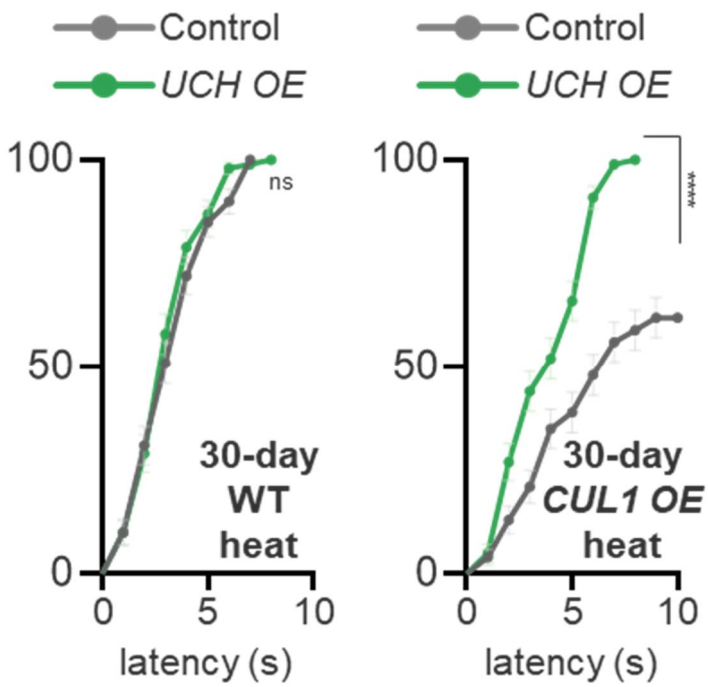

Figure 88. Decreased pain responses to the heat stimulation in CUL1 overexpressing flies were improved by UCH overexpression.

Measurement of jumping responses upon 43°C heat stimuli of 30-day-old flies with WT or CUL1 overexpression background. n = 100. Genotype, control (*OK371>+*), and UCH OE (*OK371>UCH*). Log-rank (Mantel-Cox) tests were used to identify statistical significance between different groups. ****$p < 0.0001$. All data were presented as mean ± SD.

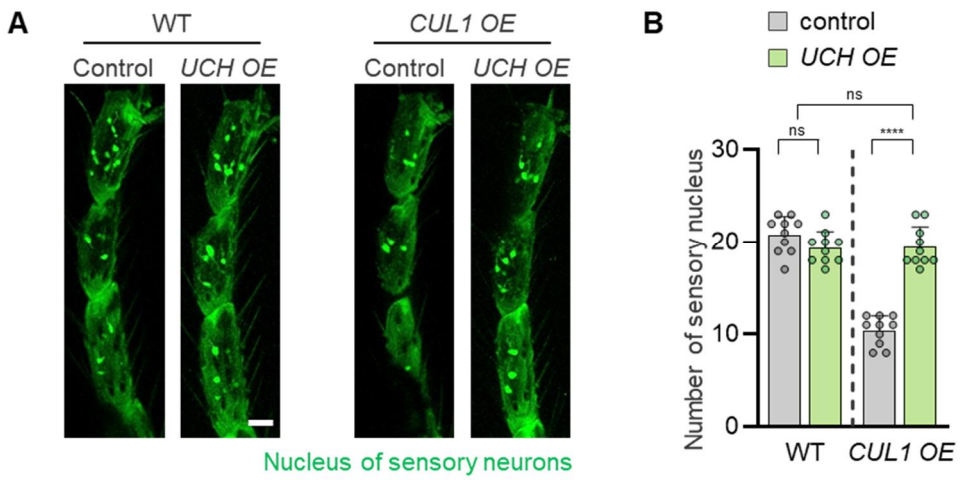

Figure 89. Loss of sensory neurons of CUL1 overexpressing flies was rescued by knocking down CUL1.

(A) Confocal fluorescence images of tarsus segment 3, 4, and 5 in 30-day-old adult *Drosophila*. Green indicates nucleus of sensory neurons. Scale bar, 20 μm. **(B)** Numbers of sensory nucleus in tarsus segment 3, 4, and 5. $n = 10$. Genotype, control (*OK371>+*), and UCH OE (*OK371>UCH*). Two-way ANOVA with Sidak's multiple comparison test was used **(B)**. ****$p < 0.0001$, ns ($p > 0.05$). All data were presented as mean + SD.

CUL1 expression was increased by HSD in *Drosophila*

According to these results, exogenous expression of UCH alleviated the diabetic flies developed by both HSD and CUL1 expression. Therefore, I hypothesized that HSD could affect the expressions of CUL1. I measured the mRNA expression levels of UCH and CUL1 while feeding high sugar food to the fruit flies. Although the expression of UCH was not altered by HSD, that of CUL1 was dramatically increased by HSD **(Fig. 90)**. Furthermore, contrary to the results that UCH expression was highly expressed in the fly heads, the expression of CUL1 did not show any tissue-specificity.

These UCH and CUL1 expression data could explain the results of **Fig. 67**. CUL1 transcription was elevated by HSD in every tissue, which made tissues resistant to insulin by ubiquitinating IRS1. Although the endogenous expression of UCH was mainly expressed in neurons, exogenous UCH overexpression in any tissues was able to improve insulin resistance induced by HSD-mediated CUL1 expression owing to its antagonistic roles of CUL1. Therefore, UCH expression in muscles or fat body could rescue the hyperglycemia developed by HSD.

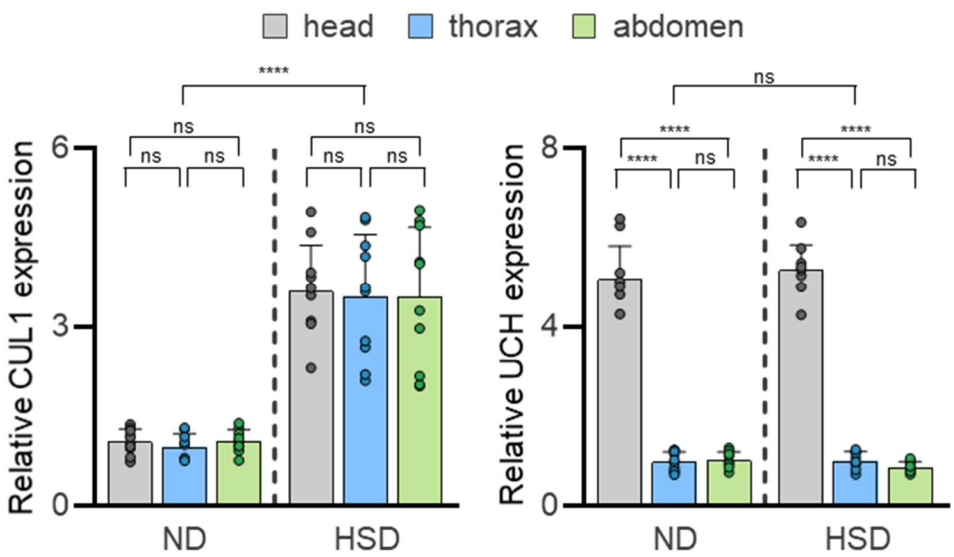

Figure 90. Gene expression levels of CUL1 were elevated by HSD.

Relative expressions of CUL1 and UCH normalized to ribosomal protein 49 (rp49) expression in the flies with normal diet (ND) or high sugar diet (HSD). $n = 10$. Student's t test was used. ****$p < 0.0001$, and ns ($p > 0.05$). All data were presented as mean + SD.

Snail is responsible for the elevated CUL1 transcription from HSD flies

I decided to identify a transcription factor which can elevate the expression of CUL1 responding to high sugar. Therefore, I used the *JASPAR* database (Castro-Mondragon et al., 2022) to specify transcription factor (TF) candidates for CUL1. The human and *Drosophila* locus around the translation start site (-350 to +150 base pair (bp)) of the CUL1 gene were analyzed. I found that a transcription factor, Snail, was able to regulate the transcription of CUL1 both in fruit flies and humans **(Fig. 91)**. Therefore, I measured CUL1 expression in the flies with ND or HSD while expressing Snail RNAi. The elevated transcription of CUL1 induced by HSD was decreased by knocking down Snail **(Fig. 92A)**. In addition, overexpressing Snail elevated the transcription of CUL1 **(Fig. 92B)**.

Therefore, I tested if the diabetic phenotypes induced by HSD can be rescued by knocking down Snail or CUL1. As expected, knockdown of Snail or CUL1 decreased the increased glycemia by high sugar feeding **(Fig. 93)**. Also, knocking down Snail or CUL1 rescued the reduced nociception **(Fig. 94)**, and the loss of sensory neurons **(Fig. 95)**.

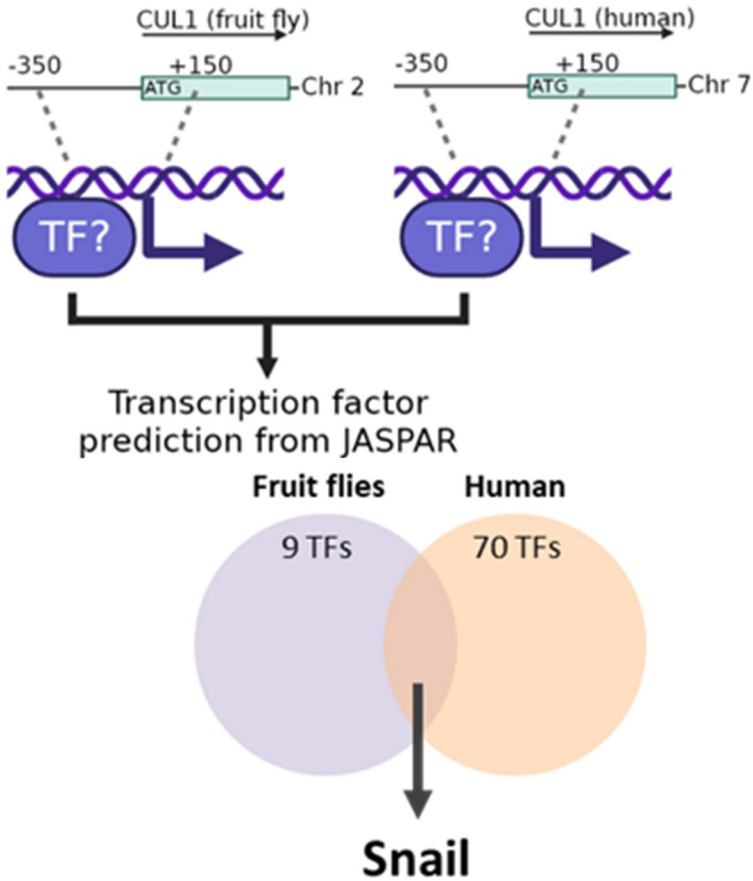

Figure 91. A schematic for finding a transcription factor for CUL1.

Nine TFs were identified as regulators for *Drosophila* CUL1 transcription and seventy TFs were identified as regulators for human CUL1 transcription. Sequences around the translation start site (-350 bp to +150 bp) in *Drosophila* and human were analyzed. Image was generated from Biorender.

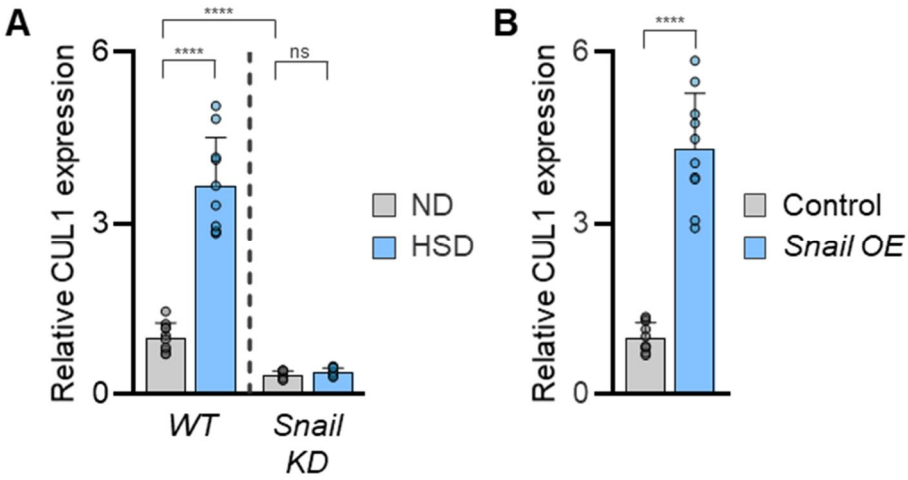

Figure 92. Gene expression levels of CUL1 correlate with Snail.

(A) Relative expression of CUL1 normalized to rp49 expression. $n = 10$. **(B)** Relative expression of CUL1 normalized to rp49 expression. $n = 10$. Genotype, WT (*hs*>+), Snail KD (*hs*>*Snail RNAi*), control (*hs*>+), and Snail OE (*hs*>*Snail*). Two-way ANOVA with Sidak's multiple comparison test was used **(A and B)**. ****$p < 0.0001$, and ns ($p > 0.05$). All data were presented as mean + SD.

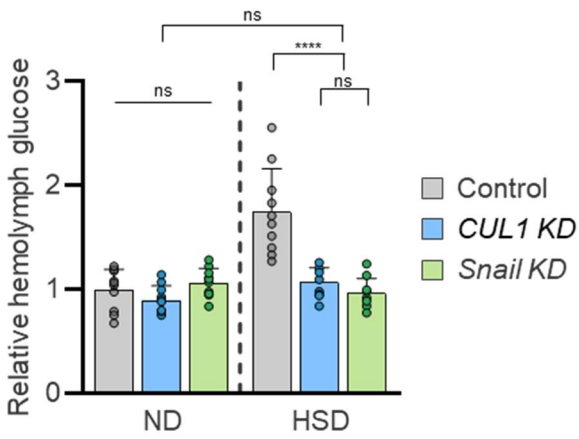

Figure 93. HSD-mediated hyperglycemia was rescued by CUL1 or Snail knockdown.

Relative levels of hemolymph glucose normalized to the glycemia of control feeding normal diet. $n = 10$. Genotype, control (*hs*>+), CUL1 KD (*hs*>*CUL1 RNAi*), and Snail KD (*hs*>*Snail RNAi*). Two-way ANOVA with Sidak's multiple comparison test was used. ****$p < 0.0001$, and ns ($p > 0.05$). All data were presented as mean + SD.

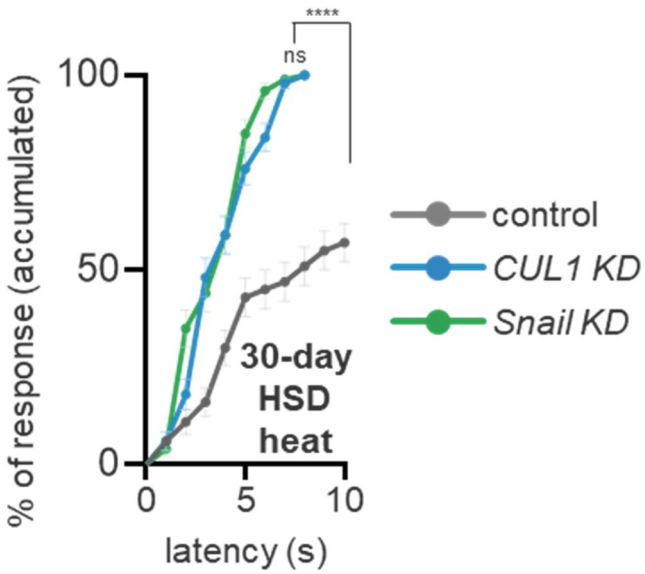

Figure 94. Decreased pain responses to the heat stimuli induced by HSD were mitigated by CUL1 or Snail knockdown.

Measurement of jumping responses upon 43℃ heat stimuli of 30-day-old flies with HSD. n = 100. Genotype, control (*OK371*>+), CUL1 KD (*OK371*>*CUL1 RNAi*), and Snail KD (*OK371*>*Snail RNAi*). Log-rank (Mantel-Cox) tests were used to identify statistical significance between different groups. ****$p < 0.0001$, and ns ($p > 0.05$). All data were presented as mean ± SD.

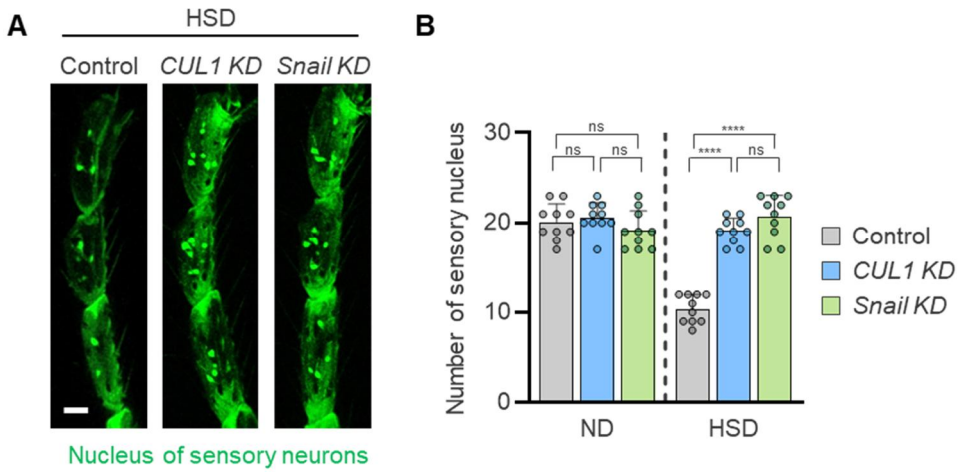

Figure 95. Loss of leg sensory neurons developed by HSD was rescued by knocking down CUL1 or Snail.

(A) Confocal fluorescence images of tarsus segment 3, 4, and 5 in 30-day-old adult flies with HSD. Green indicates nucleus of sensory neurons. Scale bar, 20 μm. **(B)** Numbers of sensory nucleus in tarsus segment 3, 4, and 5. $n = 10$. Genotype, control (*OK371>+*), CUL1 KD (*OK371>CUL1 RNAi*), and Snail KD (*OK371>Snail RNAi*). Two-way ANOVA with Sidak's multiple comparison test was used **(B)**. ****$p < 0.0001$, ns ($p > 0.05$). All data were presented as mean + SD.

Drosophila Shaggy regulated the transcription of CUL1 via Snail

According to previous studies, Snail is degraded through proteasomal degradation by glycogen synthase kinase 3 (GSK3)-mediated phosphorylation (Zhou et al., 2004). Also, the activity of GSK3 is controlled by AKT as a key component of insulin signaling (Liberman and Eldar-Finkelman, 2005). Therefore, I decided to observe the epistasis between Shaggy (Sgg), a *Drosophila* homolog of human GSK3, and Snail in the flies with HSD. I expressed the dominant negative (DN) form and constitutively active (CA) form of Sgg to measure the transcripts of CUL1. Expressing the dominant negative form of Sgg (Sgg^{DN}) elevated the transcription of CUL1 and the constitutively active form of Sgg (Sgg^{CA}) decreased the transcription of CUL1. However, HSD did not elevate the expression of CUL1 in these Sgg transgenic flies **(Fig. 96)**. Furthermore, the increased CUL1 expression in the flies with Sgg^{DN} overexpression was decreased by Snail knockdown **(Fig. 97)**. In conclusion, I ascertained that CUL1 transcription was regulated by GSK3/Snail axis under high sugar diet.

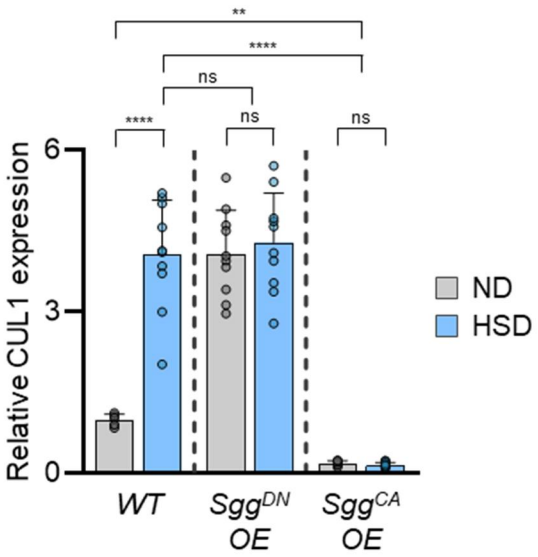

Figure 96. GSK3 negatively controlled CUL1 transcription.

Relative expression of CUL1 normalized to rp49 expression. n = 10. Genotype, WT (*hs*>+), Sgg^{DN} OE (*hs*>Sgg^{DN}), and Sgg^{CA} OE (*hs*>Sgg^{CA}). Two-way ANOVA with Sidak's multiple comparison test was used. **p < 0.01, ****p < 0.0001, and ns (p > 0.05). All data were presented as mean + SD.

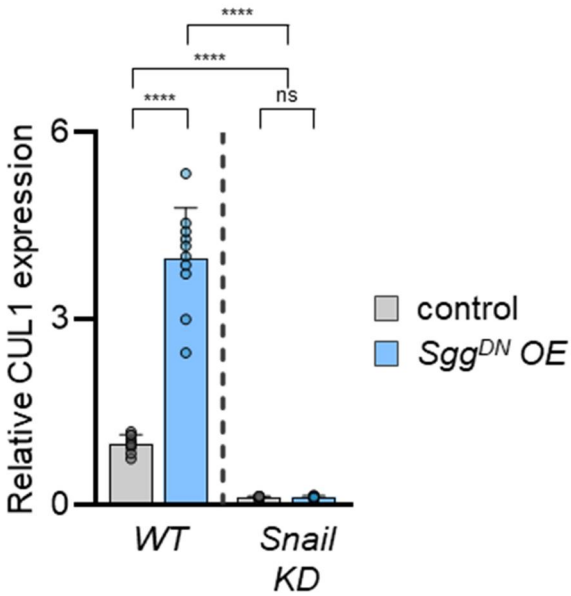

Figure 97. Snail knockdown blocked the elevated CUL1 expression from Sgg^{DN} overexpressing flies.

Relative expression of CUL1 normalized to rp49 expression. n = 10. Genotype, WT (*hs*>+), Snail KD (*hs*>*Snail RNAi*), control (*hs*>+), and Sgg^{DN} OE (*hs*>Sgg^{DN}). Two-way ANOVA with Sidak's multiple comparison test was used. ****$p < 0.0001$, and ns ($p > 0.05$). All data were presented as mean + SD.

The diabetic phenotypes induced by HSD were rescued by expressing a constitutively active form of Sgg

As Sgg activation reduced the expression of CUL1, I thought that the diabetic phenotypes induced by HSD could be alleviated by expressing Sgg^{CA} in *Drosophila*. As expected, the hyperglycemia in the flies feeding high sugar food was reduced by expressing Sgg^{CA} **(Fig. 98)**. Furthermore, numbness to noxious stimuli **(Fig. 99)** and the sensory neuronal defects **(Fig. 100)** in the high sugar feeding flies were rescued by expressing Sgg^{CA}.

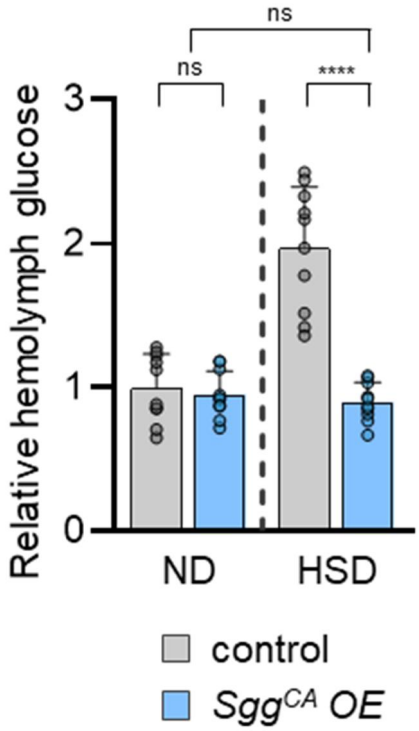

Figure 98. Hyperglycemia induced by HSD was rescued by Sgg^{CA} expression.

Relative levels of hemolymph glucose normalized to the glycemia of control feeding normal diet. n = 10. Genotype, control (*hs*>+), and Sgg^{CA} OE (*hs*>*Sgg*^{CA}). Two-way ANOVA with Sidak's multiple comparison test was used. ****p < 0.0001, and ns (p > 0.05). All data were presented as mean + SD.

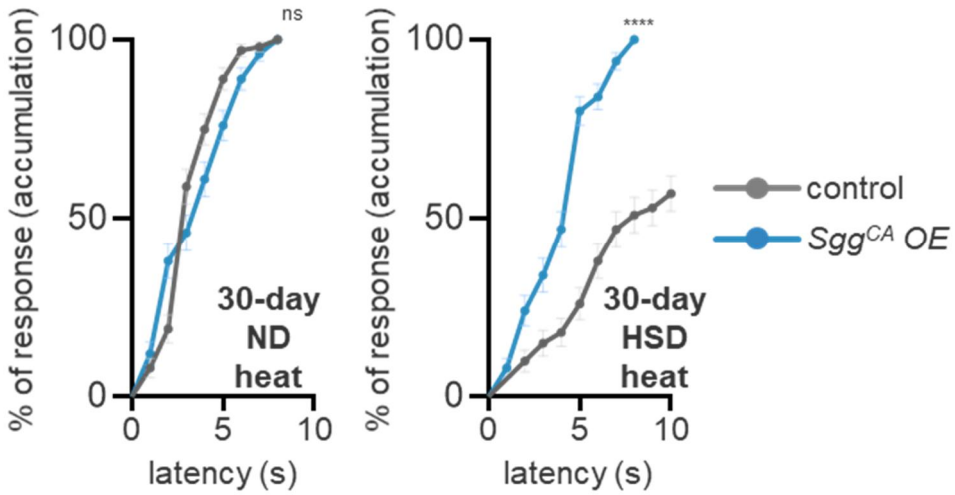

Figure 99. Decreased nociception in HSD flies was rescued by Sgg^{CA} expression.

Measurement of jumping responses upon 43°C heat stimuli of 30-day-old flies with ND or HSD. n = 100. Genotype, control (*OK371*>+), and Sgg^{CA} OE (*OK371*>Sgg^{CA}). Log-rank (Mantel-Cox) tests were used to identify statistical significance between different groups. ****p < 0.0001. All data were presented as mean ± SD.

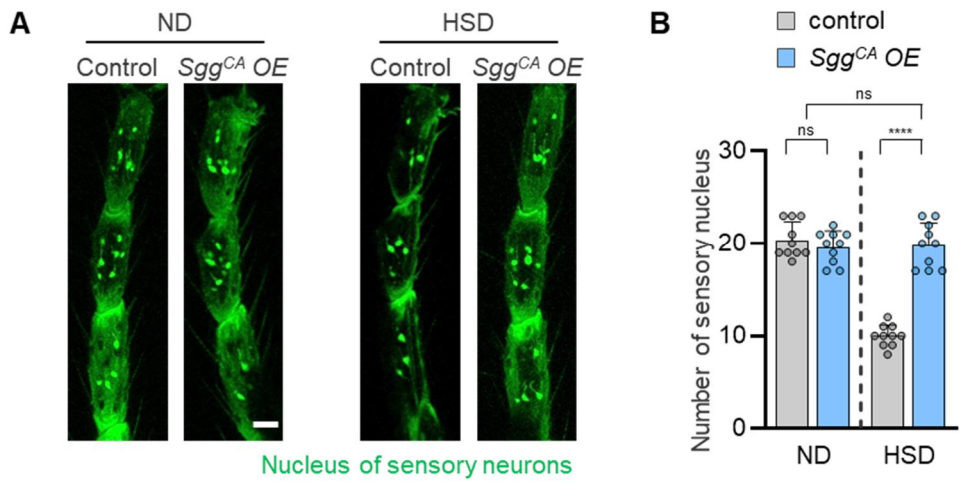

Figure 100. Loss of sensory neurons at tarsus segments induced by HSD was rescued by Sgg^{CA} expression.

(A) Confocal fluorescence images of tarsus segment 3, 4, and 5 in 30-day-old adult flies with ND or HSD. Green indicates nucleus of sensory neurons. Scale bar, 20 μm. **(B)** Numbers of sensory nucleus in tarsus segment 3, 4, and 5. n = 10. Genotype, control (*OK371*>+), and Sgg^{CA} OE (*OK371*>*Sgg^{CA}*). Two-way ANOVA with Sidak's multiple comparison test was used **(B)**. ****p < 0.0001, ns (p > 0.05). All data were presented as mean + SD.

The diabetic phenotypes induced by expressing dominant negative form of Sgg or Snail were rescued by CUL1 knockdown

Since the flies with CUL1 overexpression displayed diabetic and DN-like phenotypes, I tested if elevating CUL1 transcription by expressing the dominant negative form of Sgg or Snail in *Drosophila* developed into T2D and DN. As expected, expressing Sgg^{DN} or Snail exogenously using *hs*-GAL4 induced increased glycemia, degeneration of sensory neurons, and numbness to heat stimulation. However, the concurrent expression of CUL1 RNAi in these flies rescued all these phenotypes **(Fig. 101, 102, and 103)**.

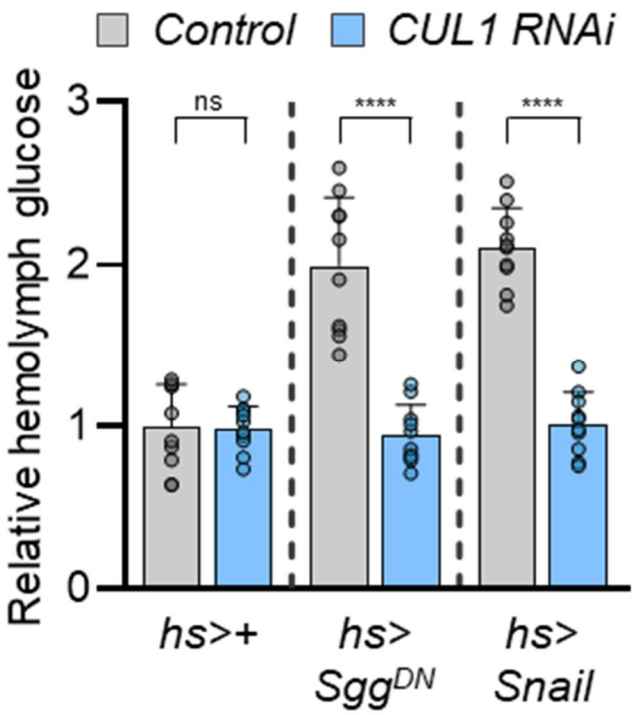

Figure 101. The increased glycemia induced by expressing Sgg^{DN} or Snail was rescued by CUL1 knockdown.

Relative levels of hemolymph glucose normalized to the glycemia of control (*hs*>+). n = 10. Genotype, control (*hs*>+), and CUL1 RNAi (*hs*>*CUL1 RNAi*). Two-way ANOVA with Sidak's multiple comparison test was used. ****$p < 0.0001$, and ns ($p > 0.05$). All data were presented as mean + SD.

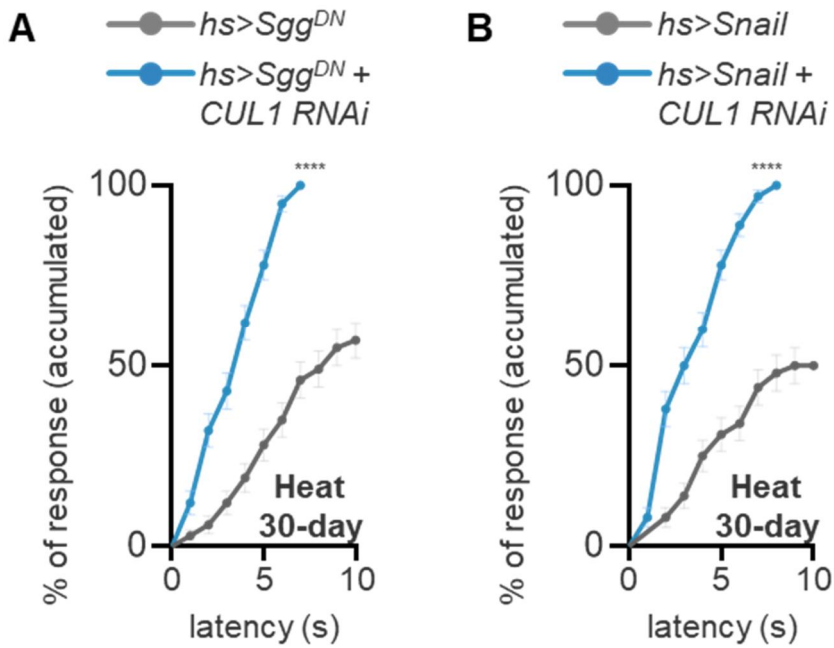

Figure 102. The numbness to the heat stimulation in the flies with Sgg^{DN} or Snail overexpression was improved by CUL1 knockdown.

(A and B) Measurement of jumping responses upon 43°C heat stimuli of 30-day-old flies. *n* = 100. Log-rank (Mantel-Cox) tests were used to identify statistical significance between different groups. ****p < 0.0001. All data were presented as mean ± SD.

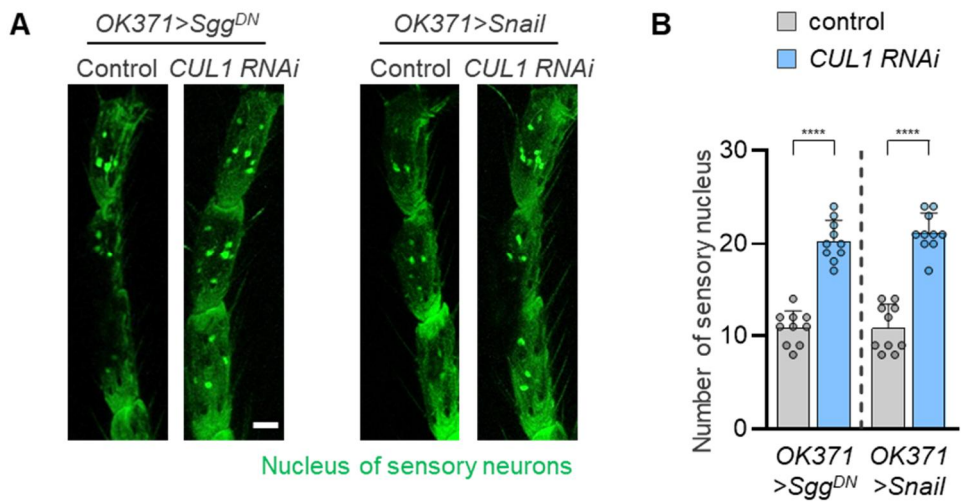

Figure 103. Loss of sensory neurons at tarsus segments induced by overexpressing Sgg^{DN} or Snail was rescued by knocking down CUL1.

(A) Confocal fluorescence images of tarsus segment 3, 4, and 5 in 30-day-old adult flies. Green indicates nucleus of sensory neurons. Scale bar, 20 μm. **(B)** Numbers of sensory nucleus in tarsus segment 3, 4, and 5. $n = 10$. Genotype, control (*OK371>+*), and CUL1 RNAi (*OK371>CUL1 RNAi*). Two-way ANOVA with Sidak's multiple comparison test was used **(B)**. ****$p < 0.0001$, ns ($p > 0.05$). All data were presented as mean + SD.

HSD-induced hyperglycemia was rescued by regulating neddylation enzymes

It has been reported that the ubiquitin ligase activity of the CUL1 complex is fully activated by conjugation of Nedd8, neddylation (Merlet et al., 2009; Schwechheimer, 2018). Therefore, I tested if the diabetic phenotypes in the flies with HSD could be rescued by regulating enzymes related to neddylation. Similar to ubiquitination, neddylation is a three-step process involving three types of enzymes, neddylation-activating enzyme (NAE; E1), nedd8-conjugating enzyme (E2), and nedd8-protein ligase (E3) (Rabut and Peter, 2008). CUL1 is a sequentially ubiquitin like modifier activating enzyme 3 (UBA3) (E1), ubiquitin conjugating enzyme E2 M (UBE2M) (E2), and ring-box 1 (RBX1) (E3) (Zhou et al., 2018) and these three enzymes are well conserved in *Drosophila*. Therefore, I measured the hemolymph glucose levels in the flies with HSD or CUL1 overexpression by knocking down UBA3, UBE2M, and RBX1. Surprisingly, the hyperglycemia in the flies feeding HSD or overexpressing CUL1 was diminished by knocking down these three enzymes associated with neddylation **(Fig. 104)**. Therefore, I thought that HSD-induced diabetic phenotypes could be rescued by neddylation inhibition.

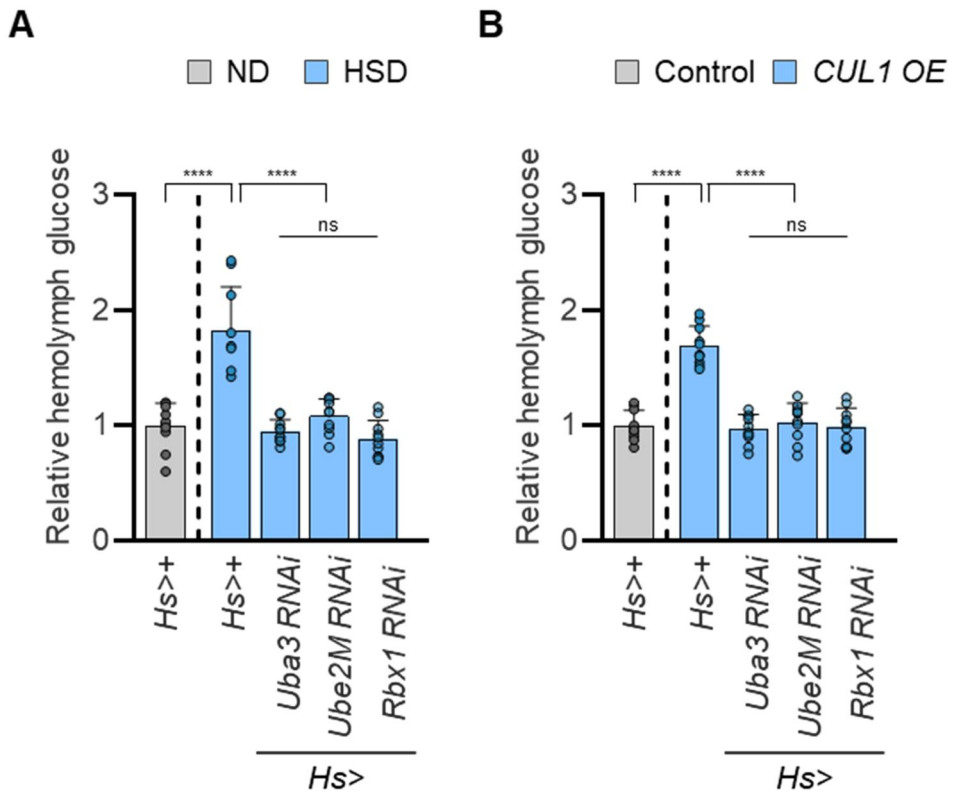

Figure 104. Knocking down neddylation enzymes rescued increased glycemia induced by HSD or CUL1 overexpression.

(A) Relative levels of hemolymph glucose normalized to the glycemia of control with ND. n = 10. **(B)** Relative levels of hemolymph glucose normalized to the glycemia of control in WT background. n = 10. Genotype, control (*hs*>+), and CUL1 OE (*hs*>*CUL1*). Two-way ANOVA with Sidak's multiple comparison test was used **(A and B)**. ****$p < 0.0001$, and ns ($p > 0.05$). All data were presented as mean + SD.

Discussion

Summary

In PART 2, I have identified that UCHL1 is a key molecule regulating insulin signaling by deubiquitinating IRS1. Using *Drosophila* models, UCHL1 mutations induce hyperglycemia and insulin resistance. Also, in the legs of UCHL1 knock-out flies, the impairments of sensory neurons led to neuronal death-causing numbness to both physically and chemically noxious stimulations. Conversely, UCHL1 overexpression alleviated these defects related to T2D from HSD flies. Furthermore, I identified that UCHL1 deubiquitinated IRS1 and regulated insulin signaling using mammalian cell lines. Also, HSD feeding induced GSK3 inactivation in *Drosophila*, stabilizing Snail. Snail elevated the transcription of CUL1, an E3 ligase playing an antagonistic role of UCHL1. Finally, I revealed that the T2D-like symptoms in fruit flies were completely rescued by genetic inhibition of CUL1 activity. Thus, I suggested that UCHL1 is a pivotal regulator of insulin signaling and type 2 diabetes **(Fig. 105)**.

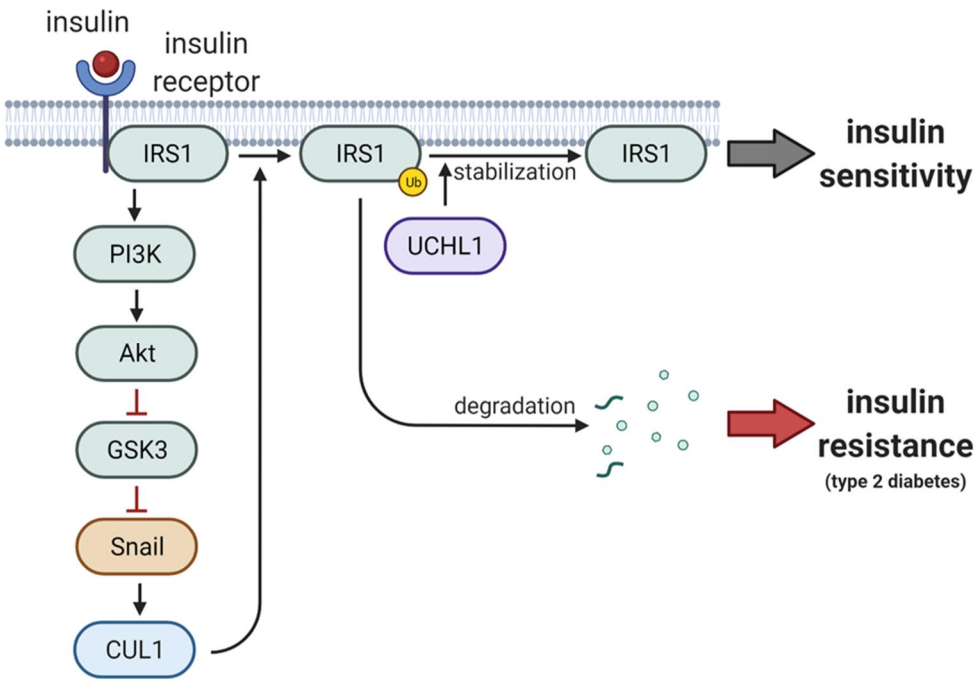

Figure 105. A proposed model summarizing PART 2.

Image was generated from Biorender.

Genetic factors for T2D development

It has been reported that genetic factors can contribute to the development of T2D (Ali, 2013). Also, these genes have been identified mainly by genome-wide association studies (GWAS) (DeFronzo et al., 2015; Mahajan et al., 2018; Polfus et al., 2021). Particularly, a GWAS result describes that UCHL1 has functional associations with T2D development (Li et al., 2015). Furthermore, I have identified that UCHL1 mutations induced T2D-related phenotypes and UCHL1 overexpression rescued these phenotypes in *Drosophila*.

Likewise, important T2D genes identified by GWAS studies were observed to induce T2D in model organisms. For example, a polymorphism in peroxisome proliferator-activated receptor-γ (PPARγ) has a genetic association with T2D (Kilpeläinen et al., 2008; Sanghera et al., 2010; Sarhangi et al., 2020). PPARγ increases the expression of insulin signaling components in adipose tissues, which elevates insulin sensitivity (Sugii et al., 2009). Also, transcription factor 7-like 2 (TCF7L2), a key molecule in Wnt signaling (Ip et al., 2012), is involved in T2D susceptibility (Cauchi et al., 2007; Cauchi and Froguel, 2008; Chen et al., 2018). After this finding, it has been revealed that TCF7L2 is responsible for regulating genes regarding insulin secretion in pancreatic islets of humans and rodents (da Silva Xavier et al., 2012; Zhou et al., 2014). Recently, a GWAS among T2D patients from sub-Saharan African leads to the identification of zinc finger RANBP2-type containing 3 (ZRANB3) as a gene related to T2D. ZRANB3 knock-out

zebrafish have apoptotic responses in islets and consequent reduction in pancreatic β-cell numbers (Adeyemo et al., 2019). In conclusion, I propose UCHL1 as a crucial gene for T2D pathogenesis.

Diabetic neuropathy (DN)

I have found that UCHL1 KO flies or HSD feeding flies showed numbness to the noxious stimulation. Also, the sensory neurons in the fly legs were dramatically impaired, similar to the neuropathy symptoms developed in T2D patients. In human T2D patients, diabetic neuropathy (DN) initially appears in the distal extremities and develops into numbness or persistent pain, which is the leading cause of foot ulcers or limb amputations in diabetic patients (Feldman et al., 2019; Said, 2007). It has been reported that activation of the polyol pathway and hexosamine pathway, and accumulation of advanced glycation end products (AGEs) might be the reasons for DN (Feldman et al., 2019).

Firstly, in the polyol pathway, aldolase reductase converts excess glucose in hyperglycemic conditions into sorbitol. The osmotic stress by increased sorbitol induces the efflux of myoinositol which is needed for the proper function of sodium/potassium ATPase. Thus, the normal nerve is damaged, developing DN (Chung et al., 2003; Oates, 2002).

Secondly, under high glycemia, the hexosamine pathway is elevated by increased levels of fructose-6-phosphate, one of the glycolytic intermediates. This pathway generates uridine 5-diphosphate-N-acetylglucosamine (GlcNac) and SP1 transcription factor (SP1), abundant in peripheral nerves, is hyperactivated by GlcNac. As lipid dyshomeostasis is induced by SP1, peripheral nerves become malfunctioned (Sandireddy et al., 2014).

In addition, AGEs are one of the factors for DN. Since amino acids in proteins react with glucose forming AGEs, numerous glycated proteins can be generated by hyperglycemia. In particular, extracellular AGEs bind the receptor for AGE (RAGE) and activate the nuclear factor κB (NF-κB) pathway. This pathway hyperactivates inflammation, causing neuronal death (Tóbon-Velasco et al., 2014). In the rodent peripheral nerve systems, AGEs accumulation and the huge expression of RAGE are observed, which develops into DN (Sugimoto et al., 2008).

However, since the drugs which can inhibit each of these three pathways, aldolase reductase inhibitor (FR74366 or AS-3201) (Ao et al., 1991; Bril and Buchanan, 2006), hexosamine pathway inhibitor (ruboxistaurin) (Bansal et al., 2013), and AGEs formation inhibitor (aminoguanidine) (Cameron et al., 1992; Chen et al., 2004), are not effective in clinical trials for treating DN, many researchers are trying to introduce new genes or pathways in DN fields. Therefore, I suggest UCHL1 and GSK3/Snail/CUL1 pathway as breakthroughs for understanding diabetic neuropathy.

AMPK activation by UCHL1 mutations and T2D

It has been reported that AMPK activation could mitigate hyperglycemia or insulin resistance. Especially, one of the most well-known drugs for curing T2D, metformin, rescues T2D in an AMPK-dependent manner. Furthermore, the muscles of patients suffering from T2D showed decreased activity of AMPK, which was completely rescued by AMPK activation by treating rosiglitazone (Ye et al., 2006). In T2D rat models induced by high fat diet (HFD), a single dose of 5-aminoimidazole-4-carboxamide ribonucleotide (AICAR), one of the AMPK activators, increased insulin sensitivity of muscle and liver (Fryer et al., 2002). Although the activity of AMPK was elevated by UCHL1 KO in PART 1 study, UCH mutant flies showed T2D phenotypes, and UCHL1 KO cell lines showed decreased insulin signaling in PART 2 study. Therefore, I tested if brain-specific overexpression of constitutively active form of AMPK ($AMPK^{CA}$) could rescue HFD-induced hyperglycemia since UCHL1 is mostly expressed in the brain. Though expressing $AMPK^{CA}$ in the muscle and fat body alleviated the increased glycemia from HFD flies, expressing exogenous $AMPK^{CA}$ in the brain did not rescue hyperglycemia caused by HFD **(Fig. 106)**. Therefore, I suggested that AMPK activation in the brain did not affect T2D.

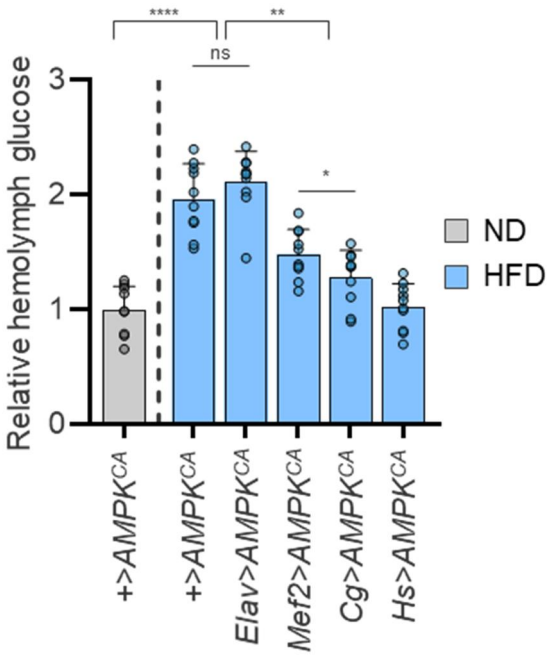

Figure 106. Expressing AMPK^{CA} in neurons did not rescue hyperglycemia.

(A) Relative levels of hemolymph glucose normalized to the glycemia of control (+>AMPK^{CA}) with ND. n = 10. Two-way ANOVA with Sidak's multiple comparison test was used. ****p < 0.0001, and ns (p > 0.05). All data were presented as mean + SD.

The lifespan of UCHL1 mutants

The two targets of UCHL1 identified in PART 1 and PART 2 studies, PKM and IRS1, are well-known factors regulating lifespan. In *Caenorhabditis elegans*, 4,4'-diaminodiphenylsulfone (DDS) treatment extends lifespan by inhibiting pyruvate kinase (Cho et al., 2010). Furthermore, in *Drosophila*, IRS1 KO mutants display an extended lifespan (Clancy et al., 2001). Similar to these results, UCH deletion mutant flies showed prolonged longevity **(Fig. 107)**. Since pyruvate kinase inhibition and IRS1 malfunction both increase lifespan, I am going to prove which factors are linked with the survival phenotypes of UCH^{KO}.

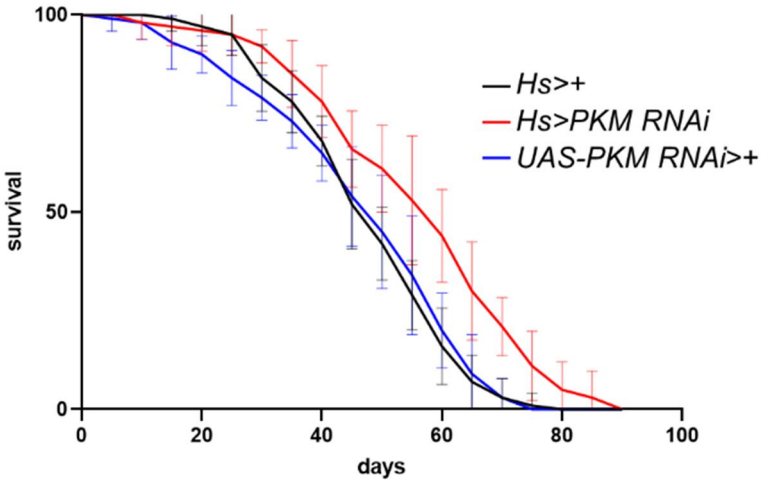

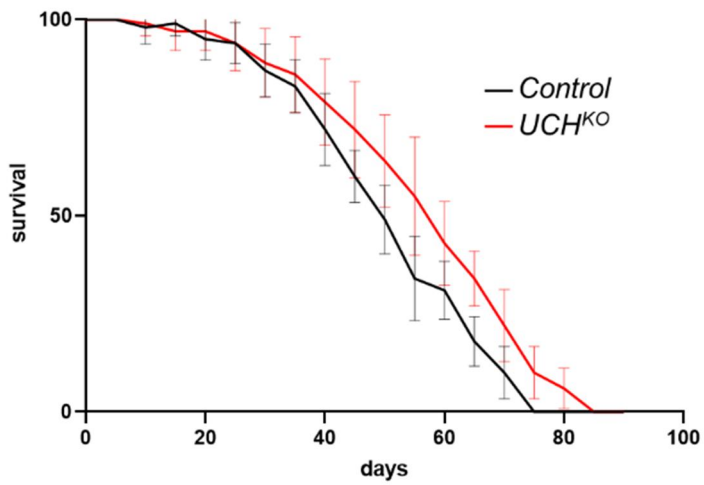

Figure 107. PKM knockdown and UCH mutant flies showed an extended lifespan.

Survival rate of flies with indicated genotypes. All data were presented as mean ± SD.

Correlations between TRIM63 and CUL1

I have identified that both TRIM63 and CUL1 can play antagonistic roles of UCHL1 in PD and T2D pathogenesis, respectively. Furthermore, I sought to observe if TRIM63 could perform opposite functions of UCHL1 in T2D pathogenesis and CUL1 could perform opposite functions of UCHL1 in PD pathogenesis. Therefore, I expressed CUL1 RNAi lines in PINK1 and UCH double knockout flies and measured climbing abilities. Surprisingly, the effects of which UCH KO ameliorated the decreased locomotor activities from PINK1 mutant flies were not blocked by CUL1 knockdown. In addition, I knocked TRIM9 RNAi down in UCH mutant flies and observed the glucose levels. The hyperglycemia of UCH^{KO} flies was not rescued by TRIM9 knockdown **(Fig. 108)**. Therefore, I concluded that TRIM63 and CUL1 did not affect each other.

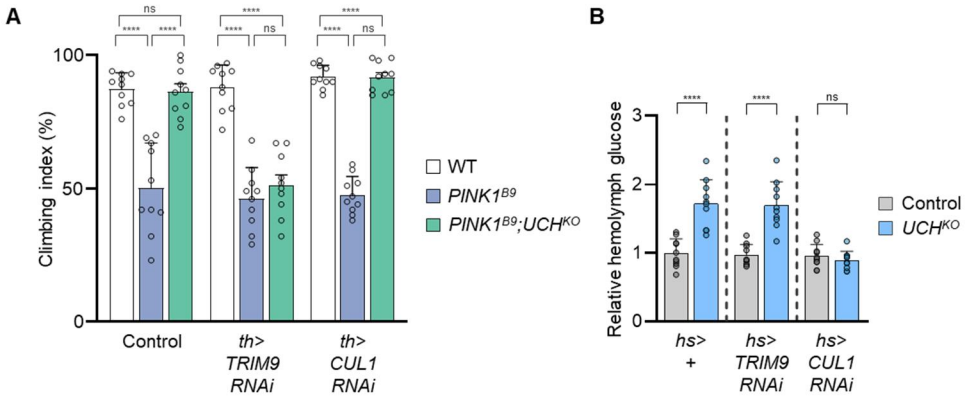

Figure 108. CUL1 knockdown did not block the PD-rescuing effects of UCH KO and TRIM9 knockdown did not inhibit the T2D phenotypes of UCH KO.

(A) Climbing abilities in the adult flies of indicated genotypes. $n = 10$. **(B)** Relative levels of hemolymph glucose normalized to the glycemia of control (*hs*>+). $n = 10$. Two-way ANOVA with Sidak's multiple comparison test was used. ****$p < 0.0001$, and ns ($p > 0.05$). All data were presented as mean + SD.

Limitations of PART1 and PART 2 study

PART 1 study explained that PD-related pathogenic mutations of UCHL1 did not induce PD-like symptoms in *Drosophila*. Despite these results, whether UCHL1 mutations are associated with PD in humans or not should be revealed clearly in future researches. Also, the outcome that the dysfunctions of UCHL1 rescued PD phenotypes has to be recapitulated using vertebrate model organisms and epidemiologic approaches in humans.

PART 2 study established that sensory neurons were vulnerable by several insulin resistance-related genetic factors. However, the mechanisms of how insulin resistance specifically induced the death of sensory neurons were not explored. I need to observe more evidence for cell death phenotypes of sensory neurons and their related signaling pathways using *Drosophila* models and mammalian cell lines.

Through both PART 1 and PART 2 studies, it has been identified well that UCHL1 plays important roles for PD and T2D pathogenesis, respectively. However, the correlations between PD and T2D are not explained clearly in these studies. Therefore, I will further study to observe PD-related symptoms while blocking glucose uptake or expressing CUL1 in dopaminergic neurons of PINK1 or Parkin mutant flies in near future.

Conclusion

In this study, I observed the implications of UCHL1 for human diseases using *Drosophila* models and identified the two novel targets of UCHL1, PKM and IRS1.

In PART 1, PD-like phenotypes in the PINK1 or Parkin mutants are completely rescued by UCHL1 deletion in *Drosophila*. Since UCHL1 deubiquitinates and stabilizes PKM, pyruvate productions are significantly decreased, and the consequent reduction of ATP levels is also observed in UCHL1 knockout cell lines. The diminished cellular energy levels activate AMPK, ULK1, and FUNDC1, one of the mitophagy receptors. These energy-sensing cascade triggers mitophagy independent from PINK1/Parkin pathway. Therefore, UCHL1 deficiency mitigated PD-related phenotypes by supplementing mitophagy in PINK1 or Parkin mutants.

In PART 2, UCHL1 mutant flies exhibit T2D-like symptoms and UCHL1 overexpression rescues T2D-associated phenotypes induced by high sugar diet. UCHL1 deubiquitinates and destabilizes IRS1, a scaffold protein delivering insulin signals. Therefore, insulin signaling is downregulated in UCHL1 KO. Furthermore, GSK3, another component of insulin signaling, is inactivated by high sugar circumstances and stabilizes a transcription factor, Snail. Snail elevates the transcription of CUL1, an E3 ligase playing an antagonistic role of UCHL1 by ubiquitinating IRS1. Therefore, T2D-like phenotypes in HSD flies are developed by GSK3/Snail/CUL1 axis and rescued by UCHL1 overexpression.

In conclusion, I enlighten the physiological roles of UCHL1 by suggesting two targets of UCHL1, PKM and IRS1. In glucose metabolism, PKM functions as a junction of glycolysis and TCA cycle, and IRS1 participates in cellular uptake of glucose in response to insulin. Accordingly, I propose UCHL1 as a pivotal regulator of glucose metabolism.

References

Adeyemo, A.A., Zaghloul, N.A., Chen, G., Doumatey, A.P., Leitch, C.C., Hostelley, T.L., Nesmith, J.E., Zhou, J., Bentley, A.R., Shriner, D., *et al.* (2019). ZRANB3 is an African-specific type 2 diabetes locus associated with beta-cell mass and insulin response. Nat Commun *10*, 3195.

Ahmed, S.S., Santosh, W., Kumar, S., and Christlet, H.T. (2009). Metabolic profiling of Parkinson's disease: evidence of biomarker from gene expression analysis and rapid neural network detection. Journal of biomedical science *16*, 63.

Ali, O. (2013). Genetics of type 2 diabetes. World journal of diabetes *4*, 114-123.

Amerik, A.Y., and Hochstrasser, M. (2004). Mechanism and function of deubiquitinating enzymes. Biochimica et Biophysica Acta (BBA) - Molecular Cell Research *1695*, 189-207.

Ao, S., Shingu, Y., Kikuchi, C., Takano, Y., Nomura, K., Fujiwara, T., Ohkubo, Y., Notsu, Y., and Yamaguchi, I. (1991). Characterization of a novel aldose reductase inhibitor, FR74366, and its effects on diabetic cataract and neuropathy in the rat. Metabolism: clinical and experimental *40*, 77-87.

Bahadorani, S., Hur, J.H., Lo, T., Jr., Vu, K., and Walker, D.W. (2010). Perturbation of mitochondrial complex V alters the response to dietary restriction in Drosophila. Aging cell *9*, 100-103.

Bansal, D., Badhan, Y., Gudala, K., and Schifano, F. (2013). Ruboxistaurin for the treatment of diabetic peripheral neuropathy: a systematic review of randomized clinical trials. Diabetes & metabolism journal *37*, 375-384.

Bassett, A., and Liu, J.L. (2014). CRISPR/Cas9 mediated genome engineering in Drosophila. Methods (San Diego, Calif) *69*, 128-136.

Bhujabal, Z., Birgisdottir Å, B., Sjøttem, E., Brenne, H.B., Øvervatn, A., Habisov, S., Kirkin, V., Lamark, T., and Johansen, T. (2017). FKBP8 recruits LC3A to mediate Parkin-independent mitophagy. EMBO reports *18*, 947-961.

Bilguvar, K., Tyagi, N.K., Ozkara, C., Tuysuz, B., Bakircioglu, M., Choi, M., Delil, S., Caglayan, A.O., Baranoski, J.F., Erturk, O., *et al.* (2013). Recessive loss of function of the neuronal ubiquitin hydrolase UCHL1 leads to early-onset progressive neurodegeneration. Proceedings of the National Academy

of Sciences of the United States of America *110*, 3489-3494.

Bingol, B., Tea, J.S., Phu, L., Reichelt, M., Bakalarski, C.E., Song, Q., Foreman, O., Kirkpatrick, D.S., and Sheng, M. (2014). The mitochondrial deubiquitinase USP30 opposes parkin-mediated mitophagy. Nature *510*, 370-375.

Blagosklonny, M.V. (2019). Fasting and rapamycin: diabetes versus benevolent glucose intolerance. Cell Death & Disease *10*, 607.

Bolam, J.P., and Pissadaki, E.K. (2012). Living on the edge with too many mouths to feed: why dopamine neurons die. Movement disorders : official journal of the Movement Disorder Society *27*, 1478-1483.

Bonello, F., Hassoun, S.M., Mouton-Liger, F., Shin, Y.S., Muscat, A., Tesson, C., Lesage, S., Beart, P.M., Brice, A., Krupp, J., *et al.* (2019). LRRK2 impairs PINK1/Parkin-dependent mitophagy via its kinase activity: pathologic insights into Parkinson's disease. Human molecular genetics *28*, 1645-1660.

Bononi, A., Giorgi, C., Patergnani, S., Larson, D., Verbruggen, K., Tanji, M., Pellegrini, L., Signorato, V., Olivetto, F., Pastorino, S., *et al.* (2017). BAP1 regulates IP3R3-mediated Ca(2+) flux to mitochondria suppressing cell transformation. Nature *546*, 549-553.

Boucher, J., Kleinridders, A., and Kahn, C.R. (2014). Insulin receptor signaling in normal and insulin-resistant states. Cold Spring Harbor perspectives in biology *6*.

Boura-Halfon, S., and Zick, Y. (2009). Phosphorylation of IRS proteins, insulin action, and insulin resistance. *296*, E581-E591.

Branson, K., Robie, A.A., Bender, J., Perona, P., and Dickinson, M.H. (2009). High-throughput ethomics in large groups of *Drosophila*. Nature Methods *6*, 451-457.

Bril, V., and Buchanan, R.A. (2006). Long-term effects of ranirestat (AS-3201) on peripheral nerve function in patients with diabetic sensorimotor polyneuropathy. Diabetes care *29*, 68-72.

Brown, E.B., Shah, K.D., Faville, R., Kottler, B., and Keene, A.C. (2020). Drosophila insulin-like peptide 2 mediates dietary regulation of sleep intensity. PLoS genetics *16*, e1008270.

Burchell, V.S., Nelson, D.E., Sanchez-Martinez, A., Delgado-Camprubi, M.,

Ivatt, R.M., Pogson, J.H., Randle, S.J., Wray, S., Lewis, P.A., Houlden, H., *et al.* (2013). The Parkinson's disease-linked proteins Fbxo7 and Parkin interact to mediate mitophagy. Nature neuroscience *16*, 1257-1265.

Callio, J., Oury, T.D., and Chu, C.T. (2005). Manganese superoxide dismutase protects against 6-hydroxydopamine injury in mouse brains. The Journal of biological chemistry *280*, 18536-18542.

Cameron, N.E., Cotter, M.A., Dines, K., and Love, A. (1992). Effects of aminoguanidine on peripheral nerve function and polyol pathway metabolites in streptozotocin-diabetic rats. Diabetologia *35*, 946-950.

Carmine Belin, A., Westerlund, M., Bergman, O., Nissbrandt, H., Lind, C., Sydow, O., and Galter, D. (2007). S18Y in ubiquitin carboxy-terminal hydrolase L1 (UCH-L1) associated with decreased risk of Parkinson's disease in Sweden. Parkinsonism & related disorders *13*, 295-298.

Castro-Mondragon, J.A., Riudavets-Puig, R., Rauluseviciute, I., Lemma, R.B., Turchi, L., Blanc-Mathieu, R., Lucas, J., Boddie, P., Khan, A., Manosalva Pérez, N., *et al.* (2022). JASPAR 2022: the 9th release of the open-access database of transcription factor binding profiles. Nucleic acids research *50*, D165-d173.

Cauchi, S., El Achhab, Y., Choquet, H., Dina, C., Krempler, F., Weitgasser, R., Nejjari, C., Patsch, W., Chikri, M., Meyre, D., *et al.* (2007). TCF7L2 is reproducibly associated with type 2 diabetes in various ethnic groups: a global meta-analysis. Journal of molecular medicine (Berlin, Germany) *85*, 777-782.

Cauchi, S., and Froguel, P. (2008). TCF7L2 genetic defect and type 2 diabetes. Current diabetes reports *8*, 149-155.

Chakraborty, J., and Ziviani, E. (2020). Deubiquitinating Enzymes in Parkinson's Disease. Frontiers in physiology *11*, 535.

Chen, A.S., Taguchi, T., Sugiura, M., Wakasugi, Y., Kamei, A., Wang, M.W., and Miwa, I. (2004). Pyridoxal-aminoguanidine adduct is more effective than aminoguanidine in preventing neuropathy and cataract in diabetic rats. Hormone and metabolic research = Hormon- und Stoffwechselforschung = Hormones et metabolisme *36*, 183-187.

Chen, C., Gu, L., Matye, D.J., Clayton, Y.-D., Hasan, M.N., Wang, Y., Friedman, J.E., and Li, T. (2022). Cullin neddylation inhibitor attenuates hyperglycemia by enhancing hepatic insulin signaling through insulin receptor substrate stabilization. *119*, e2111737119.

Chen, X., Ayala, I., Shannon, C., Fourcaudot, M., Acharya, N.K., Jenkinson, C.P., Heikkinen, S., and Norton, L. (2018). The Diabetes Gene and Wnt Pathway Effector TCF7L2 Regulates Adipocyte Development and Function. Diabetes *67*, 554-568.

Cho, S.C., Park, M.C., Keam, B., Choi, J.M., Cho, Y., Hyun, S., Park, S.C., and Lee, J. (2010). DDS, 4,4'-diaminodiphenylsulfone, extends organismic lifespan. Proceedings of the National Academy of Sciences of the United States of America *107*, 19326-19331.

Chung, S.S.M., Ho, E.C.M., Lam, K.S.L., and Chung, S.K. (2003). Contribution of Polyol Pathway to Diabetes-Induced Oxidative Stress. *14*, S233-S236.

Clancy, D.J., Gems, D., Harshman, L.G., Oldham, S., Stocker, H., Hafen, E., Leevers, S.J., and Partridge, L. (2001). Extension of life-span by loss of CHICO, a Drosophila insulin receptor substrate protein. Science (New York, NY) *292*, 104-106.

Cohen, P., and Frame, S. (2001). The renaissance of GSK3. Nature Reviews Molecular Cell Biology *2*, 769-776.

Copps, K.D., and White, M.F. (2012). Regulation of insulin sensitivity by serine/threonine phosphorylation of insulin receptor substrate proteins IRS1 and IRS2. Diabetologia *55*, 2565-2582.

Cornelissen, T., Haddad, D., Wauters, F., Van Humbeeck, C., Mandemakers, W., Koentjoro, B., Sue, C., Gevaert, K., De Strooper, B., Verstreken, P.*, et al.* (2014). The deubiquitinase USP15 antagonizes Parkin-mediated mitochondrial ubiquitination and mitophagy. Human molecular genetics *23*, 5227-5242.

Cunningham, C.N., Baughman, J.M., Phu, L., Tea, J.S., Yu, C., Coons, M., Kirkpatrick, D.S., Bingol, B., and Corn, J.E. (2015). USP30 and parkin homeostatically regulate atypical ubiquitin chains on mitochondria. Nature cell biology *17*, 160-169.

da Silva Xavier, G., Mondragon, A., Sun, G., Chen, L., McGinty, J.A., French, P.M., and Rutter, G.A. (2012). Abnormal glucose tolerance and insulin secretion in pancreas-specific Tcf7l2-null mice. Diabetologia *55*, 2667-2676.

Davies, M.J., D'Alessio, D.A., Fradkin, J., Kernan, W.N., Mathieu, C., Mingrone, G., Rossing, P., Tsapas, A., Wexler, D.J., and Buse, J.B. (2018). Management of Hyperglycemia in Type 2 Diabetes, 2018. A Consensus Report by the American Diabetes Association (ADA) and the European Association for the

Study of Diabetes (EASD). Diabetes care *41*, 2669-2701.

DeFronzo, R.A., Ferrannini, E., Groop, L., Henry, R.R., Herman, W.H., Holst, J.J., Hu, F.B., Kahn, C.R., Raz, I., Shulman, G.I., *et al.* (2015). Type 2 diabetes mellitus. Nature Reviews Disease Primers *1*, 15019.

DeFronzo, R.A., and Tripathy, D. (2009). Skeletal muscle insulin resistance is the primary defect in type 2 diabetes. Diabetes care *32 Suppl 2*, S157-163.

Dodson, M.W., and Guo, M. (2007). Pink1, Parkin, DJ-1 and mitochondrial dysfunction in Parkinson's disease. Current opinion in neurobiology *17*, 331-337.

Doktór, B., Damulewicz, M., and Pyza, E. (2019). Overexpression of Mitochondrial Ligases Reverses Rotenone-Induced Effects in a Drosophila Model of Parkinson's Disease. Frontiers in neuroscience *13*, 94.

Doran, J.F., Jackson, P., Kynoch, P.A.M., and Thompson, R.J. (1983). Isolation of PGP 9.5, a New Human Neurone-Specific Protein Detected by High-Resolution Two-Dimensional Electrophoresis. *40*, 1542-1547.

Eguez, L., Lee, A., Chavez, J.A., Miinea, C.P., Kane, S., Lienhard, G.E., and McGraw, T.E. (2005). Full intracellular retention of GLUT4 requires AS160 Rab GTPase activating protein. Cell metabolism *2*, 263-272.

Feldman, E.L., Callaghan, B.C., Pop-Busui, R., Zochodne, D.W., Wright, D.E., Bennett, D.L., Bril, V., Russell, J.W., and Viswanathan, V. (2019). Diabetic neuropathy. Nature Reviews Disease Primers *5*, 41.

Fernius, J., Starkenberg, A., and Thor, S. (2017). Bar-coding neurodegeneration: identifying subcellular effects of human neurodegenerative disease proteins using Drosophila leg neurons. Disease Models & Mechanisms *10*, 1027-1038.

Fryer, L.G., Parbu-Patel, A., and Carling, D. (2002). The Anti-diabetic drugs rosiglitazone and metformin stimulate AMP-activated protein kinase through distinct signaling pathways. The Journal of biological chemistry *277*, 25226-25232.

Fukushima, T., Gao, T., Tawara, T., Hojo, N., Isobe, A., and Yamane, Y. (1997). Inhibitory effect of nicotinamide to paraquat toxicity and the reaction site on complex I. Archives of toxicology *71*, 633-637.

Ghosh, A., Tyson, T., George, S., Hildebrandt, E.N., Steiner, J.A., Madaj, Z., Schulz, E., Machiela, E., McDonald, W.G., Escobar Galvis, M.L., *et al.* (2016). Mitochondrial pyruvate carrier regulates autophagy, inflammation, and neurodegeneration in experimental models of Parkinson's disease. Science translational medicine *8*, 368ra174.

Gual, P., Le Marchand-Brustel, Y., and Tanti, J.F. (2005). Positive and negative regulation of insulin signaling through IRS-1 phosphorylation. Biochimie *87*, 99-109.

Haeusler, R.A., McGraw, T.E., and Accili, D. (2018). Biochemical and cellular properties of insulin receptor signalling. Nature Reviews Molecular Cell Biology *19*, 31-44.

Ham, S.J., Lee, D., Yoo, H., Jun, K., Shin, H., and Chung, J. (2020). Decision between mitophagy and apoptosis by Parkin via VDAC1 ubiquitination. Proceedings of the National Academy of Sciences of the United States of America *117*, 4281-4291.

Ham, S.J., Lee, D., Xu, W.J., Cho, E., Choi, S., Min, S., Park, S., and Chung, J. (2021). Loss of UCHL1 rescues the defects related to Parkinson's disease by suppressing glycolysis. *7*, eabg4574.

Hanna, R.A., Quinsay, M.N., Orogo, A.M., Giang, K., Rikka, S., and Gustafsson Å, B. (2012). Microtubule-associated protein 1 light chain 3 (LC3) interacts with Bnip3 protein to selectively remove endoplasmic reticulum and mitochondria via autophagy. The Journal of biological chemistry *287*, 19094-19104.

Håkanson, R., Lundquist, I., and Rerup, C. (1967). On the hyperglycaemic effect of DOPA and dopamine. European Journal of Pharmacology *1*, 114-119.

Healy, D.G., Abou-Sleiman, P.M., Casas, J.P., Ahmadi, K.R., Lynch, T., Gandhi, S., Muqit, M.M.K., Foltynie, T., Barker, R., Bhatia, K.P., *et al.* (2006). UCHL-1 is not a Parkinson's disease susceptibility gene. *59*, 627-633.

Hicke, L. (2001). Protein regulation by monoubiquitin. Nature Reviews Molecular Cell Biology *2*, 195-201.

Hoxhaj, G., and Manning, B.D. (2020). The PI3K–AKT network at the interface of oncogenic signalling and cancer metabolism. Nature Reviews Cancer *20*, 74-88.

Ip, W., Chiang, Y.T., and Jin, T. (2012). The involvement of the wnt signaling

pathway and TCF7L2 in diabetes mellitus: The current understanding, dispute, and perspective. Cell & bioscience *2*, 28.

Islam, M.S., and Loots du, T. (2009). Experimental rodent models of type 2 diabetes: a review. Methods and findings in experimental and clinical pharmacology *31*, 249-261.

Iwashita, H., Torii, S., Nagahora, N., Ishiyama, M., Shioji, K., Sasamoto, K., Shimizu, S., and Okuma, K. (2017). Live Cell Imaging of Mitochondrial Autophagy with a Novel Fluorescent Small Molecule. ACS chemical biology *12*, 2546-2551.

Jastroch, M., Divakaruni, A.S., Mookerjee, S., Treberg, J.R., and Brand, M.D. (2010). Mitochondrial proton and electron leaks. Essays in biochemistry *47*, 53-67.

Karlsson, H.K., and Zierath, J.R. (2007). Insulin signaling and glucose transport in insulin resistant human skeletal muscle. Cell biochemistry and biophysics *48*, 103-113.

Katsarou, A., Gudbjörnsdottir, S., Rawshani, A., Dabelea, D., Bonifacio, E., Anderson, B.J., Jacobsen, L.M., Schatz, D.A., and Lernmark, Å. (2017). Type 1 diabetes mellitus. Nature Reviews Disease Primers *3*, 17016.

Kilpeläinen, T.O., Lakka, T.A., Laaksonen, D.E., Lindström, J., Eriksson, J.G., Valle, T.T., Hämäläinen, H., Ilanne-Parikka, P., Keinänen-Kiukaanniemi, S., Lindi, V.*, et al.* (2008). SNPs in PPARG associate with type 2 diabetes and interact with physical activity. Medicine and science in sports and exercise *40*, 25-33.

Komander, D., and Rape, M. (2012). The Ubiquitin Code. Annual Review of Biochemistry *81*, 203-229.

Kyratzi, E., Pavlaki, M., and Stefanis, L. (2008). The S18Y polymorphic variant of UCH-L1 confers an antioxidant function to neuronal cells. Human molecular genetics *17*, 2160-2171.

Lachmann, A., Torre, D., Keenan, A.B., Jagodnik, K.M., Lee, H.J., Wang, L., Silverstein, M.C., and Ma'ayan, A. (2018). Massive mining of publicly available RNA-seq data from human and mouse. Nature Communications *9*, 1366.

Laker, R.C., Drake, J.C., Wilson, R.J., Lira, V.A., Lewellen, B.M., Ryall, K.A., Fisher, C.C., Zhang, M., Saucerman, J.J., Goodyear, L.J.*, et al.* (2017). Ampk phosphorylation of Ulk1 is required for targeting of mitochondria to

lysosomes in exercise-induced mitophagy. Nat Commun *8*, 548.

Larsen, C.N., Krantz, B.A., and Wilkinson, K.D. (1998). Substrate specificity of deubiquitinating enzymes: ubiquitin C-terminal hydrolases. Biochemistry *37*, 3358-3368.

Lee, C.S., Yi, J.S., Jung, S.Y., Kim, B.W., Lee, N.R., Choo, H.J., Jang, S.Y., Han, J., Chi, S.G., Park, M.*, et al.* (2010). TRIM72 negatively regulates myogenesis via targeting insulin receptor substrate-1. Cell Death & Differentiation *17*, 1254-1265.

Lee, J.H., Koh, H., Kim, M., Kim, Y., Lee, S.Y., Karess, R.E., Lee, S.H., Shong, M., Kim, J.M., Kim, J.*, et al.* (2007). Energy-dependent regulation of cell structure by AMP-activated protein kinase. Nature *447*, 1017-1020.

Leroy, E., Boyer, R., Auburger, G., Leube, B., Ulm, G., Mezey, E., Harta, G., Brownstein, M.J., Jonnalagada, S., Chernova, T.*, et al.* (1998). The ubiquitin pathway in Parkinson's disease. Nature *395*, 451-452.

Li, B., Ye, J., Liu, R., Weng, L., Cao, Y., Jia, S., Xu, C., Liu, Y., Yan, S., and Zheng, M. (2021). Programmed cell death 5 improves skeletal muscle insulin resistance by inhibiting IRS-1 ubiquitination through stabilization of MDM2. Life sciences *285*, 119918.

Li, M.J., Liu, Z., Wang, P., Wong, M.P., Nelson, M.R., Kocher, J.-P.A., Yeager, M., Sham, P.C., Chanock, S.J., Xia, Z.*, et al.* (2015). GWASdb v2: an update database for human genetic variants identified by genome-wide association studies. Nucleic acids research *44*, D869-D876.

Liberman, Z., and Eldar-Finkelman, H. (2005). Serine 332 Phosphorylation of Insulin Receptor Substrate-1 by Glycogen Synthase Kinase-3 Attenuates Insulin Signaling*. Journal of Biological Chemistry *280*, 4422-4428.

Lim, G.G., and Lim, K.L. (2017). Parkin-independent mitophagy-FKBP8 takes the stage. EMBO reports *18*, 864-865.

Lincoln, S., Vaughan, J., Wood, N., Baker, M., Adamson, J., Gwinn-Hardy, K., Lynch, T., Hardy, J., and Farrer, M. (1999). Low frequency of pathogenic mutations in the ubiquitin carboxy-terminal hydrolase gene in familial Parkinson's disease. Neuroreport *10*, 427-429.

Liu, K., Li, F., Han, H., Chen, Y., Mao, Z., Luo, J., Zhao, Y., Zheng, B., Gu, W., and Zhao, W. (2016). Parkin Regulates the Activity of Pyruvate Kinase M2. The Journal of biological chemistry *291*, 10307-10317.

Liu, L., Feng, D., Chen, G., Chen, M., Zheng, Q., Song, P., Ma, Q., Zhu, C., Wang, R., Qi, W., *et al.* (2012). Mitochondrial outer-membrane protein FUNDC1 mediates hypoxia-induced mitophagy in mammalian cells. Nature cell biology *14*, 177-185.

Liu, Y., Lashuel, H.A., Choi, S., Xing, X., Case, A., Ni, J., Yeh, L.A., Cuny, G.D., Stein, R.L., and Lansbury, P.T., Jr. (2003). Discovery of inhibitors that elucidate the role of UCH-L1 activity in the H1299 lung cancer cell line. Chemistry & biology *10*, 837-846.

Mahajan, A., Taliun, D., Thurner, M., Robertson, N.R., Torres, J.M., Rayner, N.W., Payne, A.J., Steinthorsdottir, V., Scott, R.A., Grarup, N., *et al.* (2018). Fine-mapping type 2 diabetes loci to single-variant resolution using high-density imputation and islet-specific epigenome maps. Nature genetics *50*, 1505-1513.

Mallette, F.A., Mattiroli, F., Cui, G., Young, L.C., Hendzel, M.J., Mer, G., Sixma, T.K., and Richard, S. (2012). RNF8- and RNF168-dependent degradation of KDM4A/JMJD2A triggers 53BP1 recruitment to DNA damage sites. EMBO J *31*, 1865-1878.

Maraganore, D.M., Lesnick, T.G., Elbaz, A., Chartier-Harlin, M.-C., Gasser, T., Krüger, R., Hattori, N., Mellick, G.D., Quattrone, A., Satoh, J.-I., *et al.* (2004a). UCHL1 is a Parkinson's disease susceptibility gene. *55*, 512-521.

Maraganore, D.M., Lesnick, T.G., Elbaz, A., Chartier-Harlin, M.C., Gasser, T., Krüger, R., Hattori, N., Mellick, G.D., Quattrone, A., Satoh, J., *et al.* (2004b). UCHL1 is a Parkinson's disease susceptibility gene. Annals of neurology *55*, 512-521.

Mîinea, C.P., Sano, H., Kane, S., Sano, E., Fukuda, M., Peränen, J., Lane, W.S., and Lienhard, G.E. (2005). AS160, the Akt substrate regulating GLUT4 translocation, has a functional Rab GTPase-activating protein domain. The Biochemical journal *391*, 87-93.

Merlet, J., Burger, J., Gomes, J.E., and Pintard, L. (2009). Regulation of cullin-RING E3 ubiquitin-ligases by neddylation and dimerization. Cellular and molecular life sciences : CMLS *66*, 1924-1938.

Min, S., Chae, H.-S., Jang, Y.-H., Choi, S., Lee, S., Jeong, Yong T., Jones, Walton D., Moon, Seok J., Kim, Y.-J., and Chung, J. (2016). Identification of a Peptidergic Pathway Critical to Satiety Responses in Drosophila. Current Biology *26*, 814-820.

Moraru, A., Wiederstein, J., Pfaff, D., Fleming, T., Miller, A.K., Nawroth, P., and Teleman, A.A. (2018). Elevated Levels of the Reactive Metabolite Methylglyoxal Recapitulate Progression of Type 2 Diabetes. Cell metabolism *27*, 926-934.e928.

Naganos, S., Horiuchi, J., and Saitoe, M. (2012). Mutations in the Drosophila insulin receptor substrate, CHICO, impair olfactory associative learning. Neuroscience Research *73*, 49-55.

Nakao, R., Hirasaka, K., Goto, J., Ishidoh, K., Yamada, C., Ohno, A., Okumura, Y., Nonaka, I., Yasutomo, K., Baldwin, K.M.*, et al.* (2009). Ubiquitin ligase Cbl-b is a negative regulator for insulin-like growth factor 1 signaling during muscle atrophy caused by unloading. Molecular and cellular biology *29*, 4798-4811.

Ng, C.H., Guan, M.S., Koh, C., Ouyang, X., Yu, F., Tan, E.K., O'Neill, S.P., Zhang, X., Chung, J., and Lim, K.L. (2012). AMP kinase activation mitigates dopaminergic dysfunction and mitochondrial abnormalities in Drosophila models of Parkinson's disease. The Journal of neuroscience : the official journal of the Society for Neuroscience *32*, 14311-14317.

Oates, P.J. (2002). Polyol pathway and diabetic peripheral neuropathy. International review of neurobiology *50*, 325-392.

Olokoba, A.B., Obateru, O.A., and Olokoba, L.B. (2012). Type 2 diabetes mellitus: a review of current trends. Oman medical journal *27*, 269-273.

Oughtred, R., Stark, C., Breitkreutz, B.J., Rust, J., Boucher, L., Chang, C., Kolas, N., O'Donnell, L., Leung, G., McAdam, R.*, et al.* (2019). The BioGRID interaction database: 2019 update. Nucleic acids research *47*, D529-d541.

Ouyang, L., Yan, B., Liu, Y., Mao, C., Wang, M., Liu, N., Wang, Z., Liu, S., Shi, Y., Chen, L.*, et al.* (2020). The deubiquitylase UCHL3 maintains cancer stem-like properties by stabilizing the aryl hydrocarbon receptor. Signal Transduction and Targeted Therapy *5*, 78.

Palikaras, K., Lionaki, E., and Tavernarakis, N. (2018). Mechanisms of mitophagy in cellular homeostasis, physiology and pathology. Nature cell biology *20*, 1013-1022.

Pankiv, S., Clausen, T.H., Lamark, T., Brech, A., Bruun, J.A., Outzen, H., Øvervatn, A., Bjørkøy, G., and Johansen, T. (2007). p62/SQSTM1 binds directly to Atg8/LC3 to facilitate degradation of ubiquitinated protein aggregates by autophagy. The Journal of biological chemistry *282*, 24131-

24145.

Park, J., Lee, S.B., Lee, S., Kim, Y., Song, S., Kim, S., Bae, E., Kim, J., Shong, M., Kim, J.M., *et al.* (2006). Mitochondrial dysfunction in *Drosophila* PINK1 mutants is complemented by parkin. Nature *441*, 1157-1161.

Park, J.S., Lee, H., Choi, B.W., Ro, S., Lee, D., Na, J.E., Hong, J.-H., Lee, J.-S., Kim, B.-W., and Ko, Y.-G. (2018). An MG53-IRS1-interaction disruptor ameliorates insulin resistance. Experimental & Molecular Medicine *50*, 1-12.

Pickrell, A.M., and Youle, R.J. (2015). The roles of PINK1, parkin, and mitochondrial fidelity in Parkinson's disease. Neuron *85*, 257-273.

Plun-Favreau, H., Klupsch, K., Moisoi, N., Gandhi, S., Kjaer, S., Frith, D., Harvey, K., Deas, E., Harvey, R.J., McDonald, N., *et al.* (2007). The mitochondrial protease HtrA2 is regulated by Parkinson's disease-associated kinase PINK1. Nature cell biology *9*, 1243-1252.

Poewe, W., Seppi, K., Tanner, C.M., Halliday, G.M., Brundin, P., Volkmann, J., Schrag, A.-E., and Lang, A.E. (2017). Parkinson disease. Nature Reviews Disease Primers *3*, 17013.

Polfus, L.M., Darst, B.F., Highland, H., Sheng, X., Ng, M.C.Y., Below, J.E., Petty, L., Bien, S., Sim, X., Wang, W., *et al.* (2021). Genetic discovery and risk characterization in type 2 diabetes across diverse populations. Human Genetics and Genomics Advances *2*, 100029.

Rabey, J.M., and Hefti, F. (1990). Neuromelanin synthesis in rat and human substantia nigra. Journal of neural transmission Parkinson's disease and dementia section *2*, 1-14.

Rabut, G., and Peter, M. (2008). Function and regulation of protein neddylation. 'Protein modifications: beyond the usual suspects' review series. EMBO reports *9*, 969-976.

Ran, F.A., Hsu, P.D., Wright, J., Agarwala, V., Scott, D.A., and Zhang, F. (2013). Genome engineering using the CRISPR-Cas9 system. Nature protocols *8*, 2281-2308.

Rape, M. (2018). Ubiquitylation at the crossroads of development and disease. Nature reviews Molecular cell biology *19*, 59-70.

Repici, M., and Giorgini, F. (2019). DJ-1 in Parkinson's Disease: Clinical

Insights and Therapeutic Perspectives. Journal of clinical medicine *8*.

Richardson, J.R., Quan, Y., Sherer, T.B., Greenamyre, J.T., and Miller, G.W. (2005). Paraquat neurotoxicity is distinct from that of MPTP and rotenone. Toxicological sciences : an official journal of the Society of Toxicology *88*, 193-201.

Said, G. (2007). Diabetic neuropathy—a review. Nature Clinical Practice Neurology *3*, 331-340.

Saigoh, K., Wang, Y.-L., Suh, J.-G., Yamanishi, T., Sakai, Y., Kiyosawa, H., Harada, T., Ichihara, N., Wakana, S., Kikuchi, T.*, et al.* (1999). Intragenic deletion in the gene encoding ubiquitin carboxy-terminal hydrolase in gad mice. Nature genetics *23*, 47-51.

Sanchez-Diaz, P.C., Chang, J.C., Moses, E.S., Dao, T., Chen, Y., and Hung, J.Y. (2017). Ubiquitin carboxyl-terminal esterase L1 (UCHL1) is associated with stem-like cancer cell functions in pediatric high-grade glioma. PLoS One *12*, e0176879-e0176879.

Sandireddy, R., Yerra, V.G., Areti, A., Komirishetty, P., and Kumar, A. (2014). Neuroinflammation and oxidative stress in diabetic neuropathy: futuristic strategies based on these targets. International journal of endocrinology *2014*, 674987.

Sanghera, D.K., Demirci, F.Y., Been, L., Ortega, L., Ralhan, S., Wander, G.S., Mehra, N.K., Singh, J., Aston, C.E., Mulvihill, J.J.*, et al.* (2010). PPARG and ADIPOQ gene polymorphisms increase type 2 diabetes mellitus risk in Asian Indian Sikhs: Pro12Ala still remains as the strongest predictor. Metabolism: clinical and experimental *59*, 492-501.

Sarhangi, N., Sharifi, F., Hashemian, L., Hassani Doabsari, M., Heshmatzad, K., Rahbaran, M., Jamaldini, S.H., Aghaei Meybodi, H.R., and Hasanzad, M. (2020). PPARG (Pro12Ala) genetic variant and risk of T2DM: a systematic review and meta-analysis. Scientific Reports *10*, 12764.

Schindler, C.E., Partap, U., Patchen, B.K., and Swoap, S.J. (2014). Chronic rapamycin treatment causes diabetes in male mice. *307*, R434-R443.

Schwechheimer, C. (2018). NEDD8-its role in the regulation of Cullin-RING ligases. Current opinion in plant biology *45*, 112-119.

Shih, S.C., Sloper-Mould, K.E., and Hicke, L. (2000). Monoubiquitin carries a novel internalization signal that is appended to activated receptors. EMBO J

19, 187-198.

Sirtori, C.R., Bolme, P., and Azarnoff, D.L. (1972). Metabolic Responses to Acute and Chronic l-Dopa Administration in Patients with Parkinsonism. *287*, 729-733.

Springer, W., and Kahle, P.J. (2011). Regulation of PINK1-Parkin-mediated mitophagy. Autophagy *7*, 266-278.

Stott, N.L., and Marino, J.S. (2020). High Fat Rodent Models of Type 2 Diabetes: From Rodent to Human. Nutrients *12*.

Sugii, S., Olson, P., Sears, D.D., Saberi, M., Atkins, A.R., Barish, G.D., Hong, S.-H., Castro, G.L., Yin, Y.-Q., Nelson, M.C., *et al.* (2009). PPAR gamma activation in adipocytes is sufficient for systemic insulin sensitization. *106*, 22504-22509.

Sugimoto, K., Yasujima, M., and Yagihashi, S. (2008). Role of advanced glycation end products in diabetic neuropathy. Current pharmaceutical design *14*, 953-961.

Sui, R., and Piao, H.Z. (2020). UCHL1 enhances the malignant development of glioma via targeting GAS2. European review for medical and pharmacological sciences *24*, 6195-6203.

Sun, S.-C. (2008). Deubiquitylation and regulation of the immune response. Nat Rev Immunol *8*, 501-511.

Surmeier, D.J., Obeso, J.A., and Halliday, G.M. (2017). Selective neuronal vulnerability in Parkinson disease. Nat Rev Neurosci *18*, 101-113.

Swatek, K.N., and Komander, D. (2016). Ubiquitin modifications. Cell Research *26*, 399-422.

Szczepanski, A.P., and Wang, L. (2021). Emerging multifaceted roles of BAP1 complexes in biological processes. Cell Death Discovery *7*, 20.

Tain, L.S., Mortiboys, H., Tao, R.N., Ziviani, E., Bandmann, O., and Whitworth, A.J. (2009). Rapamycin activation of 4E-BP prevents parkinsonian dopaminergic neuron loss. Nature neuroscience *12*, 1129-1135.

Tang, Y., Tu, H., Zhang, J., Zhao, X., Wang, Y., Qin, J., and Lin, X. (2019). K63-linked ubiquitination regulates RIPK1 kinase activity to prevent cell

death during embryogenesis and inflammation. Nat Commun *10*, 4157.

Tian, W., Li, W., Chen, Y., Yan, Z., Huang, X., Zhuang, H., Zhong, W., Chen, Y., Wu, W., Lin, C., *et al.* (2015). Phosphorylation of ULK1 by AMPK regulates translocation of ULK1 to mitochondria and mitophagy. FEBS letters *589*, 1847-1854.

Tóbon-Velasco, J.C., Cuevas, E., and Torres-Ramos, M.A. (2014). Receptor for AGEs (RAGE) as mediator of NF-kB pathway activation in neuroinflammation and oxidative stress. CNS & neurological disorders drug targets *13*, 1615-1626.

Um, S.H., D'Alessio, D., and Thomas, G. (2006). Nutrient overload, insulin resistance, and ribosomal protein S6 kinase 1, S6K1. Cell metabolism *3*, 393-402.

Verma, R., Aravind, L., Oania, R., McDonald, W.H., Yates, J.R., 3rd, Koonin, E.V., and Deshaies, R.J. (2002). Role of Rpn11 metalloprotease in deubiquitination and degradation by the 26S proteasome. Science (New York, NY) *298*, 611-615.

Vila, M., and Przedborski, S. (2003). Targeting programmed cell death in neurodegenerative diseases. Nat Rev Neurosci *4*, 365-375.

Vives-Bauza, C., Zhou, C., Huang, Y., Cui, M., Vries, R.L.A.d., Kim, J., May, J., Tocilescu, M.A., Liu, W., Ko, H.S., *et al.* (2010). PINK1-dependent recruitment of Parkin to mitochondria in mitophagy. *107*, 378-383.

Wick, A.N., Drury, D.R., Nakada, H.I., and Wolfe, J.B. (1957). Localization of the primary metabolic block produced by 2-deoxyglucose. The Journal of biological chemistry *224*, 963-969.

Wilkinson, K.D., Lee, K.M., Deshpande, S., Duerksen-Hughes, P., Boss, J.M., and Pohl, J. (1989). The neuron-specific protein PGP 9.5 is a ubiquitin carboxyl-terminal hydrolase. Science (New York, NY) *246*, 670-673.

Wu, W., Tian, W., Hu, Z., Chen, G., Huang, L., Li, W., Zhang, X., Xue, P., Zhou, C., Liu, L., *et al.* (2014). ULK1 translocates to mitochondria and phosphorylates FUNDC1 to regulate mitophagy. EMBO reports *15*, 566-575.

Xilouri, M., Kyratzi, E., Pitychoutis, P.M., Papadopoulou-Daifoti, Z., Perier, C., Vila, M., Maniati, M., Ulusoy, A., Kirik, D., Park, D.S., *et al.* (2012). Selective neuroprotective effects of the S18Y polymorphic variant of UCH-L1 in the dopaminergic system. Human molecular genetics *21*, 874-889.

Xu, X., Sarikas, A., Dias-Santagata, D.C., Dolios, G., Lafontant, P.J., Tsai, S.C., Zhu, W., Nakajima, H., Nakajima, H.O., Field, L.J., *et al.* (2008). The CUL7 E3 ubiquitin ligase targets insulin receptor substrate 1 for ubiquitin-dependent degradation. Molecular cell *30*, 403-414.

Yamazaki, K., Wakasugi, N., Tomita, T., Kikuchi, T., Mukoyama, M., and Ando, K. (1988). Gracile axonal dystrophy (GAD), a new neurological mutant in the mouse. Proceedings of the Society for Experimental Biology and Medicine Society for Experimental Biology and Medicine (New York, NY) *187*, 209-215.

Yang, L., Li, R., Kaneko, T., Takle, K., Morikawa, R.K., Essex, L., Wang, X., Zhou, J., Emoto, K., Xiang, Y., *et al.* (2014). Trim9 regulates activity-dependent fine-scale topography in Drosophila. Current biology : CB *24*, 1024-1030.

Yaribeygi, H., Farrokhi, F.R., Butler, A.E., and Sahebkar, A. (2019). Insulin resistance: Review of the underlying molecular mechanisms. Journal of cellular physiology *234*, 8152-8161.

Ye, J.-M., Dzamko, N., Hoy, A.J., Iglesias, M.A., Kemp, B., and Kraegen, E. (2006). Rosiglitazone Treatment Enhances Acute AMP-Activated Protein Kinase–Mediated Muscle and Adipose Tissue Glucose Uptake in High-Fat–Fed Rats. Diabetes *55*, 2797-2804.

Yi, J.-S., Park, J.S., Ham, Y.-M., Nguyen, N., Lee, N.-R., Hong, J., Kim, B.-W., Lee, H., Lee, C.-S., Jeong, B.-C., *et al.* (2013). MG53-induced IRS-1 ubiquitination negatively regulates skeletal myogenesis and insulin signalling. Nature Communications *4*, 2354.

Youle, R.J., and Narendra, D.P. (2011). Mechanisms of mitophagy. Nature reviews Molecular cell biology *12*, 9-14.

Yu, W., Singh, R., Wang, Z., O'Malley, B.W., and Yi, P. (2021). The E3 ligase TRAF4 promotes IGF signaling by mediating atypical ubiquitination of IRS-1. The Journal of biological chemistry *296*, 100739.

Zakaria, N.F., Hamid, M., and Khayat, M.E. (2021). Amino Acid-Induced Impairment of Insulin Signaling and Involvement of G-Protein Coupling Receptor. *13*, 2229.

Zhou, B.P., Deng, J., Xia, W., Xu, J., Li, Y.M., Gunduz, M., and Hung, M.C. (2004). Dual regulation of Snail by GSK-3beta-mediated phosphorylation in control of epithelial-mesenchymal transition. Nature cell biology *6*, 931-940.

Zhou, W., Xu, J., Tan, M., Li, H., Li, H., Wei, W., and Sun, Y. (2018). UBE2M Is a Stress-Inducible Dual E2 for Neddylation and Ubiquitylation that Promotes Targeted Degradation of UBE2F. Molecular cell *70*, 1008-1024.e1006.

Zhou, Y., Park, S.-Y., Su, J., Bailey, K., Ottosson-Laakso, E., Shcherbina, L., Oskolkov, N., Zhang, E., Thevenin, T., Fadista, J., *et al.* (2014). TCF7L2 is a master regulator of insulin production and processing. Human molecular genetics *23*, 6419-6431.

Zhu, H., Zhu, X., Liu, Y., Jiang, F., Chen, M., Cheng, L., and Cheng, X. (2020). Gene Expression Profiling of Type 2 Diabetes Mellitus by Bioinformatics Analysis. Computational and Mathematical Methods in Medicine *2020*, 9602016.

Abstract in Korean/국문 초록

UCHL1 의 생체기능 연구

UCHL1 은 탈유비퀴틴화 효소로서, 기질과 유비퀴틴 사이의 펩타이드 결합을 가수분해하여 세포 내에 유비퀴틴 단량체를 공급하는 역할을 한다. UCHL1 은 인간 뇌 전체 프로테옴의 1~2% 가량을 차지한다고 알려져 있음에도 불구하고, UCHL1 이 세포내에서 어떠한 기능을 하는지, 이것이 인간의 질병과 어떠한 연관이 있는지는 아직까지 밝혀지지 않았다. 따라서, 이번 연구에서 나는 초파리 모델동물과 사람 세포주를 이용하여 UCHL1 의 생체 내에서의 기능을 규명하고자 하였다.

1 부에서는, UCHL1 과 세포내 에너지에 반응하는 미토파지 경로 및 파킨슨병의 상관관계에 대해 연구했다. 초파리 스크리닝을 통하여, UCHL1 의 제거가 PINK1 혹은 Parkin 유전자가 손실되어 나타나는 운동성 저하, 도파민 뉴런 사멸과 같은 파킨슨병 연관형질들을 완화할 수 있음을 보였다. 또한, UCHL1 이 없는 세포주를 제작하여 해당 세포주에서 피루브산 생산 및 ATP 농도가 줄어 있음을 관찰했다. 따라서, UCHL1 이 없으면, 피루브산을 만드는데 필수적인 효소인 PKM 의 유비퀴틴을

떼어내지 못해 안정성을 떨어뜨림을 보였다. 결과적으로, 해당과정이 억제됨과 동시에 세포내 ATP 농도가 줄어들어 AMPK 가 활성화되었다. AMPK 는 ULK1 과 미토파지 수용체 중 하나인 FUNDC1 을 차례로 활성화하여 미토파지를 유도했다. 이렇게 UCHL1 의 돌연변이로 발생한 미토파지가 PINK1 혹은 Parkin 돌연변이에서 부족했던 미토파지를 보충하여 파킨슨병 형질을 완화할 수 있다고 증명했다. 더 나아가서, PKM 에 유비퀴틴을 붙이는 E3 리가아제인 TRIM63 을 찾아냈고, TRIM63 이 PKM 에 붙인 유비퀴틴을 UCHL1 이 떼어내는 것을 확인했다. 따라서, TRIM63 을 과발현하는 것이 미토파지를 유도함과 동시에 파킨슨병 형질을 완화할 수 있다는 것을 밝혔다.

2부에서는, UCHL1 과 인슐린 신호전달 및 제 2 형 당뇨병에 대해 연구했다. UCHL1 돌연변이 초파리에서 제 2 형 당뇨병의 기본 증상인 고혈당과 인슐린 저항성, 당뇨병의 합병증인 당뇨성 신경병증의 형질이 나타남을 확인했다. 반대로, 당분이 많이 포함된 식이 섭취로 제 2 형 당뇨병 형질이 생긴 초파리에서 UCHL1 을 과발현했을 시, 해당 형질이 모두 완화되는 것 또한 확인했다. UCHL1 결손 세포주를 통해 UCHL1 이 IRS1 의 유비퀴틴을 떼어내어 인슐린 신호전달을 조절할 수 있음을 밝혔다. 또한, 고농도의 당이 초파리 내에서 GSK3 의 활성을 억제하여

전사인자인 Snail 의 안정성을 올리는 것을 보았다. Snail 은 IRS1 의 E3 리가아제인 CUL1 의 전사를 담당했고, UCHL1 은 CUL1 이 IRS1 에 붙인 유비퀴틴을 떼어내는 것임을 증명했다. 따라서, CUL1 의 활성도를 올릴 수 있는 유전자들을 억제하여 제 2 형 당뇨병의 형질을 완화할 수 있음을 보였고, 해당 질병을 치료하는 새로운 치료법을 제시했다.

주요어: UCHL1, 파킨슨병, 미토파지, PKM, 제 2 형 당뇨병, 인슐린 신호전달, IRS1

학번: 2015-22638